

8-31-1991

A three-dimensional finite element stress analysis of interface conditions in porous coated hip prosthesis

Siu-For Yau
New Jersey Institute of Technology

Follow this and additional works at: <https://digitalcommons.njit.edu/theses>



Part of the [Mechanical Engineering Commons](#)

Recommended Citation

Yau, Siu-For, "A three-dimensional finite element stress analysis of interface conditions in porous coated hip prosthesis" (1991). *Theses*. 2681.

<https://digitalcommons.njit.edu/theses/2681>

This Thesis is brought to you for free and open access by the Electronic Theses and Dissertations at Digital Commons @ NJIT. It has been accepted for inclusion in Theses by an authorized administrator of Digital Commons @ NJIT. For more information, please contact digitalcommons@njit.edu.

Copyright Warning & Restrictions

The copyright law of the United States (Title 17, United States Code) governs the making of photocopies or other reproductions of copyrighted material.

Under certain conditions specified in the law, libraries and archives are authorized to furnish a photocopy or other reproduction. One of these specified conditions is that the photocopy or reproduction is not to be “used for any purpose other than private study, scholarship, or research.” If a user makes a request for, or later uses, a photocopy or reproduction for purposes in excess of “fair use” that user may be liable for copyright infringement,

This institution reserves the right to refuse to accept a copying order if, in its judgment, fulfillment of the order would involve violation of copyright law.

Please Note: The author retains the copyright while the New Jersey Institute of Technology reserves the right to distribute this thesis or dissertation

Printing note: If you do not wish to print this page, then select “Pages from: first page # to: last page #” on the print dialog screen

The Van Houten library has removed some of the personal information and all signatures from the approval page and biographical sketches of theses and dissertations in order to protect the identity of NJIT graduates and faculty.

21 A THREE-DIMENSIONAL FINITE ELEMENT STRESS ANALYSIS OF
INTERFACE CONDITIONS IN POROUS COATED HIP PROSTHESIS

by

11 Siu-For Yau
/

Thesis submitted to the Faculty of the Graduate School of the
New Jersey Institute of Technology in partial fulfillment of the
requirements for the degree of Master Science in Mechanical
Engineering

1991

APPROVAL SHEET

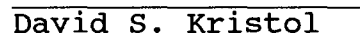
Title of thesis : A three-dimensional finite element stress analysis of interface conditions in porous coated hip prosthesis

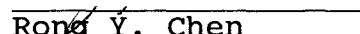
Name of candidate :
Siu-For Yau
Master Science of Mechanical Engineering

Thesis and Abstract
approved by :


Michael J. Pappas, Ph.D, P.E.

Signatures of thesis
committee members :


David S. Kristol
Director of program in Biomedical Engineering


Rong Y. Chen
Professor of Mechanical Engineering
Department of Mechanical and Industrial
Engineering
Acting associate chairman of graduate studies

VITA

Name : Siu-For Yau

Permanent address :

Degree and date to
be conferred : M.S.M.E., May 1991

Date of birth :

Place of birth :

Colleges attended :

<u>College</u>	<u>Years</u>	<u>Degree</u>	<u>Date of degree</u>
N.J.I.T.	84-87	B.S.M.E.	May, 1987
N.J.I.T.	87-91	M.S.M.E.	October, 1991

ABSTRACT

Title of thesis :

A three-dimensional finite element stress analysis of interface conditions in porous coated hip prosthesis

Thesis written by :

Siu-For Yau, M.S.M.E., 1991

Thesis directed by :

Michael J. Pappas, Ph.D, P.E.

A three-dimensional finite element model of a collar-type hip stem and both the cortical and cancellous bones is used to investigate the stress distributions on an implanted femoral stem, adjacent bone, and specifically at the bone/implant interface for various amounts of porous coating and different stem materials. The finite element model consists of 909 nodes comprising 536 linear eight-node solid brick elements and 176 two-node interface elements. The finite element analysis code employed is SUPERTAB from SDRC. The interface elements consist of coincident-node spring elements and gap elements which model the rigidly bonded and loose interfaces respectively. Local coordinate systems are defined at the bone/implant interface to represent interface normal stresses. A nonhomogeneous isotropic distribution of elastic constants is used to account for the varying material properties in the model. Four different loading conditions (4%, 9%, 41% and 52%) of the normal walking cycle are analysed. The hip joint reaction force, abductor muscle force and adductor muscle force are applied to the collar of stem and the

greater and lesser trochanters.

The resulting stress distributions indicate that for the fully porous coated inhomogeneous model, the proximal bone region is highly relieved of stresses. The proximally coated model generates more interface compression and higher bone stresses in the proximal region. The laterally coated model exhibits similar stress pattern to that of proximally coated. However, when compared to the proximally coated, the slanted coated model has a higher proximal bone stress and higher interface stress values at the bone/implant interface. Thus, the laterally coated stem is the most effective at loading the proximal femur and reducing the loading bypass mechanism in the region. The effects of cobalt-chromium-molybdenum (CoCrMo) and titanium as the stem materials are also assessed. The titanium stems demonstrate more favorable results than the CoCrMo stems. Therefore, the use of laterally coated titanium stem appears to be the optimal alternative in the total hip replacement system.

ACKNOWLEDGEMENT

I would like to take this opportunity to express my sincere gratitude to my thesis advisor, Michael J. Pappas, for his continual support and invaluable guidance toward the completion of the thesis work. Also, it is great honor to represent him and New Jersey Institute of Technology for the presentation of my thesis at the Sixteen Annual Meeting of the Society For Biomaterials in May, 1990.

I would also like to thank departments of Mechanical Engineering and Computer-Aided Design for providing computer facilities and special arrangements during the course of my thesis work.

Siu-For Yau

TABLE OF CONTENTS

	PAGE
TITLE	
APPROVAL SHEET	i
VITA	ii
ABSTRACT	iii
ACKNOWLEDGEMENT	v
TABLE OF CONTENTS	vi
LIST OF FIGURES	viii
CHAPTERS :	
1. INTRODUCTION	
1.1 HISTORICAL PERSPECTIVE	1
1.2 AN ALTERNATIVE TO CEMENTED PROSTHESIS	2
1.3 ADVANCES IN POROUS COATED IMPLANTS	3
1.4 PREVIOUS FINITE ELEMENT STUDIES	5
2. MODEL DESCRIPTION	
2.1 OBJECTIVE	9
2.2 COMPONENTS OF TOTAL HIP REPLACEMENT MODEL	9
2.2.1 FEMUR	9
2.2.2 POROUS COATED PROSTHESIS	13
2.3 INPUT BOUNDARY AND LOADING CONDITIONS	18
3. RESULTS	
3.1 VON MISES STRESSES OF THE IMPLANTS	24
3.1.1 EFFECT OF DIFFERENT MATERIALS	31
3.1.2 EFFECT OF POROUS COATING CONFIGURATIONS	32

	PAGE
3.2 COMPRESSIVE STRESSES AT BONE INTERFACE	48
3.2.1 EFFECT OF DIFFERENT MATERIALS	49
3.2.2 EFFECT OF POROUS COATING CONFIGURATIONS	49
3.3 MAXIMUM SHEAR STRESSES AT BONE INTERFACE	59
3.3.1 EFFECT OF DIFFERENT MATERIALS	59
3.3.2 EFFECT OF POROUS COATING CONFIGURATIONS	59
3.4 STRESSES IN FEMUR	73
3.4.1 EFFECT OF DIFFERENT MATERIALS	73
3.4.2 EFFECT OF POROUS COATING CONFIGURATIONS	73
4. DISCUSSION OF RESULTS	75
5. CONCLUSION	77
REFERENCES	78
APPENDIX ILLUSTRATIONS OF COORDINATE SYSTEMS TRANSFORMATION	A-1

<u>LIST OF FIGURES</u>	<u>PAGE</u>
2.2.1-1 Components of total hip replacement structure	12
2.2.2-1 Fixation geometries studied	15
2.2.2-2 Interface description of THR using lateral coated stem	17
2.3-1 Loads at 4 percent phase of the walking cycle	20
2.3-2 Loads at 9 percent phase of the walking cycle	21
2.3-3 Loads at 41 percent phase of the walking cycle	22
2.3-4 Loads at 52 percent phase of the walking cycle	23
3.1-1 Von mises stresses on the surface of laterally coated stems at 4% phase of the walking cycle	25
3.1-2 Von mises stresses on the surface of laterally coated stems at 41% phase of the walking cycle	26
3.1-3 Von mises stresses on the surface of proximally coated stems at 4% phase of the walking cycle	27
3.1-4 Von mises stresses on the surface of proximally coated stems at 41% phase of the walking cycle	28
3.1-5 Von mises stresses on the surface of fully coated stems at 4% phase of the walking cycle	29
3.1-6 Von mises stresses on the surface of fully coated stems at 41% phase of the walking cycle	30
3.2-1 Interface compressive stresses on THR using fully coated Co-Cr stem at 4% phase of the walking cycle	33

LIST OF FIGURES, CONTINUED

	PAGE
3.2-2 Interface compressive stresses on THR using fully coated Ti stem at 4% phase of the walking cycle	34
3.2-3 Interface compressive stresses on THR using fully coated Co-Cr stem at 41% phase of the walking cycle	35
3.2-4 Interface compressive stresses on THR using fully coated Ti stem at 41% phase of the walking cycle	36
3.2-5 Interface compressive stresses on THR using proximally coated Co-Cr stem at 4% phase of the walking cycle	37
3.2-6 Interface compressive stresses on THR using proximally coated Ti stem at 4% phase of the walking cycle	38
3.2-7 Interface compressive stresses on THR using proximally coated Co-Cr stem at 41% phase of the walking cycle	39
3.2-8 Interface compressive stresses on THR using proximally coated Ti stem at 41% phase of the walking cycle	40
3.2-9 Interface compressive stresses on THR using laterally coated Co-Cr stem at 4% phase of the walking cycle	41
3.2-10 Interface compressive stresses on THR using laterally coated Ti stem at 4% phase of the walking cycle	42
3.2-11 Interface compressive stresses on THR using laterally coated Co-Cr stem at 41% phase of the walking cycle	43
3.2-12 Interface compressive stresses on THR using laterally coated Ti stem at 41% phase of the walking cycle	44
3.2-13 Interface compressive stress for fully coated Ti and Co-Cr stems at bone interface	45

LIST OF FIGURES, CONTINUED

	PAGE
3.2-14 Interface compressive stress for proximally coated Ti and Co-Cr stems at bone interface	46
3.2-15 Interface compressive stress for laterally coated Ti and Co-Cr stems at bone interface	47
3.3-1 Maximum shear at bone interface surrounding fully coated stems at 4% load case	50
3.3-2 Maximum shear at bone interface surrounding fully coated stems at 41% load case	51
3.3-3 Maximum shear at bone interface surrounding proximally coated stems at 4% load case	52
3.3-4 Maximum shear at bone interface surrounding proximally coated stems at 41% load case	53
3.3-5 Maximum shear at bone interface surrounding laterally coated stems at 4% load case	54
3.3-6 Maximum shear at bone interface surrounding laterally coated stems at 41% load case	55
3.3-7 Maximum shear stress for fully coated Ti and Co-Cr stems at bone interface	56
3.3-8 Maximum shear stress for proximally coated Ti and Co-Cr stems at bone interface	57
3.3-9 Maximum shear stress for laterally coated Ti and Co-Cr stems at bone interface	58
3.4-1 Maximum compressive stresses at bone interface and surrounding bone on THR using fully coated stem Ti at 4% phase of the walking cycle	61

LIST OF FIGURES, CONTINUED

	PAGE
3.4-2 Maximum compressive stresses at bone interface and surrounding bone on THR using proximally coated stem Ti at 4% phase of the walking cycle	62
3.4-3 Maximum compressive stresses at bone interface and surrounding bone on THR using laterally coated Ti stem at 4% phase of the walking cycle	63
3.4-4 Von mises stress on cortical bone surface of THR using fully coated stems at 4% phase of the walking cycle	64
3.4-5 Von mises stress on cortical bone surface of THR using fully coated Co-Cr stem at 41% phase of the walking cycle	65
3.4-6 Von mises stress on cortical bone surface of THR using fully coated Ti stem at 41% phase of the walking cycle	66
3.4-7 Von mises stress on cortical bone surface of THR using proximally coated stems at 4% phase of the walking cycle	67
3.4-8 Von mises stress on cortical bone surface of THR using proximally coated Co-Cr stem at 41% phase of the walking cycle	68
3.4-9 Von mises stress on cortical bone surface of THR using proximally coated Ti stem at 41% phase of the walking cycle	69

LIST OF FIGURES, CONTINUED

	PAGE
3.4-10 Von mises stress on cortical bone surface of THR using laterally coated stems at 4% phase of the walking cycle	70
3.4-11 Von mises stress on cortical bone surface of THR using laterally coated Co-Cr stem at 41% phase of the walking cycle	71
3.4-12 Von mises stress on cortical bone surface of THR using laterally coated Ti stem at 41% phase of the walking cycle	72
A-1 Force actions on left femur at 4 percent phase of the walking cycle	A-2
A-2 Force actions on left femur at 9 percent phase of the walking cycle	A-5
A-3 Force actions on left femur at 41 percent phase of the walking cycle	A-8
A-4 Force actions on left femur at 52 percent phase of the walking cycle	A-11

CHAPTER ONE

INTRODUCTION

1.1 HISTORICAL PERSPECTIVE

Smith-Peterson[1] developed the techniques of Pyrex cup arthroplasty for treatment of arthritic hips in 1939. Later he used Vitallium molds in place of the Pyrex cups. These metallic cup arthroplasties were used in the United States until cemented total hip replacements became available in the late 1960s. In the 1940s Moore and Bohlman[2] as well as the Judet brothers[3] independently designed and developed a replacement prosthesis for the femoral head and neck, which is still being used in the treatment of femoral neck fractures. In 1960, John Charnley[4] first reported his clinical experiences with replacement of the human hip joint using stainless steel and Teflon fixed to bone with methylmethacrylate. Due to excessive wear of the Teflon cups, high density polyethylene (HDPE) was substituted. In the early 1970s, Giliberty[5] and Bateman[6] independently developed a press-fit bipolar prosthesis. This consisted of a femoral head and stem capped by a shell of HDPE over which a metallic cup was placed. Luncford[7] used the technique of combining McBride cup[8]

and Moore prosthesis without cement to perform total hip replacement. In the late 1970s Lord et al.[9] and Judet et al.[10] designed and developed press-fit femoral components with roughened surfaces for implantation in the femur which did not necessitate using acrylic bone cement. Since 1977, noncemented prosthesis with a Moore-type stem and a porous coating have been developed by surgeons like Engh, Chandler, and Lunceford[11].

Active individuals with healthy bone stock are ideal candidates for noncemented implants. With the increasing cases of aseptic femoral loosening with each subsequent revision of cemented hip implants[12][13], porous coated implants are finding wide acceptance in the orthopaedic community[14][15] and are considered a better alternative to avoid the problems being encountered with cement.

1.2 AN ALTERNATIVE TO CEMENTED PROSTHESIS

Acrylic cement provides immediate fixation of the implant to bone by virtue of its space-filling role. No real adhesive bonding of the element to bone or implant occurs. The incidence of loosened cemented total hip replacement can be attributed by cement failure and resulting lysis[16] often called "cement disease". Chwirut[17] found significant creep deformation subsequent to repetitive loading with

interpore cracks appearing in vitro. Furthermore, a 73% reduction in the cement strains has been shown to occur in the proximal-medial region after 4.1 million cycles. This is another indication of creep deformation. Acrylic cement may undergo "aging" with time. Long term studies[18] suggest that the intrinsic changes of methyl methacrylate over time decrease the biomechanical suitability of cement for long-term fixation. Studies[19] have documented the stress shielding in the proximal-medial margin of the femur. It is evident that the proximal femur is subject to conditions that may hinder the ability of the cement to transfer load from the prosthesis to the surrounding bone. Therefore, the elimination of "cement disease" can only occur with the elimination of cement. An attractive alternative is the use of porous coated implants to achieve biologic fixation, permitting the so-called micro-interlock[20].

Cementless components offer several potential advantages over cemented ones, including less foreign material, long term interface stability, and improved biocompatibility. The implant stems are fabricated from cast cobalt-chromium alloy or titanium alloy and they are coated with a sintered bead porous surface[21].

1.3 ADVANCES IN POROUS COATED IMPLANTS

Early designs of cementless total hip prosthesis have stems which are fully coated. Their clinical results

demonstrate that bony ingrowth has occurred into the coating of the distal part of the femoral components and stress shieldings result[22]. Stems with distal coating appear to transfer more load distally and stress-relieve proximally. Engh and Bobyn[23] find in their study that the more extensive the connection between the implant and the bone, the greater the amount of bone will be stress-shielded and become resorbed. Similar findings have also been reported by Turner et al.[24] in studies of canine porous-coated femoral implants.

Later designs have confined the porous coating to the proximal portion of the femoral component. Several advantages can potentially accrue from a proximally coated implant design : less surface area for corrosion and metal ion release[25], reduced likelihood of rigid distal fixation causing cantilever stem loading and fatigue failure, and easier implant removal if necessary. With partially coated stem, even if the proximal porous region is well-connected to the femur by bony ingrowth, the distal femur is free to move somewhat relative to the smooth distal surface of the implant. This decoupling of implant and bone increases the strain and stresses in the femur and noticeably reduces the distal bone resorption.

Histologic analyses of proximally coated human and canine femoral implants[26] have often shown rigid fixation of the proximal stem region by bone microinterlock and encapsulation of the smooth distal stem region by a thin

shell of bone separated from the implant by fibrous tissue. However, Engh and Bobyn indicate in their study[23] that proximally coated implants do not reduce proximal bone resorption in the region of porous coating. The gain in conservation of bone stock with one-third coated implants appears to result from the region which is not porous coated.

1.4 PREVIOUS FINITE ELEMENT STUDIES

The finite element method (FEM), an advanced computer technique of structural stress analysis developed in engineering mechanics, was introduced in 1972 to orthopaedic biomechanics for evaluating stresses in human bone. Since then, this method has been applied with increasing frequency for stress analyses of bones and bone-prosthesis structures. Artificial joint design and fixation is probably the most popular application of the FEM in orthopaedic biomechanics. Three dimensional, 2-D and beam analyses of total hip replacement structure have been widely performed.

In 2-D FEM analysis, varying degrees of mesh refinement are used and different prosthetic designs are simulated. A simple load case such as hip joint reaction force is commonly used. Andriacchi et al.[27] use a 2-D model consisting of constant strain triangular elements used

separately, or combined into groups of four, to represent a quadrilateral. A unit load is applied to the femoral head in different angles with respect to the longitudinal axis of the femur. The model results in errors of 50% when compared to experimental results. This could be attributed to the consideration of the model as a 'sandwich' construction in a plane with no connection between the lateral and medial bone slabs. Probably the best method to restore the 3-D integrity of the bone in 2-D models is by using a layer of 'spanning ' elements or 'sideplate' elements. Svensson et al.[28] use this method to include the effects of bone cement and cortex in the anterior-posterior dimension. The medial and lateral cortices are connected, without being connected to the stem elements. A single hip joint force is applied to the model. However, the accuracy of the model improves sufficiently enough to be considered as realistic evaluation.

Another way of accounting for the 3-D structural integrity of the composite in simplified models is to assume axisymmetric geometry. By using Fourier analysis, 3-D loading and stress states can be incorporated. Huiskes[29] assumes the idea of axisymmetric geometry and uses a simplified model with a three dimensional joint force. He applies axisymmetric ring elements, FEM beam elements, 2-D plane-strain elements, beam-on-elastic foundation theory, and strain gauge analysis to compare modelling options and to obtain a more generalized description of the intramedullary fixation structure. Anatomic models, applying

the 3-D FEM with varying degrees of refinement have been investigated. 3-D FEA is quite useful for predicting the changes in stress distribution that result from variations in design. The three dimensional and variable nature of the in vivo stem loads and of the various muscle loads would produce significantly variable patterns of stress distribution. Crowninshield et al.[30] study the various aspects of the stem design using a simplified 3-D model of hip replacement. The loading conditions include a force on the head of prosthesis and an abduction force inserted through the greater trochanter. This chosen loading situation is one of the most demanding situations during prosthetic function.

Since the cementless porous coated prosthesis becomes to replace the cemented method, analytical studies have been shifted to this area. Rohlman et al.[31] investigate load transfer between a porous coated (partly and fully) hip stem and a femur. The stance phase of walking is used as the load case for the model. No muscle forces is taken into consideration. Only a pure bending moment is applied to the model. The stress distributions for linear and nonlinear interface conditions are determined. Their results indicate that maximum values for relative motion in the interface occur on implants with the same elastic modulus as compact bone and the elastic modulus of the coating has only a small influence on bone stresses. Rohlmann et al.[32] later model a nonlinear bone-implant

interface with a finite element program employing stress-based method to represent the loose interface. Stress-based iterations are less suitable because they are calculated as derivatives of the displacement field and hence are less accurate than displacement. The more accurate method using nodal displacements has been described by Bathe and Chaudhary[33].

With the advantages of fast growing computer technologies, the finite element codes are far more capable of dealing with complicated but more realistic approaches. The fundamental 2-D finite element analysis should be replaced with 3-D which can offer better accurate results. One of the greater challenges, which has not been met in the recent hip replacement analyses lies in the input of major muscle forces in particular the applied adductor force during normal gait. The major muscles acting on the hip joint are the gluteus maximus as well as the gluteus medius and minimus. Gluteus maximus, the largest muscle in the body, is the hip extensor, adductor and the most powerful lateral rotator of the thigh. The gluteus medius and minimus are the abductors and medial rotators of the thigh. The hip abductor and adductor play a major role during gait to stabilize the pelvic girdle over the weight-receiving limb so that the opposite limb would move forward and in turn receive the body's weight.

CHAPTER TWO

MODEL DESCRIPTION

2.1 OBJECTIVE

The aim of this study is to investigate the effects of implant materials and porous coating geometries on load transfer in total hip replacement (THR). The implant materials involved are cobalt-chromium-molybdenum alloy and titanium alloy. The porous coating geometries under study will be the configurations of complete coating, proximal coating and lateral coating. Emphases are placed on interface stress patterns which would characterize the initial postoperative conditions in THR.

2.2 COMPONENTS OF TOTAL HIP REPLACEMENT MODEL

2.2.1 FEMUR

A normal femur basically consists of two structures, one is compact cortical bone surrounding the other spongy cancellous bone. The structure of the femur was preliminary interpreted by J. Wolff's hypothesis [34] : statical importance and necessity are deduced from the

density of trajectories in the Culmann's crane model, high density of trajectories meaning large stresses and consequently the necessity of compact bone, low density meaning cancellous bone, and no density meaning the medullary cavity. Later Koch[35] adopts Wolff's hypothesis to investigate the inner structure of the femur on a mathematical basis. He dissects a normal left femur into 75 transverse sections and computes their mechanical properties individually.

The femur is an inhomogeneous, anisotropic, and elastic material[36][37]. Huiskes[38] indicates the stress analysis of a human femur is adequately served with an isotropic elastic model. Isotropic materials are described by only two independent elastic constants, Young's Modulus and Poisson's Ratio. As a result of review of published literature[39][40], the following data are assumed to be appropriate as typical values for analysis :

Cortical bone

Young's Modulus=18 GPa

Poisson's Ratio=0.29

Cancellous bone

Young's Modulus=0.32 GPa

Poisson's Ratio=0.29

These are the average values from several workers whose results show good agreement. Young's Modulus is the

ratio of normal stress to normal strain produced in a simple one-dimensional tension or compression test. The simple tensile test may be the best way to characterize bone. When bone is bent, it will fail in tension on convex side. The tensile strength of bone has often been considered its most important mechanical property. In a tensile test, the whole bone is not used, test pieces are machined from the cortex. Cancellous bone is a difficult tissue to test and estimates of its properties are few. It is almost impossible to test in tension because of the difficulty of gripping it without crushing it. Evans and King[41] tested its modulus of elasticity and compressive strength in small prisms taken from all parts of human femora. From the data obtained during tests, a stress-strain curve was drawn for each specimen and was used to calculate the tangent modulus of elasticity.

The finite element model of the femur(Fig. 2.2.1-1[1-2]) is made of linear eight-node brick element using SUPERTAB analysis program developed by Structural Dynamics Research Corporation (SDRC). The solid brick element is designed to construct approximate solutions to the equations of three dimensional linear elasticity[42]. It also provides flexibility for the mesh formation of the odd geometries of cortical and cancellous bone. The profiles that form the cortical and cancellous structures in this study are extracted from part of the sections in the study by Koch[35].

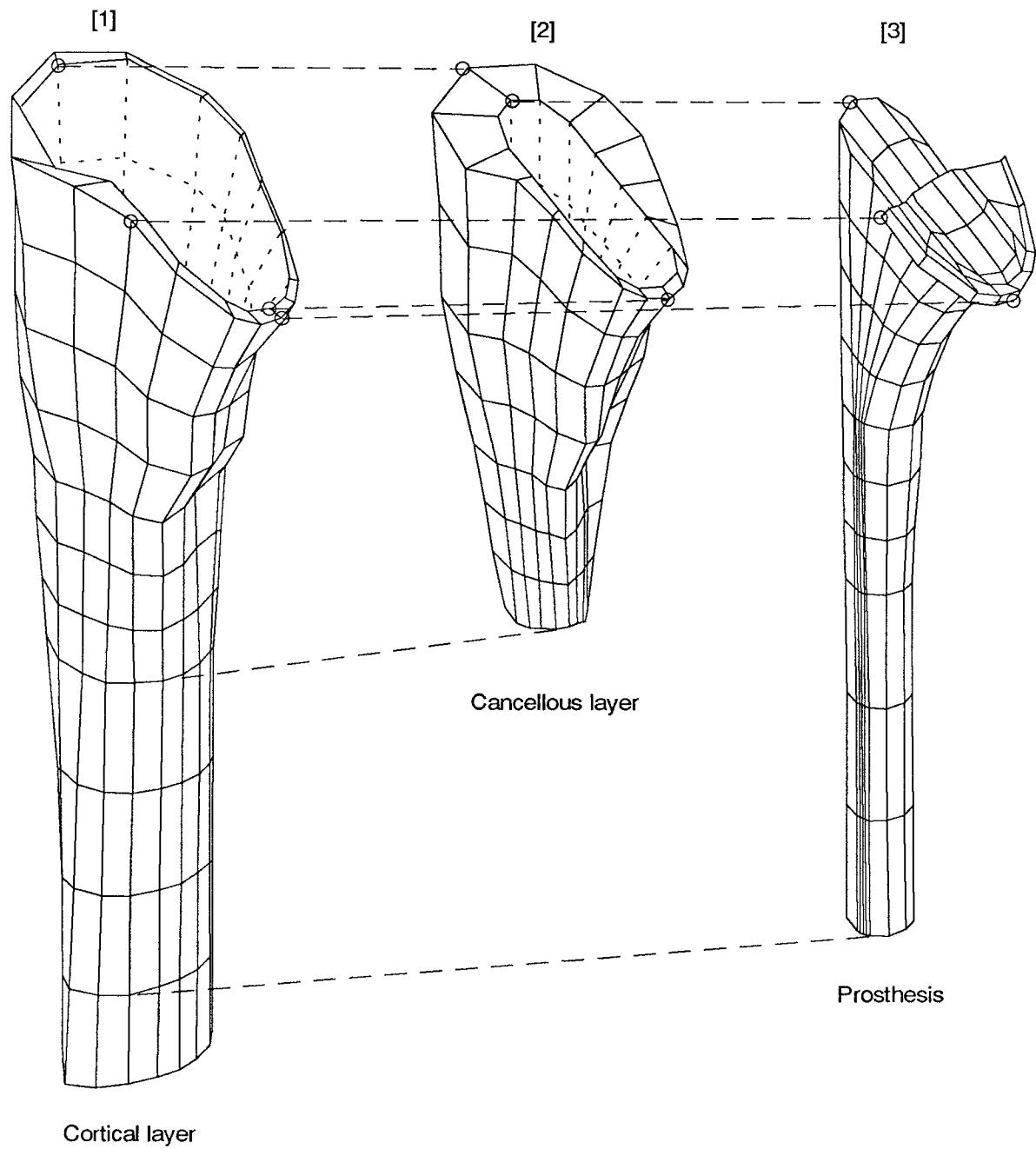


Fig.2.2.1-1 Components of total hip replacement structure :
[1] Cortical bone. [2] Cancellous bone. and [3] Prosthesis.

2.2.2 POROUS COATED PROSTHESIS

The stem used in this study is a simplified form of the Buechel-Pappas femoral stem whose body is basically straight tapered, cylindrical and porous coated. The model has a 12-mm diameter and a length of 7 inches (Fig. 2.2.1-1[3]). The stem has collar seating whose main effects are to transfer compressive load through the calcar [43] and to control distal settling (subsidence) of the implant with repetitive loads [44]. A stem without collar would increase the hoop stresses in the calcar as reported in the study by Crowninshield et al. [31]. The tensile stress component which is mode of unphysiological loading might lead to the bone resorption in the calcar region of the femur.

The implant materials which are compared in this study are cobalt-chromium-molybdenum alloy and titanium alloy used for biologically fixed metal implants [45]. Titanium alloy is stronger than Co-Cr-Mo alloy in both fatigue and yielding resistance. Due to its lower stiffness, titanium implants should reduce the stress shielding effect in the calcar region of the femur and therefore help alleviate the bone resorption problem. The mechanical properties of these alloys are as follow :

Cobalt-Chromium-Molybdenum alloy (Co-Cr-Mo)

Young's Modulus = 200 GPa

Poisson's ratio = 0.30

Titanium alloy ELI grade (Ti-6%Al-4%V)

Young's Modulus = 110 GPa

Poisson's ratio = 0.30

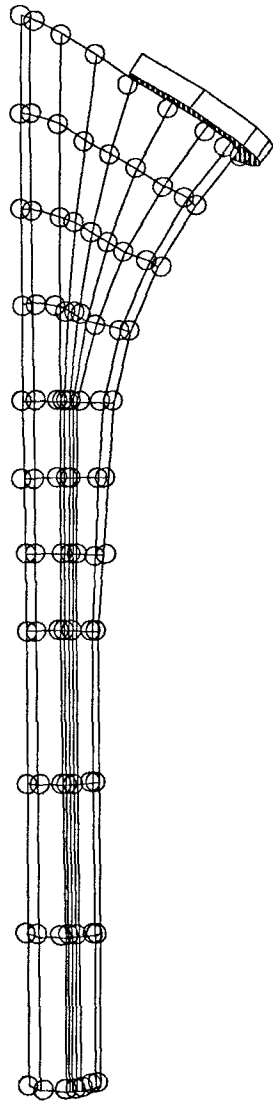
Three types of porous coating configurations on the stem model[figure 2.2.2-1] are studied. These are :

(1) Complete coating : An entirely coated stem would be proved as least efficient in terms of load transfer from the prosthesis to the bone.

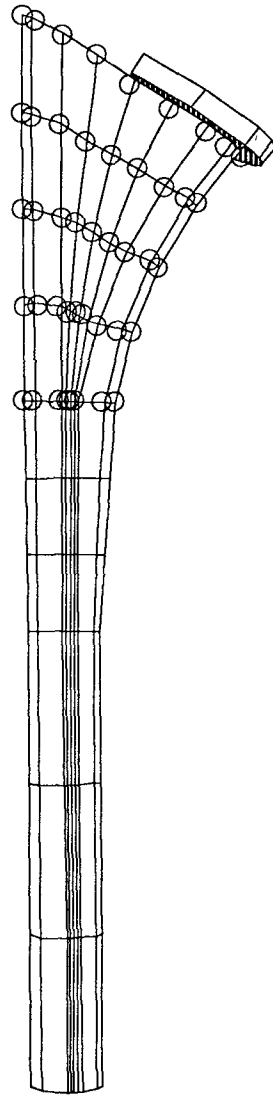
(2) Proximal coating : a proximally coated stem providing extensive decoupling area which facilitates more bending to the bone and enables to achieve natural stress patterns.

(3) Lateral coating : This type of configuration differs from the proximal one that the coating extends gradually from the medial side of the stem to lateral side. The slanted coating tends to produce a load path that transfers load directly to the medial calcar region and distributes the load laterally. This study attempts to verify it as optimal coating geometry for minimizing the stress shielding effect.

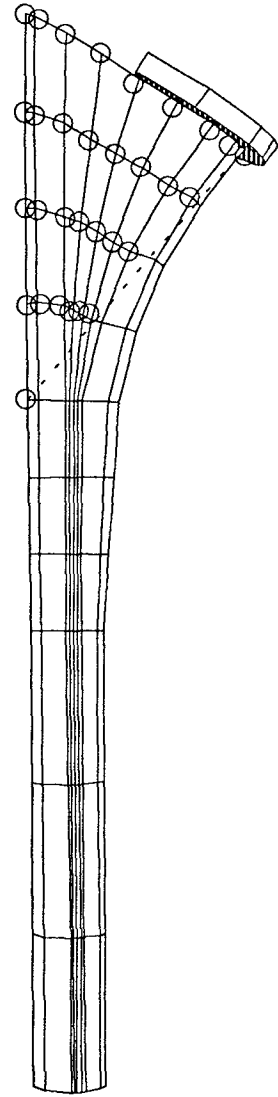
○ NODAL FIXATION



COMPLETE
FIXATION



PROXIMAL
FIXATION



LATERAL
FIXATION

Fig.2.2.2-1 Fixation geometries studied

The stem mesh is solid brick elements as is the femur. The porous coating region is modelled by node-to-node interface spring element connecting one node on the stem to another node on the bone. Since there is no gap between the stem and the bone, the spring element becomes a pair of coincident nodes. The nodes are bonded with a stiffness constant of 200×10^9 Newtons per unit Meter equal to the value of Young's Modulus of CoCr to ensure fixation. The bonded interface allows transfer of tension, compression and frictional shear.

SUPERTAB provides the node-to-node nonlinear frictionless gap element which simulates the non-coating interface. The gap element interprets a tensile nodal force as impermissible. Thus the gap is ignored whenever tensile force is required to maintain contact. The non coating region is treated as a loose interface which allows slip without frictional shear. The gap element also functions to limit the relative motion of its pairs of nodes in a specified direction. This prevents the penetration of elements attached to one node into the elements attached to the other node.

A local cartesian coordinate system is created for each of the interface connecting nodes. The main purpose of this coordinate system is to have the local negative z-axis normal to the interface represent compressive interface stresses. Figure 2.2.2-2 shows a brief interface description in two sections .

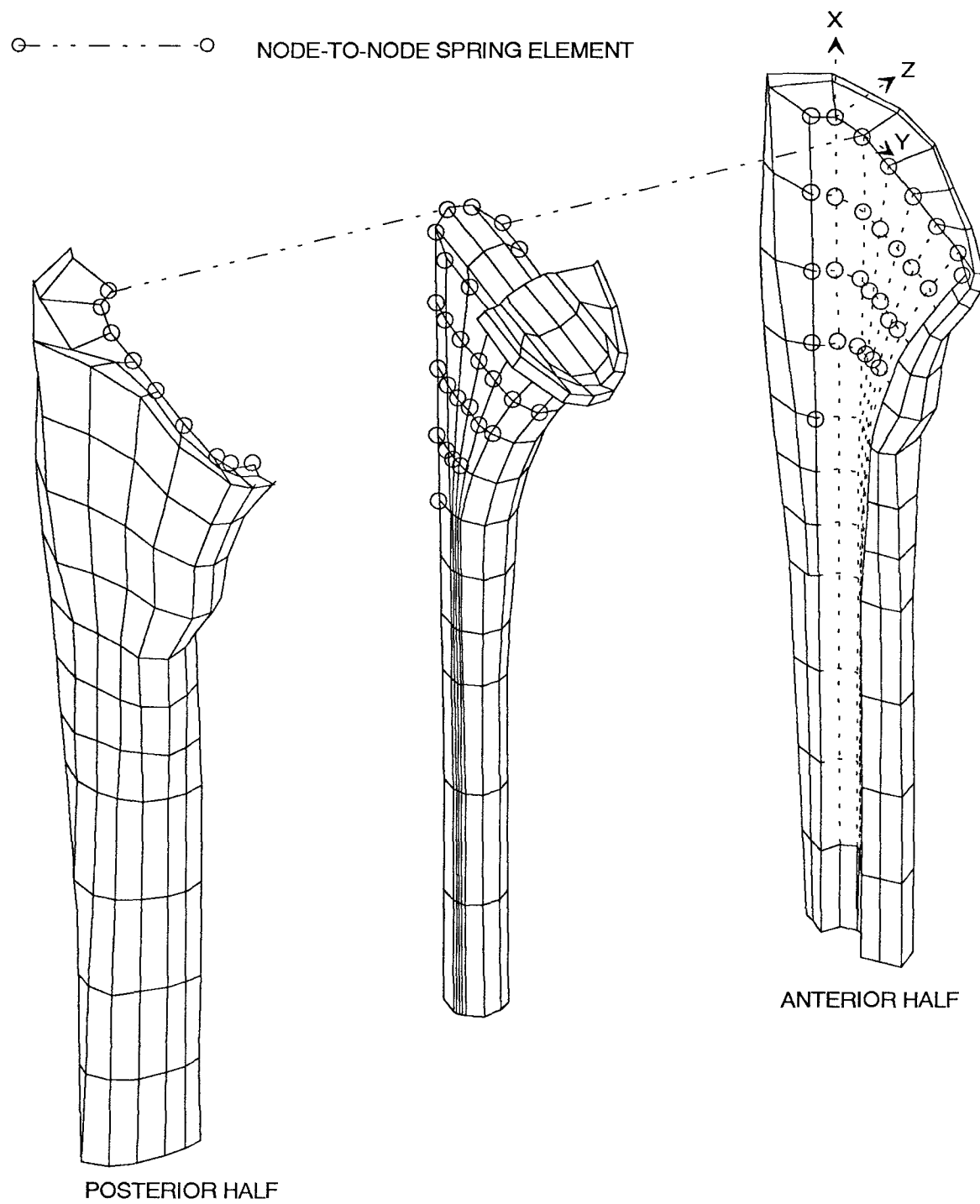


Fig.2.2.2-2 Interface description of THR using laterally coated stem

2.3 INPUT BOUNDARY AND LOADING CONDITIONS

The model is constrained at the bottom which is far from being the area of interest in this study.

The input load is the muscle forces and hip joint force during normal gait. The analysis by John P. Paul[46] is adopted as reference for the loading conditions in this study. Paul photographically measure the three dimensional configuration of the leg segments during a walking cycle in which the ground-to-foot force actions were measured by a force-plate dynamometer. From the measurement data, the resultant forces and moments transmitted between segments were calculated. The hip joint forces are presented as orthogonal components through the hip joint. The stress values are analyzed at the 4 percent, 9 percent, 41 percent and 52 percent phases of the walking cycle after heel strike.

The input loads are abductor and adductor muscle forces and hip joint reaction force during normal gait. The hip joint and muscle forces determined by Paul[46] are used in this study. The resultant muscle forces(abductors and gluteus maximus) and orthogonal hip joint forces are transformed here into new sets of force components to coincide with the orientation of the model used by coordinate transformation. The initial step is to determine the I,J,K component forces from three different views

including top, lateral and front. At each view, a three by three transformation matrix is established to relate the old axes to the new axes with directional cosines. Multiplying the individual matrixes together get the overall transformation matrix T of the model. This would become the transformation factor to obtain the new set of components(I',J',K') from the product between the matrix factor and old components matrix. Here is the governing equation :

$$\begin{vmatrix} I' \\ J' \\ K' \end{vmatrix} = |T| \begin{vmatrix} I \\ J \\ K \end{vmatrix} \quad \text{where}$$

I',J',K' represents axes applied to current study

I,J,K represents axes applied to Paul's study

T represents transformation matrix factor converting I,J,K coordinate system to I',J',K' c.s.

These procedures are repeated for four different loading phases and are illustrated in the Appendix I. Three dimensional force components of hip joint and major muscles at 4%, 9%, 41% and 52% phases are shown in fig.2.3-1 thru fig.2.3-4.

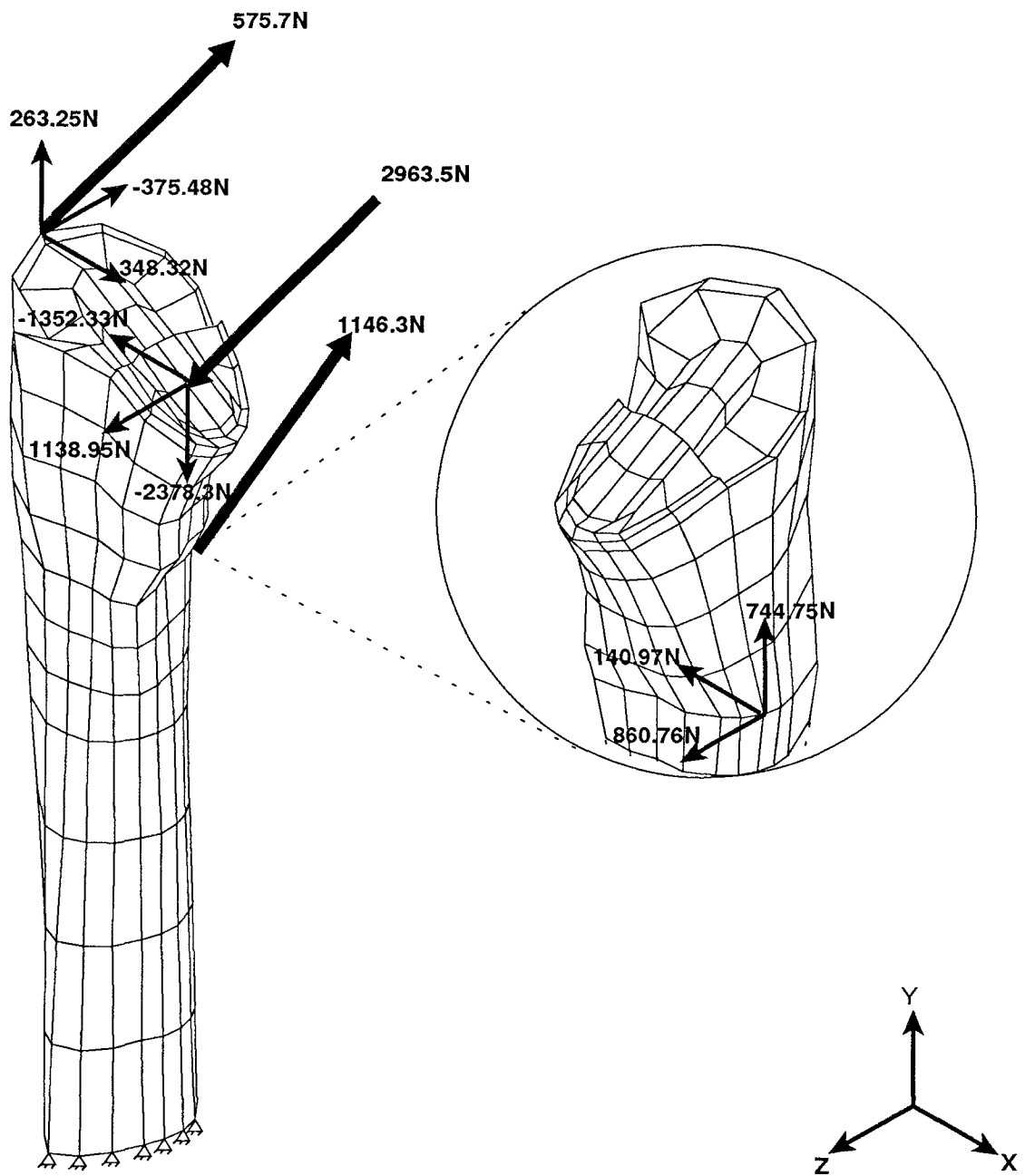


Fig. 2.3-1 Loads at 4 percent phase of the walking cycle

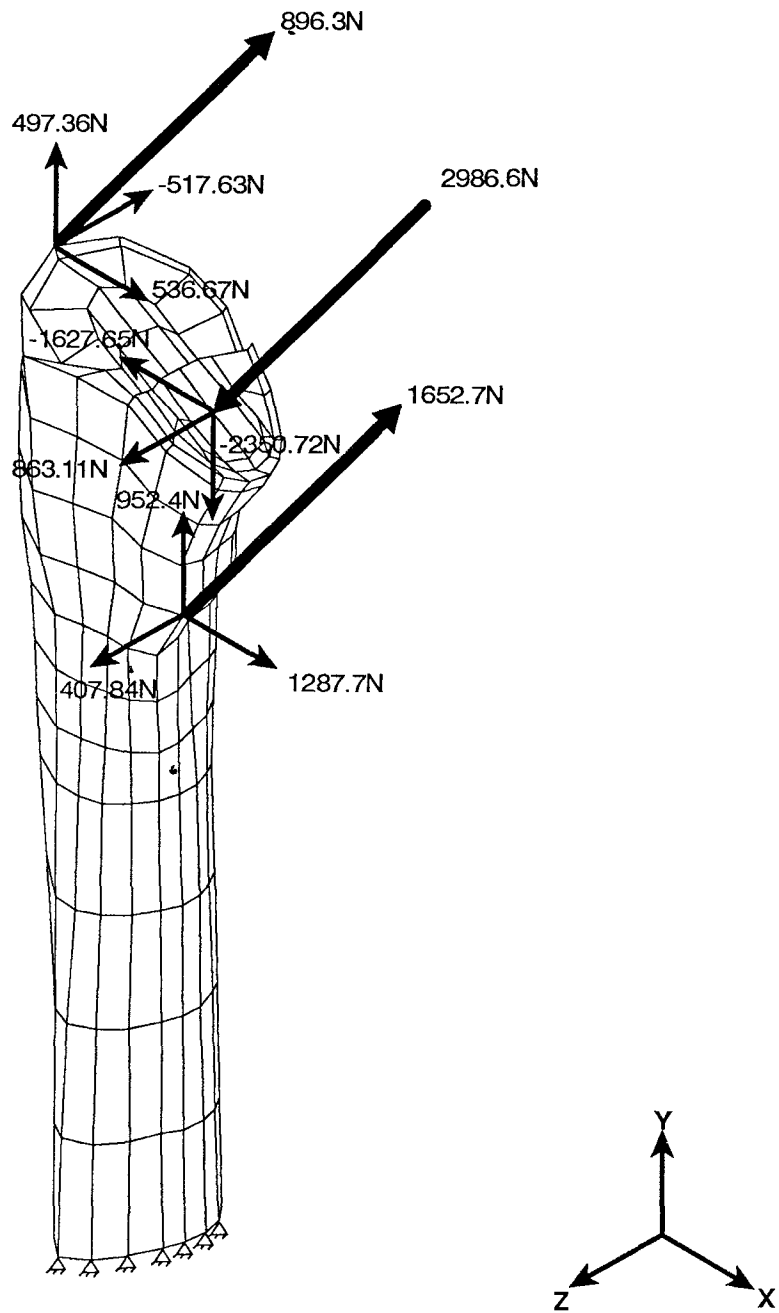


Fig.2.3-2 Loads at 9 percent phase of the walking cycle

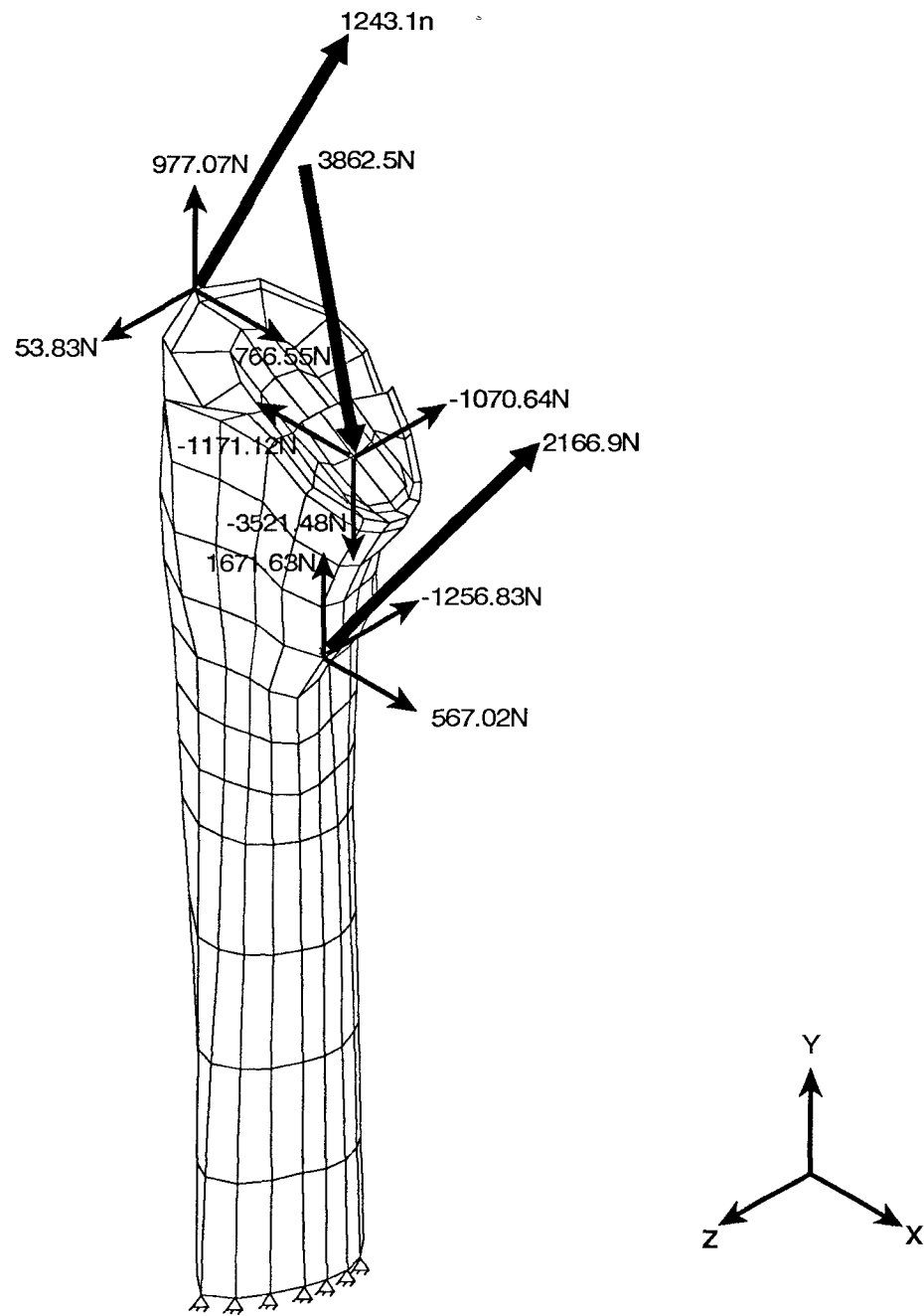


Fig.2.3-3 Loads at 41 percent phase of the walking cycle

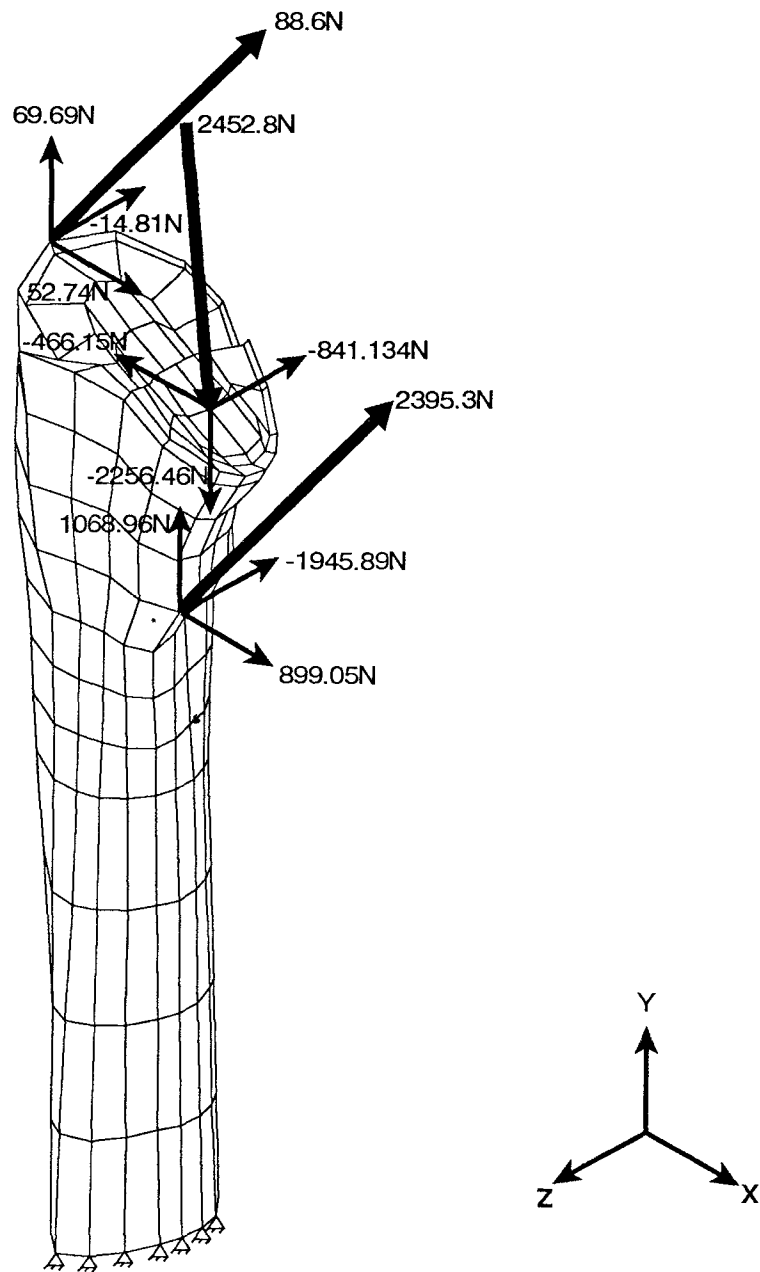


Fig.2.3-4 Loads at 52 percent phase of the walking cycle

CHAPTER THREE

RESULTS

A total of six finite element models of total hip replacement structure using titanium and Co-Cr implants with lateral, proximal and complete coating configurations are analyzed. Results for 4 percent and 41 percent phases of the walking cycle are presented. These two load cases differ substantially from each other in terms of directions and magnitudes of the loading forces. For the 4 percent load case, the dominant positive z components result in a more posterior displacement of the model. The vector magnitudes of the 4 percent load case are lower than the 41 percent load case which displaces the model in a more anterior direction due to the dominant negative z components.

3.1 VON MISES STRESSES ON THE IMPLANTS

Von Mises stress is used to characterize the three dimensional nature of stresses on the implant. It is generally considered as the yield indicator for ductile materials such as those used in the implants.

VON MISES STRESS, MPa
(1MPa = 145 PSI)

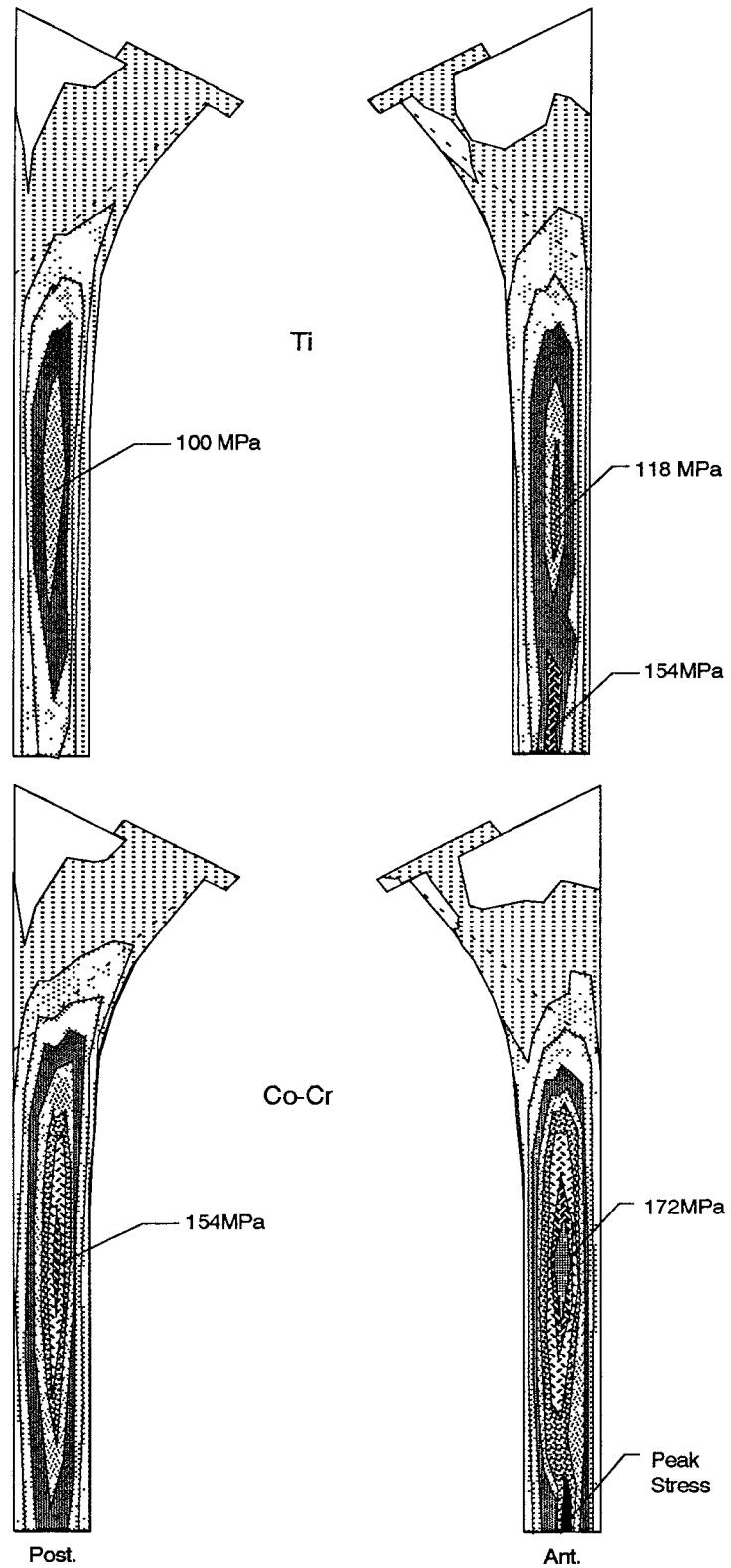
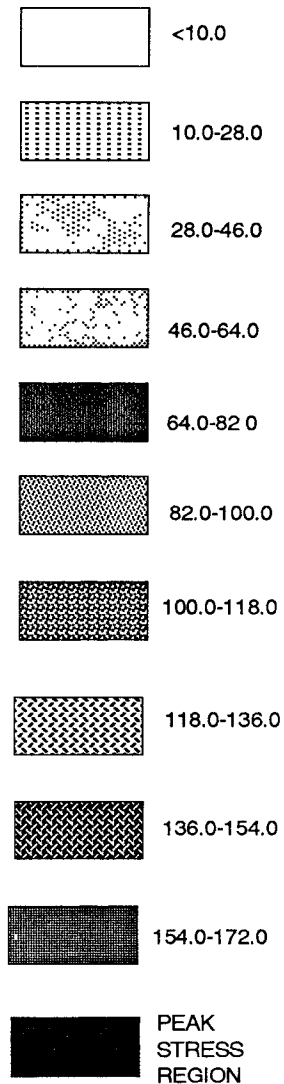


Fig.3.1-1 Von Mises stresses on the surface of laterally coated stems at 4% phase of the walking cycle

VON MISES STRESS, MPa
(1MPa = 145 PSI)

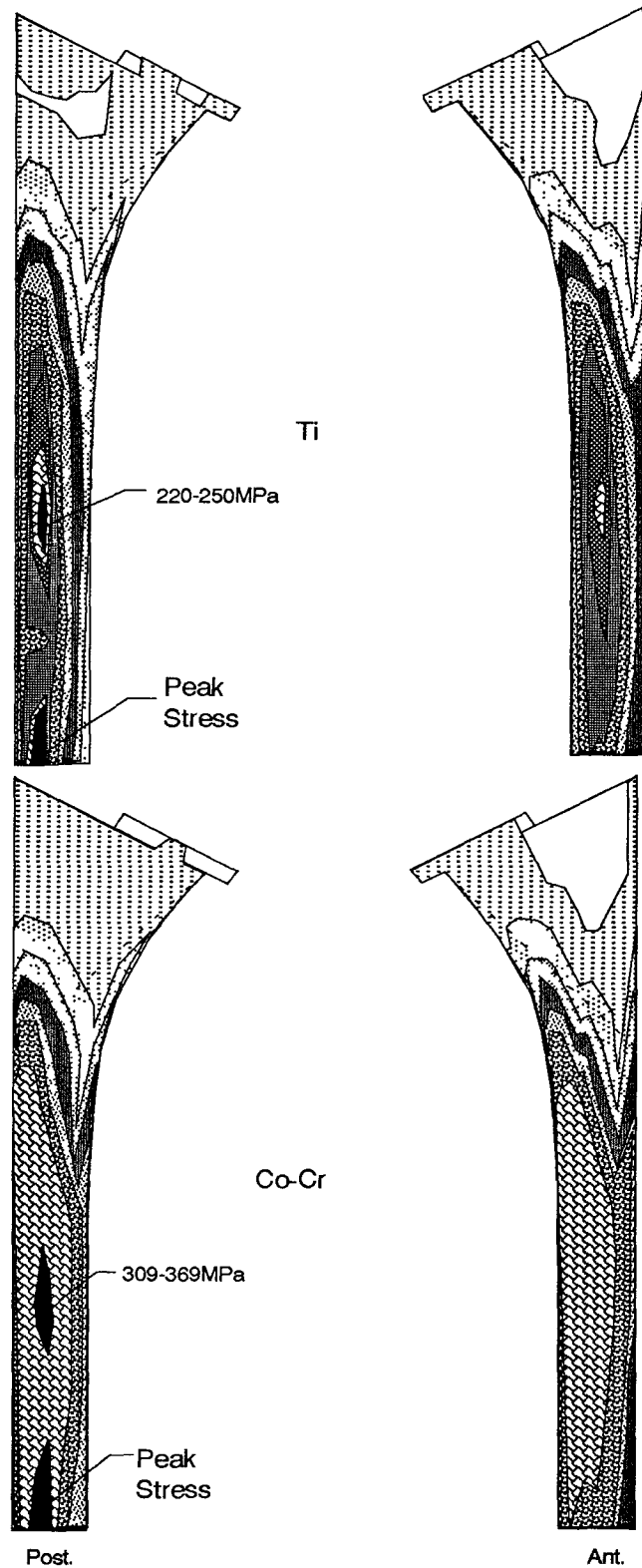
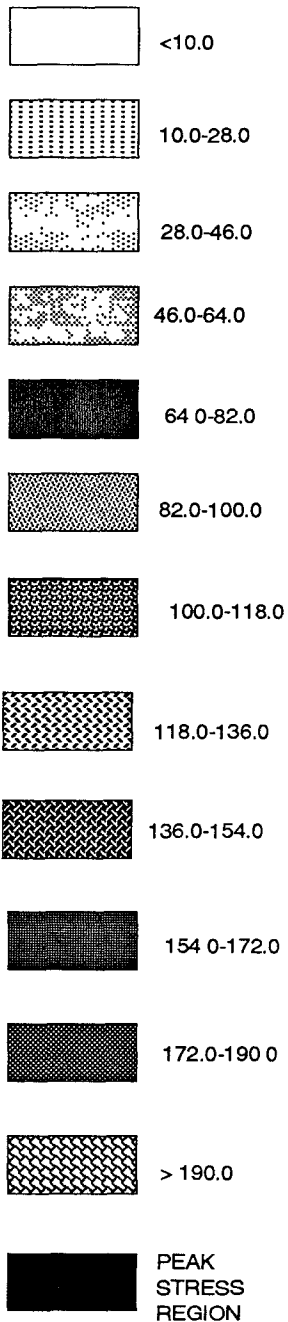
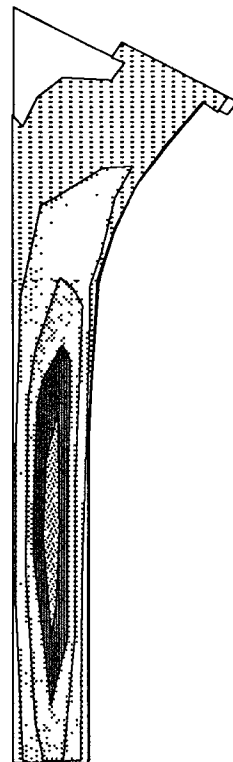
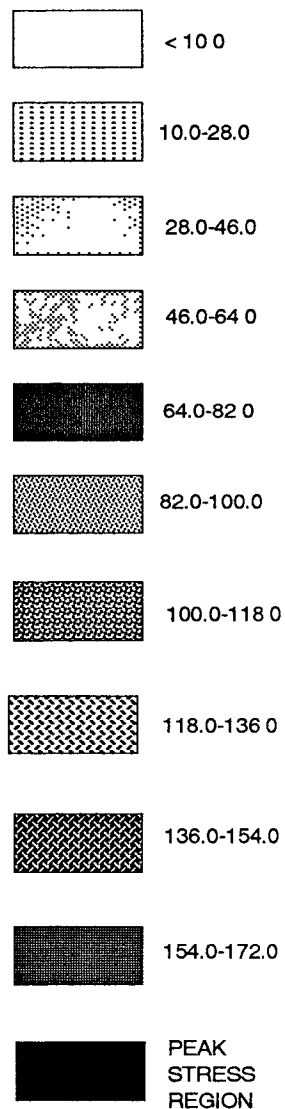
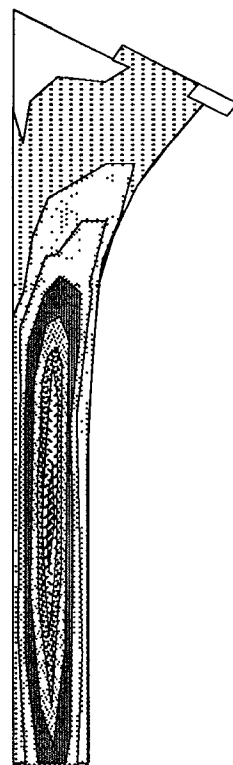
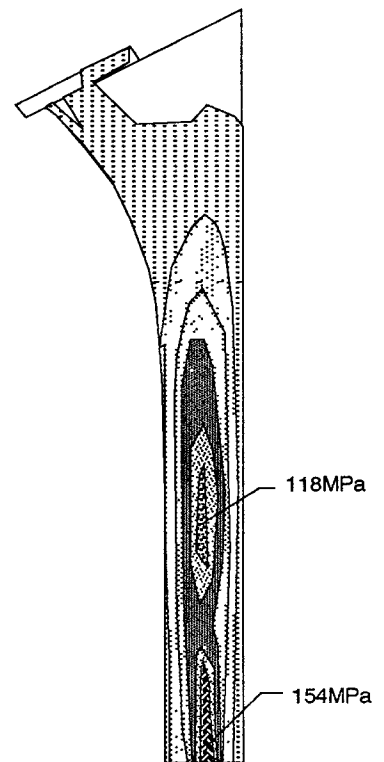


Fig.3.1-2 Von Mises stress on the surface of laterally coated stems at 41% phase of the walking cycle

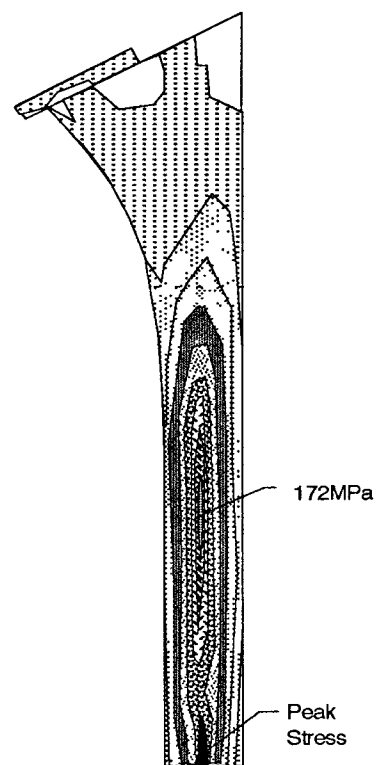
VON MISES STRESS, MPa
(1MPa = 145 PSI)



Ti



Co-Cr



Post.

Ant.

Fig.3.1-3 Von Mises stress on the surface of proximaly coated stems at 4% phase of the walking cycle

VON MISES STRESS, MPa
(1MPa = 145 PSI)

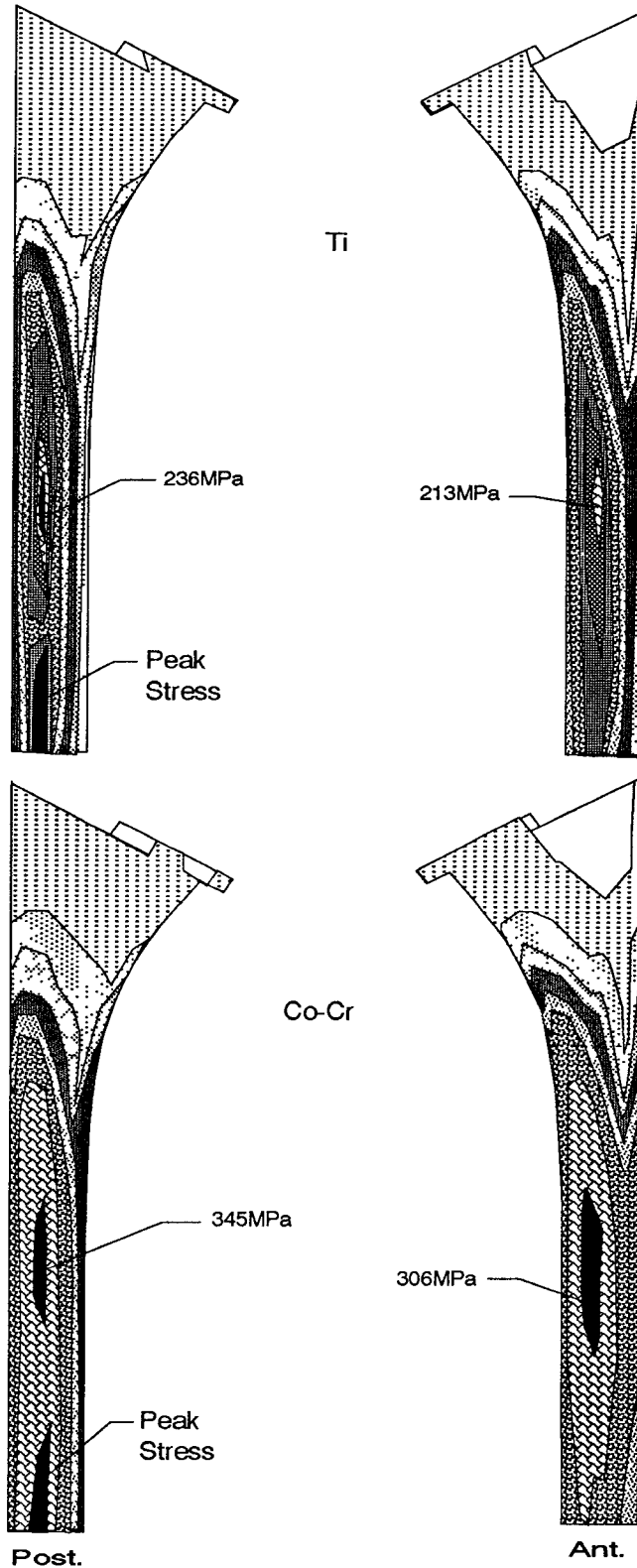
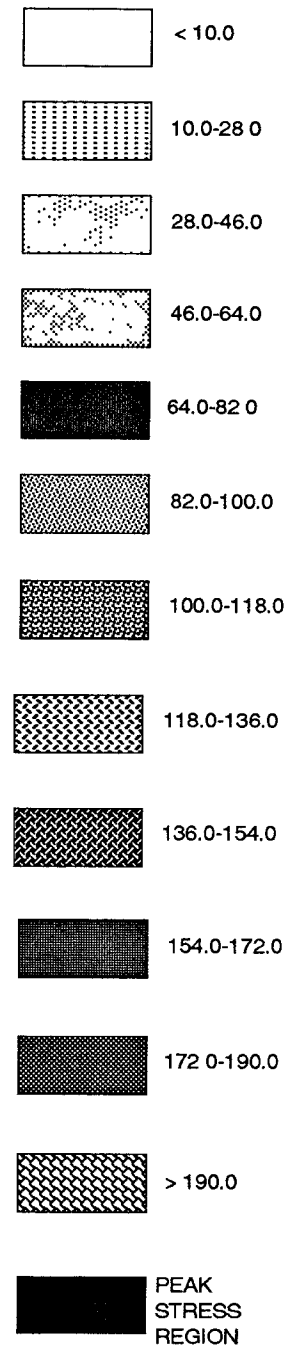


Fig.3.1-4 Von Mises Stress on the surface of proximally coated stems at 41% phase of the walking cycle

VON MISES STRESS, MPa
(1MPa = 145 PSI)

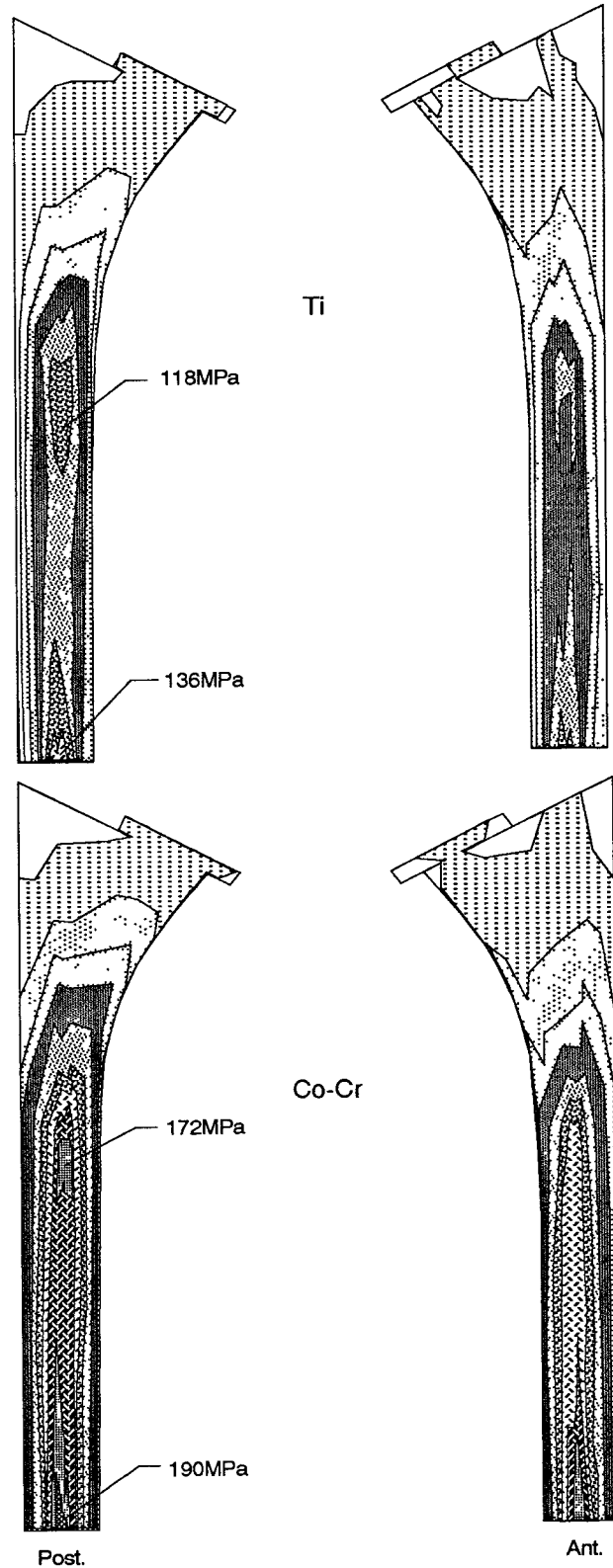
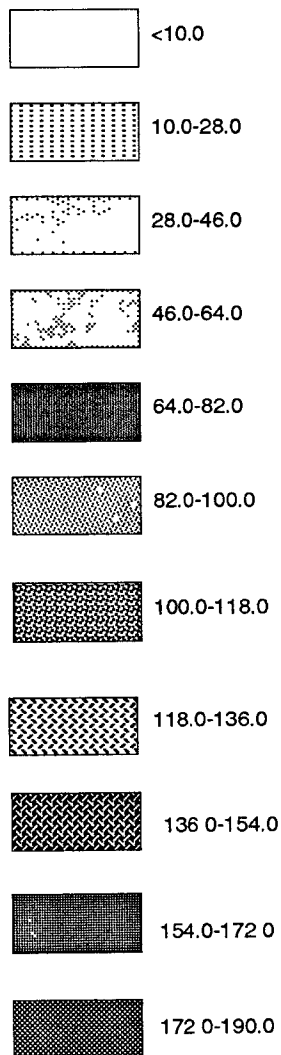


Fig.3.1-5 Von Mises stresses on the surface of fully coated stems at 4% phase of the walking cycle

VON MISES STRESS, MPa
(1MPa = 145 PSI)

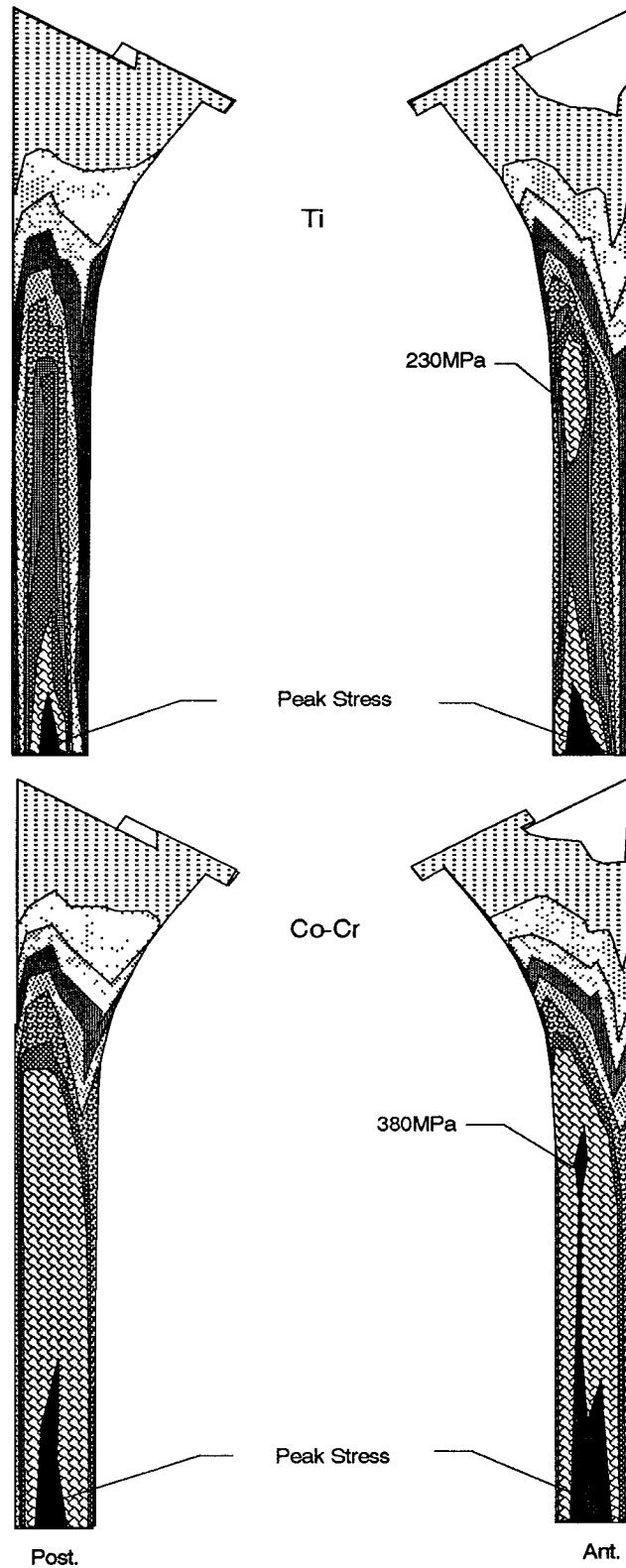
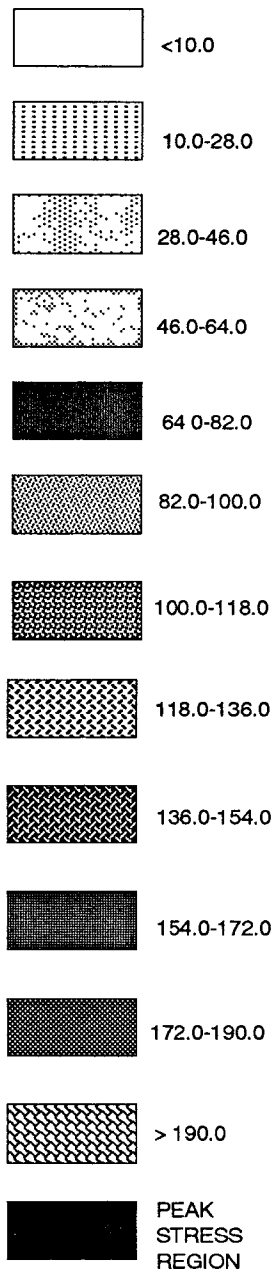


Fig.3.1-6 Von Mises stresses on the surface of fully coated stems at 41% phase of the walking cycle

The von Mises stresses on the stem surface for the 4% and 41% load cases are illustrated in fig. 3.1-1 thru 3.1-6. The variations in stress magnitude are mainly contributed by the varying material stiffness and the amount of porous coating.

3.1.1 EFFECT OF DIFFERENT MATERIALS

The average stresses on the surface of the Co-Cr implants range from 25 to 29 percent higher than the titanium implants. This is primarily due to Co-Cr having modulus of elasticity roughly twice that of titanium. When the stiff Co-Cr implant is surrounded by spongy bone tissue, it preferentially takes more of the shared load.

The fatigue strength values for titanium in coated and uncoated forms are 25ksi(172MPa) and 60ksi(414MPa) respectively. For Co-Cr, these values are 25ksi(172MPa) and 40ksi(276MPa) respectively. With the common factor of safety of 2 applied to the fatigue limits, failure by fatigue loading occurs whenever the titanium stem reaches the stress values of 81MPa and 207MPa and the Co-Cr stem reaches the stress values of 81MPa and 138MPa in coated and uncoated forms respectively. The maximum stresses on the Co-Cr implants at the 41 percent phase exceeds its fatigue strength in all coating configurations. These excessive stresses would result in eventual implant failure under fatigue loadings. The titanium implants fall in the same category despite that the peak stresses are not in much excess of the fatigue strength except for the complete coating geometry.

3.1.2 EFFECT OF POROUS COATING CONFIGURATIONS

Maximum stresses are found at the tip of the stems in all coating configurations. This unrealistic occurrence is caused by modelling and is not considered further.

The common behavior pattern of the partly coated stems is that levels of stress intensity are approximately ten times lower in the coated proximal region than in the uncoated distal region. The highest stresses is located about lower two-third down the length of the stem. For the 4 percent and 41 percent load cases, the highest stresses exist on the anterior side and posterior side of the stem respectively. Maximum stresses for the partly coated stems are generated on the tensile side of the stem. Overall, the partly coated stems share similar stress patterns although peak values are somewhat higher in the laterally coated stem than in the proximally coated stem.

For the fully coated stems, the maximum stresses is near middle of the stem. Unlike the partly coated stems, the peak stress is on the compressive side of the stem and the stress distribution is more uniform on the stem surface.

INTERFACE
COMPRESSIVE
STRESSES, -MPa
(1MPa = 145PSI)

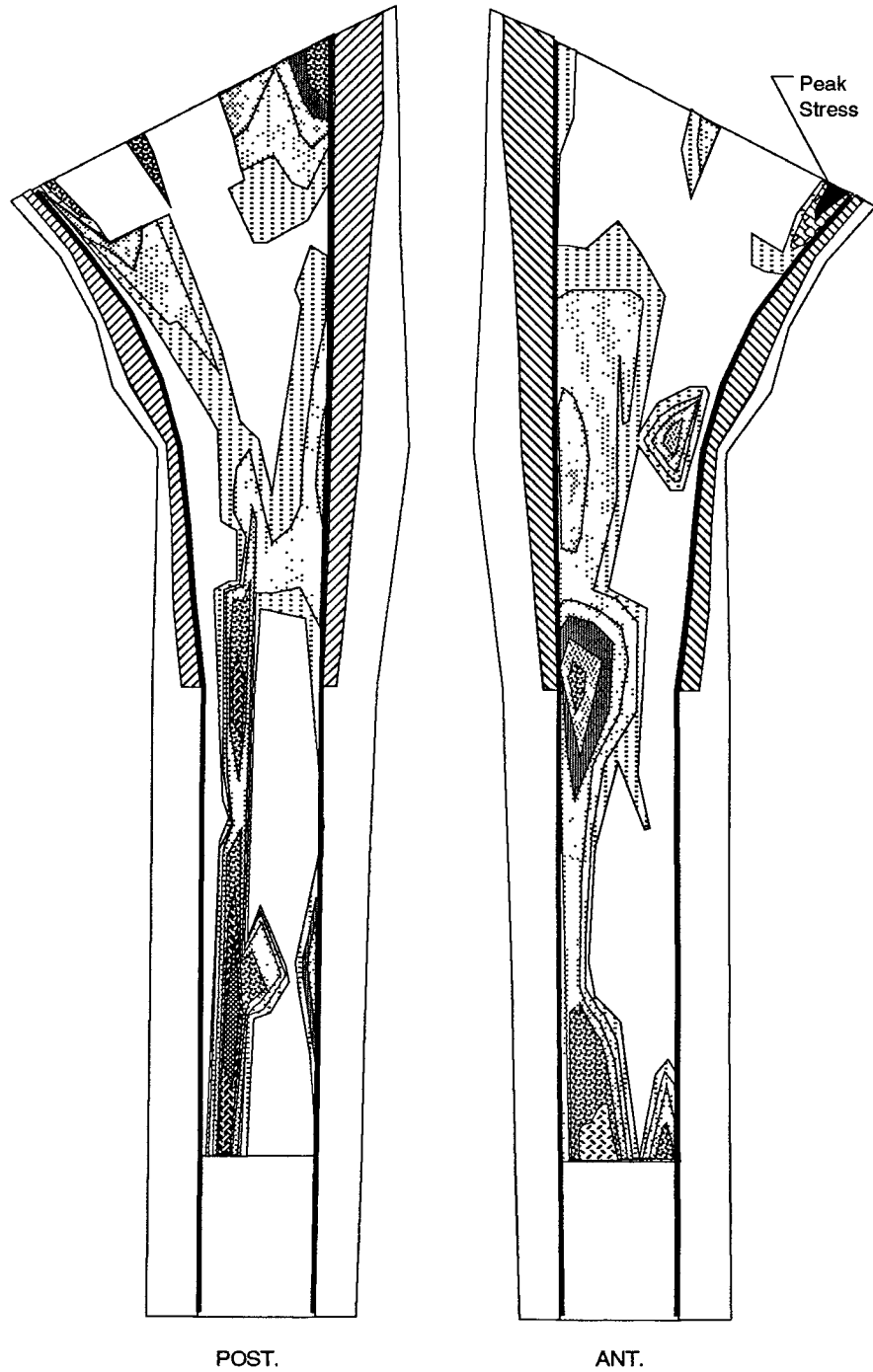
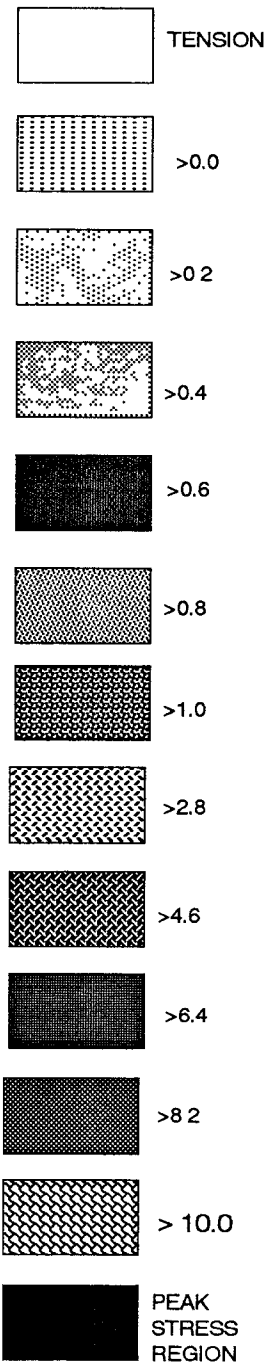


Fig.3.2-1 Interface compressive stresses on THR using fully coated Co-Cr stem at 4% phase of the walking cycle

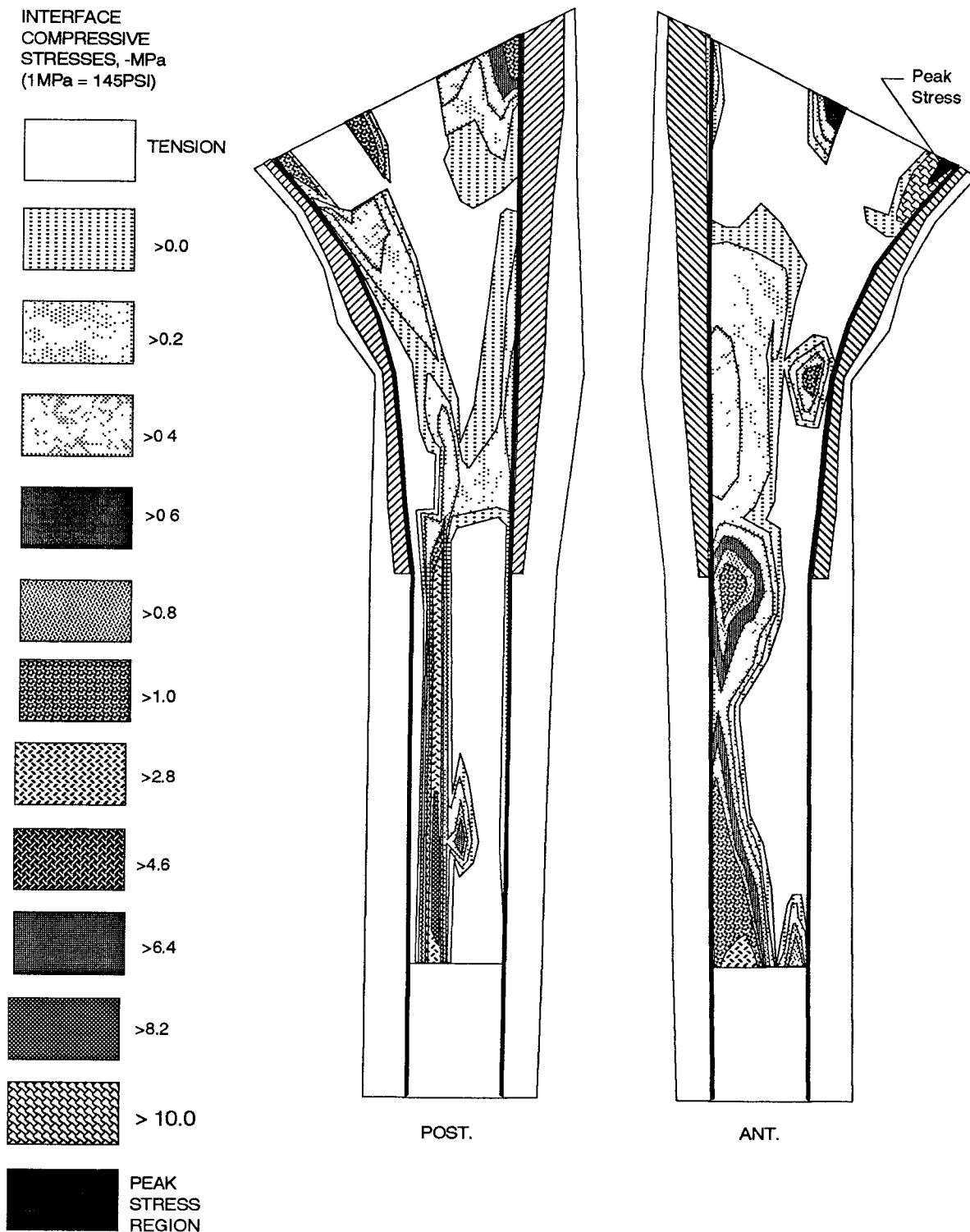


Fig.3.2-2 Interface compressive stresses on THR using fully coated Ti stem at 4% phase of the walking cycle

INTERFACE
COMPRESSIVE
STRESSES, -MPa
(1MPa = 145PSI)

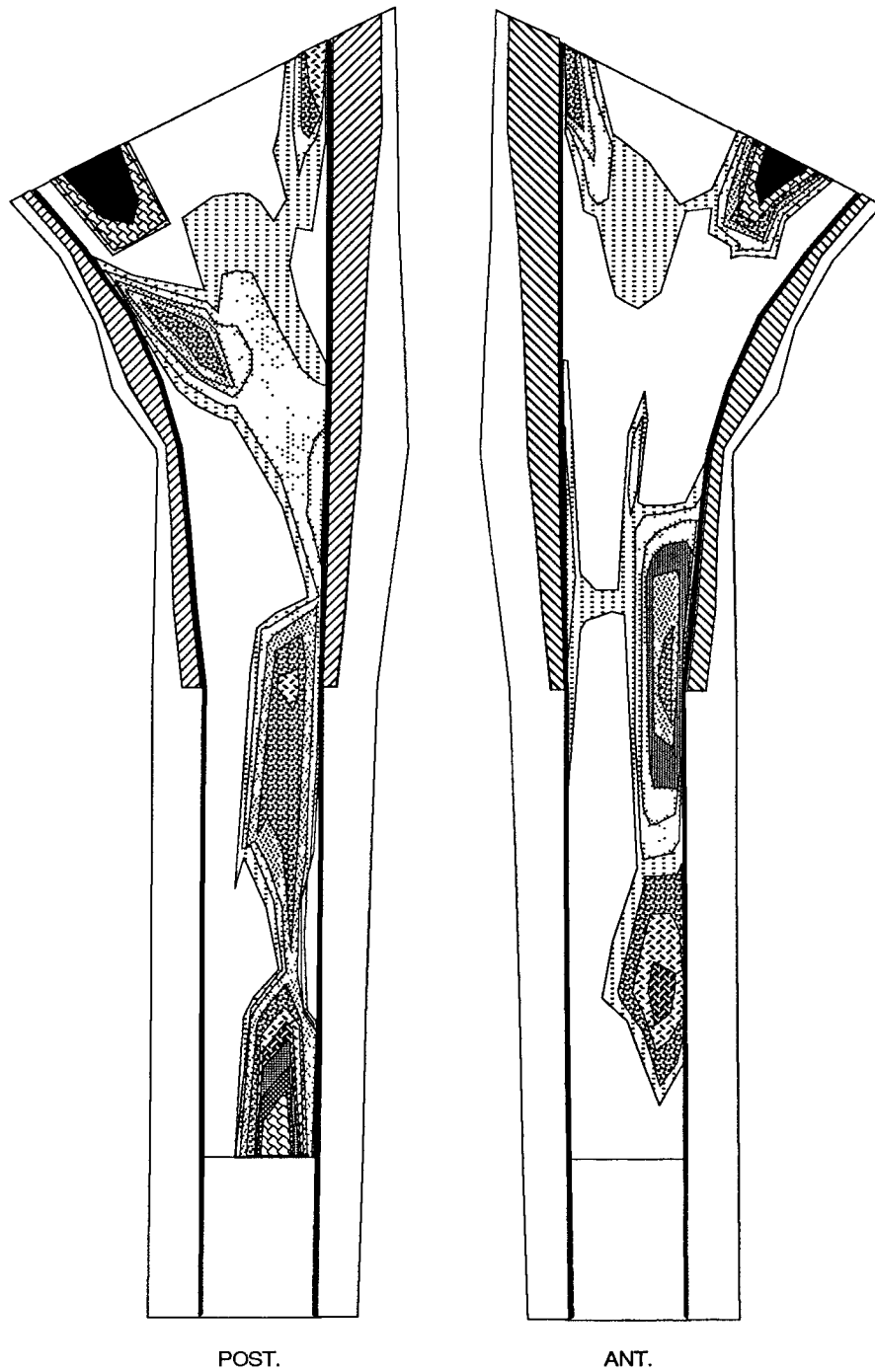
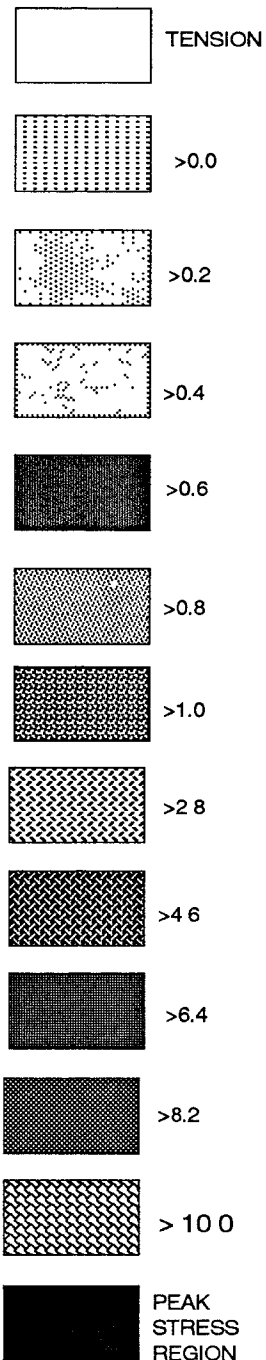


Fig.3.2-3 Interface compressive stresses on THR using fully coated Co-Cr stem at 41% phase of the walking cycle

INTERFACE
COMPRESSIVE
STRESSES, -MPa
(1MPa = 145PSI)

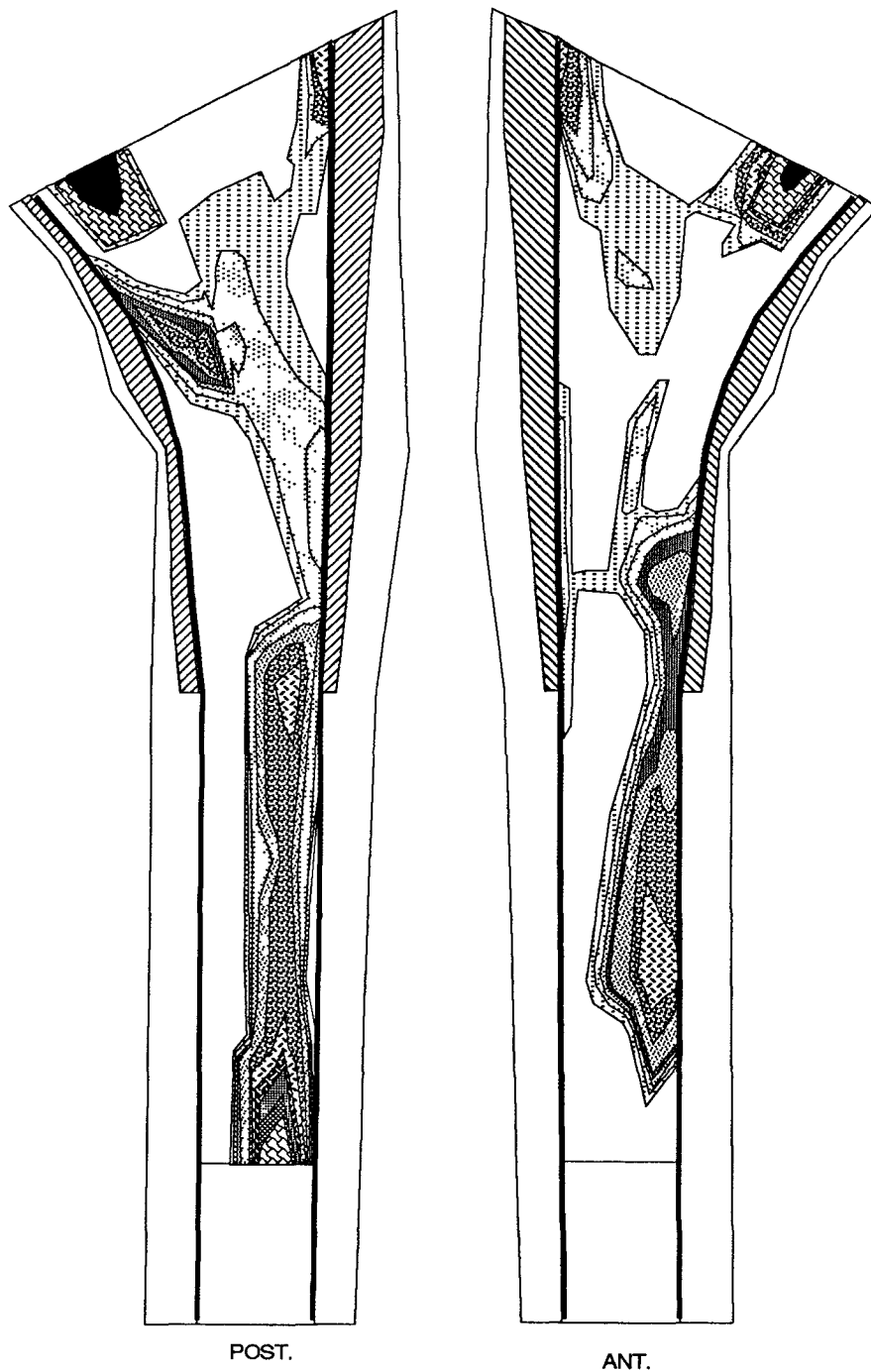
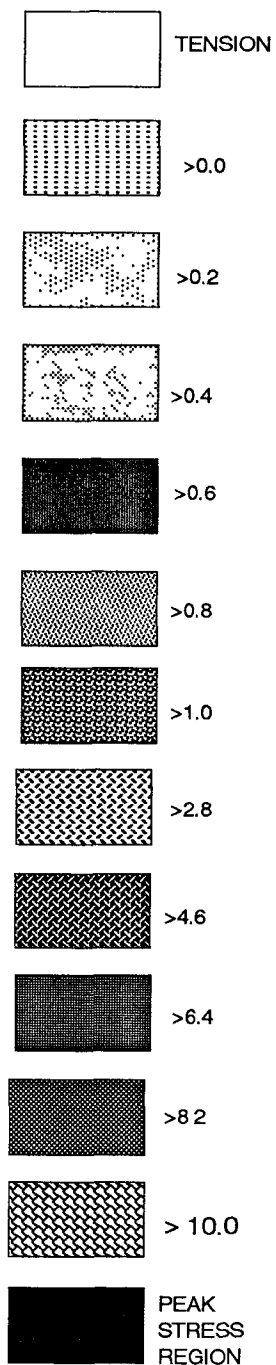


Fig.3.2-4 Interface compressive stresses on THR using fully coated Ti stem at 41% phase of the walking cycle

INTERFACE
COMPRESSIVE
STRESSES, -MPa
(1MPa = 145PSI)

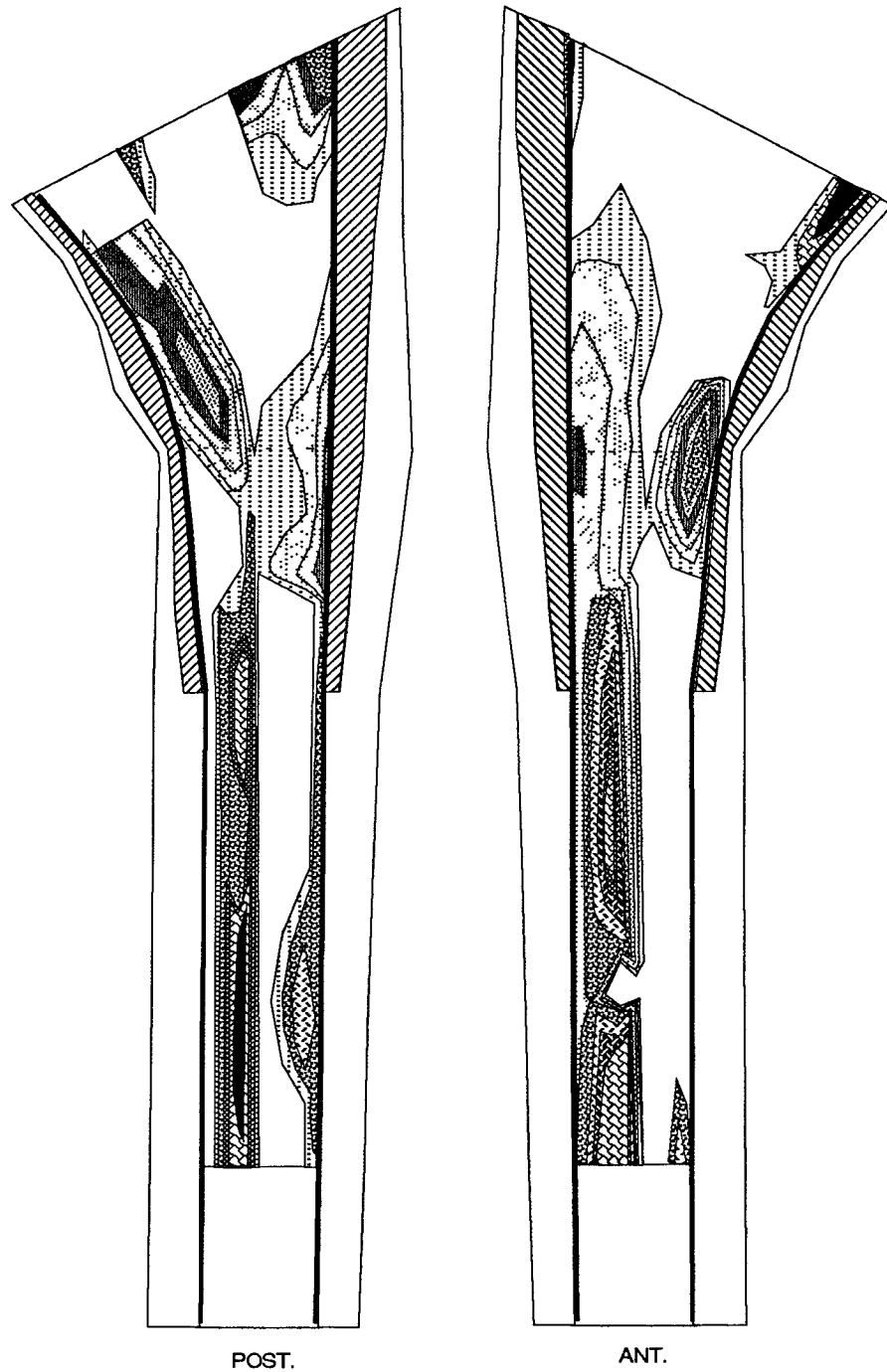
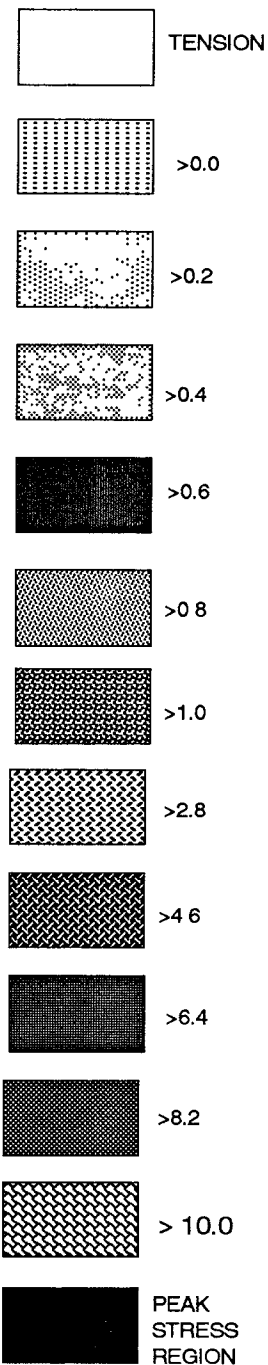


Fig.3.2-5 Interface compression on THR using proximally coated Co-Cr stem at 4% phase of the walking cycle

INTERFACE
COMPRESSIVE
STRESSES, -MPa
(1MPa = 145PSI)

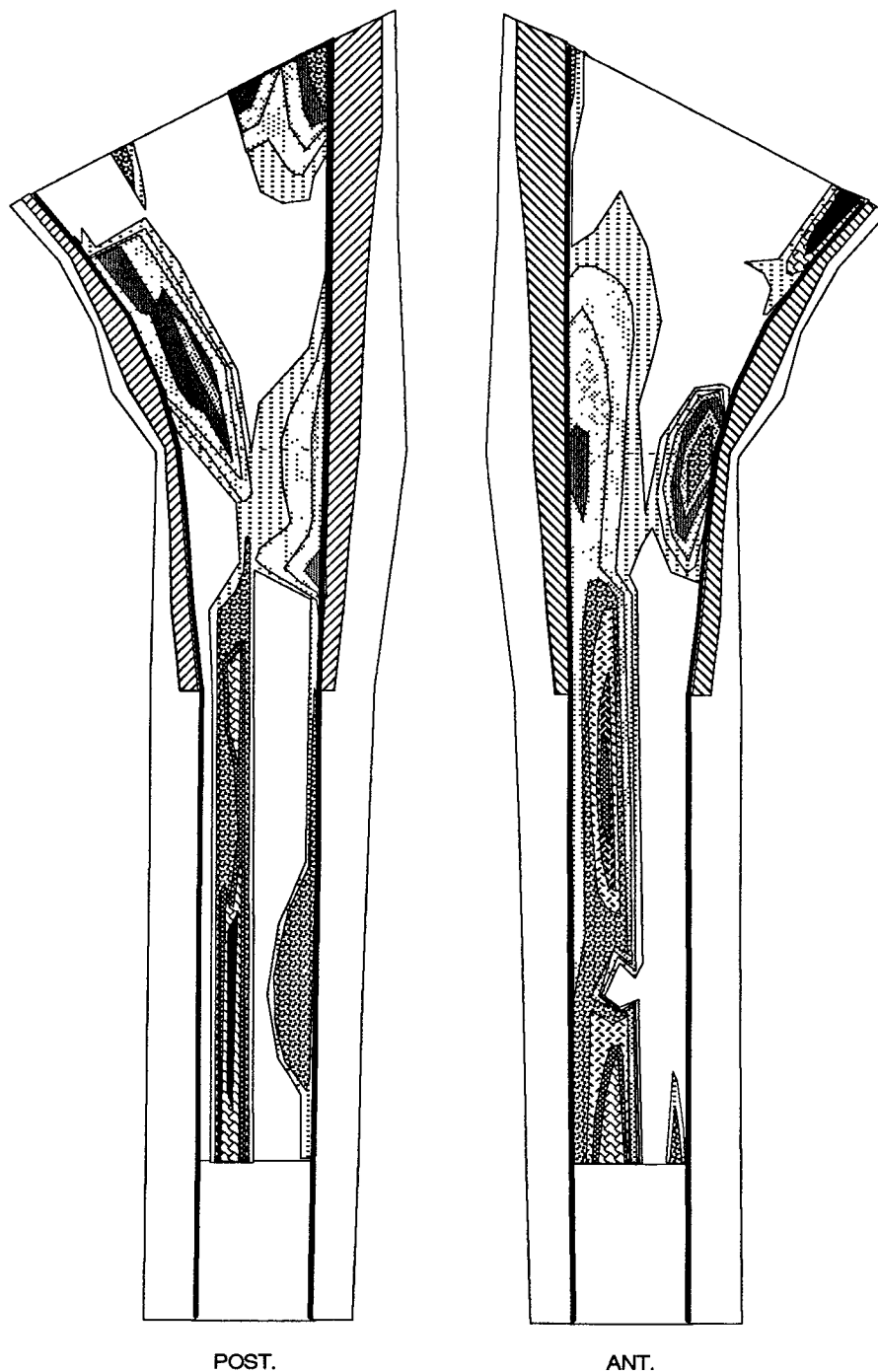
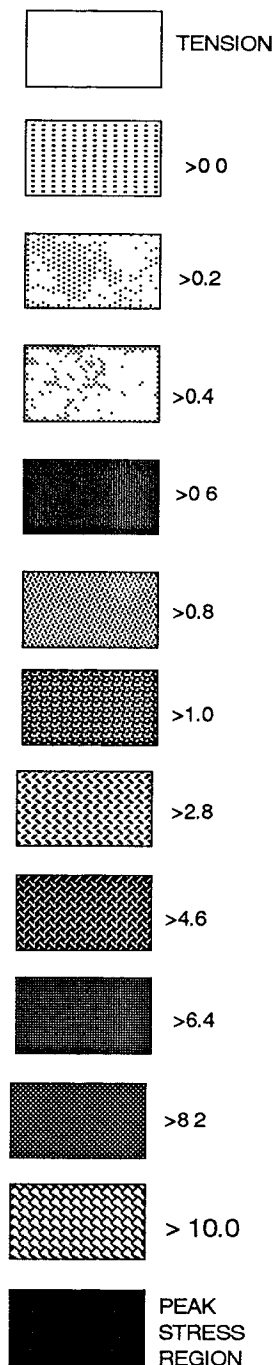


Fig.3.2-6 Interface compression on THR using proximally coated Ti stem at 4% phase of the walking cycle

INTERFACE
COMPRESSIVE
STRESSES, -MPa
(1MPa = 145PSI)

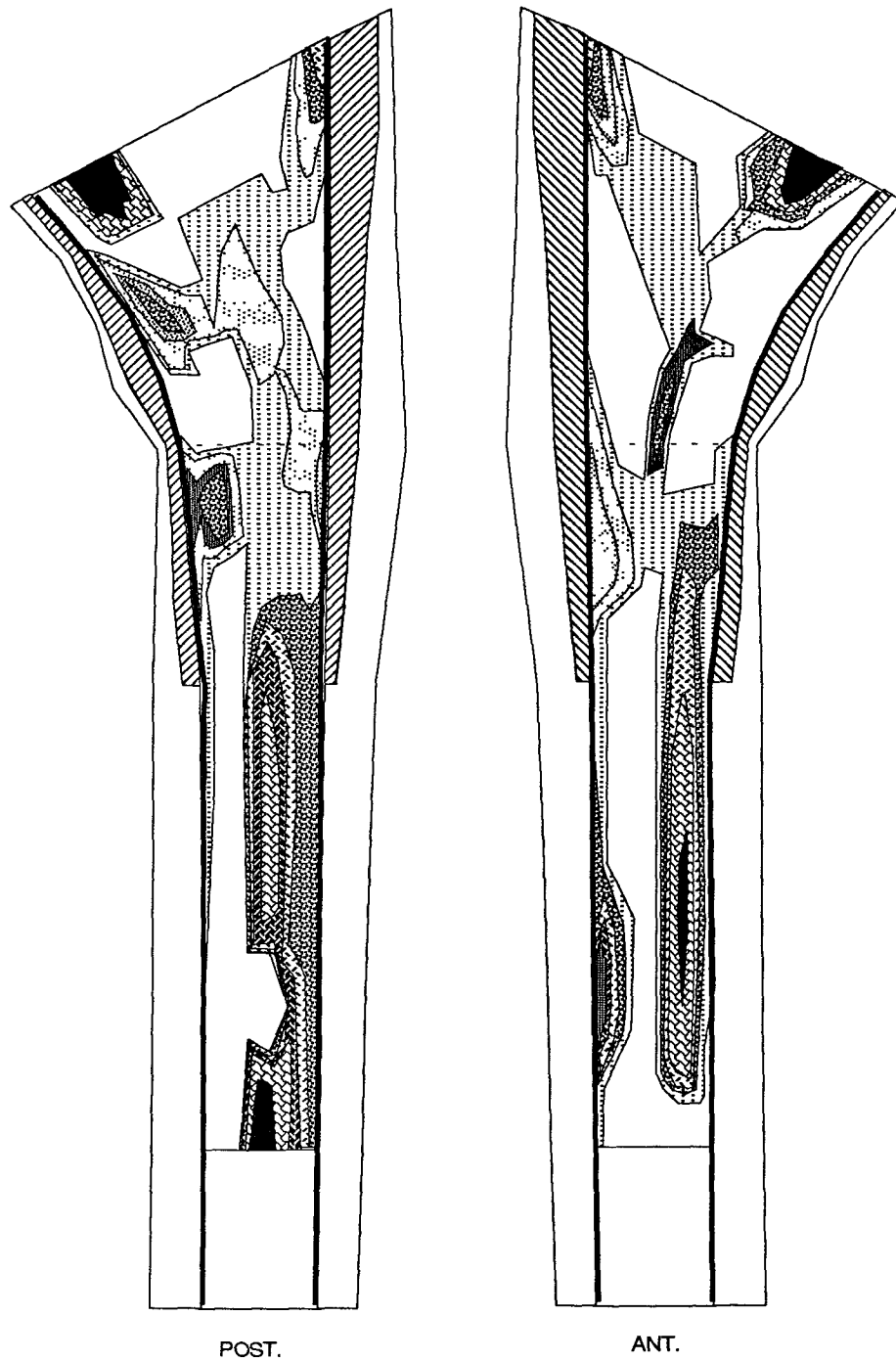
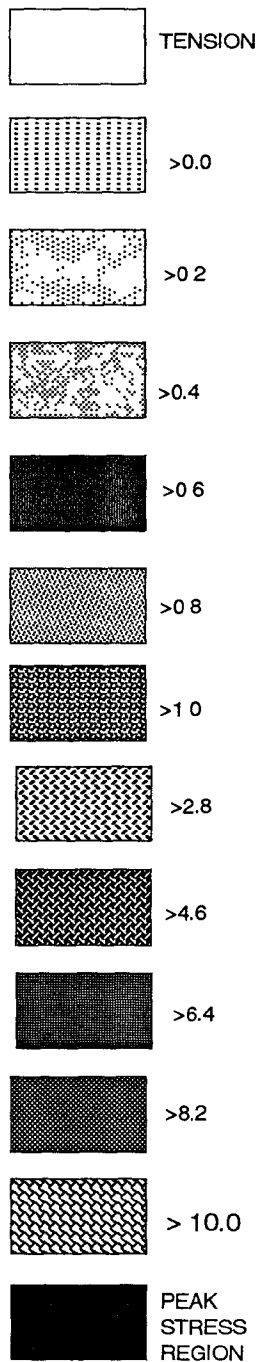


Fig.3.2-7 Interface compression on THR using proximaly coated Co-Cr stem at 41% phase of the walking cycle

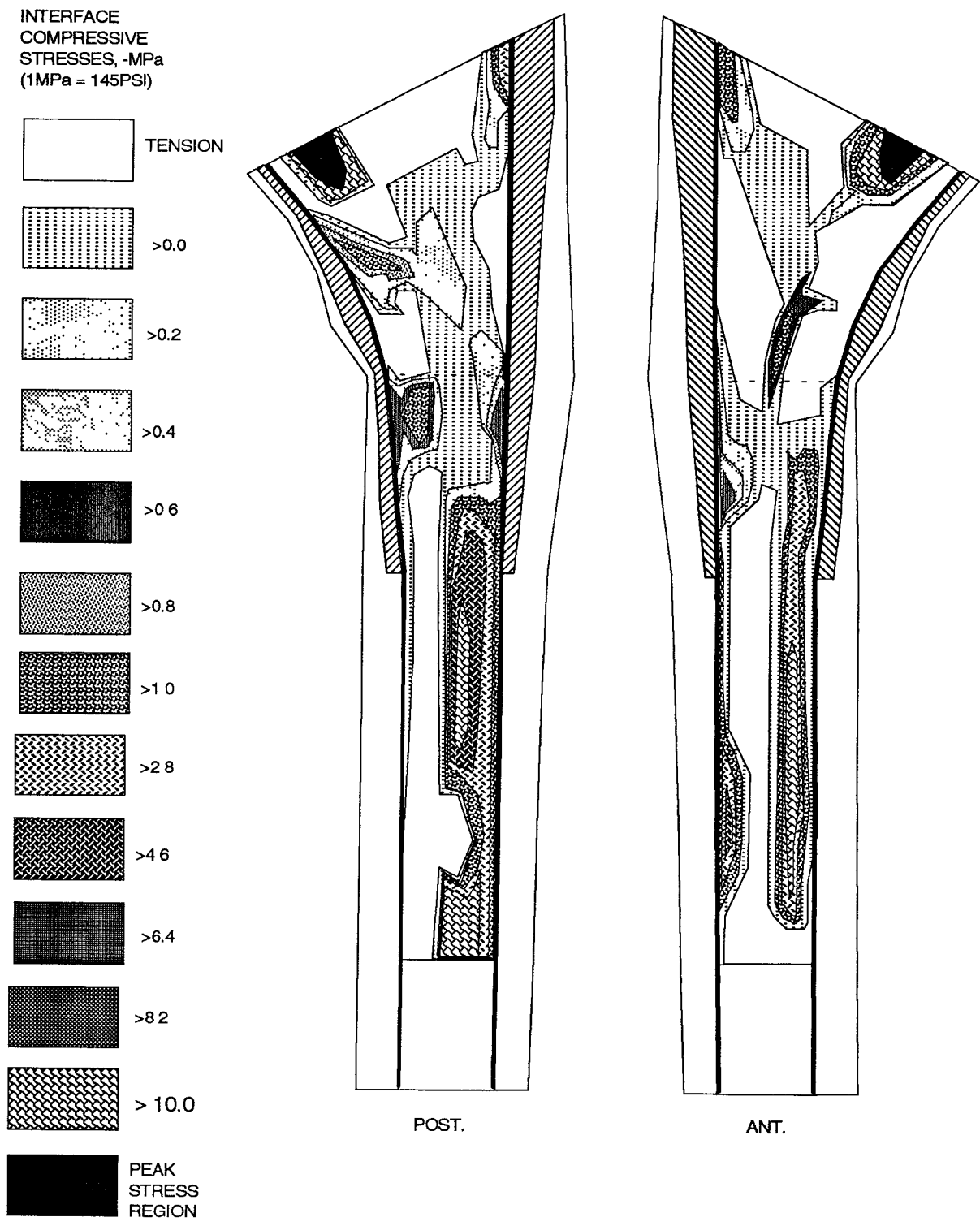


Fig.3.2-8 Interface compression on THR using proximally coated Ti stem at 41% phase of the walking cycle

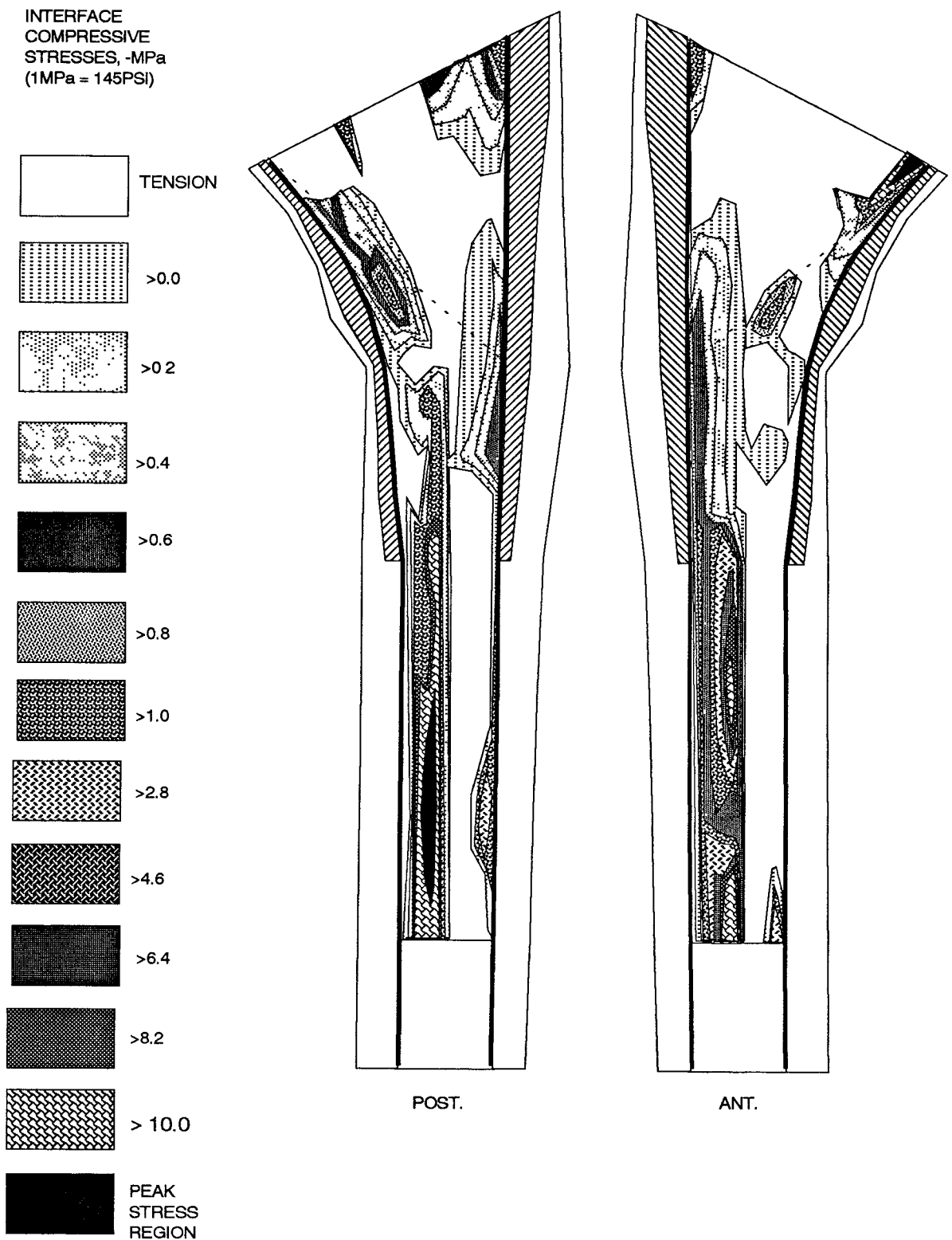


Fig.3.2-9 Interface compressive stresses on THR using laterally coated Co-Cr stem at 4% phase of the walking cycle

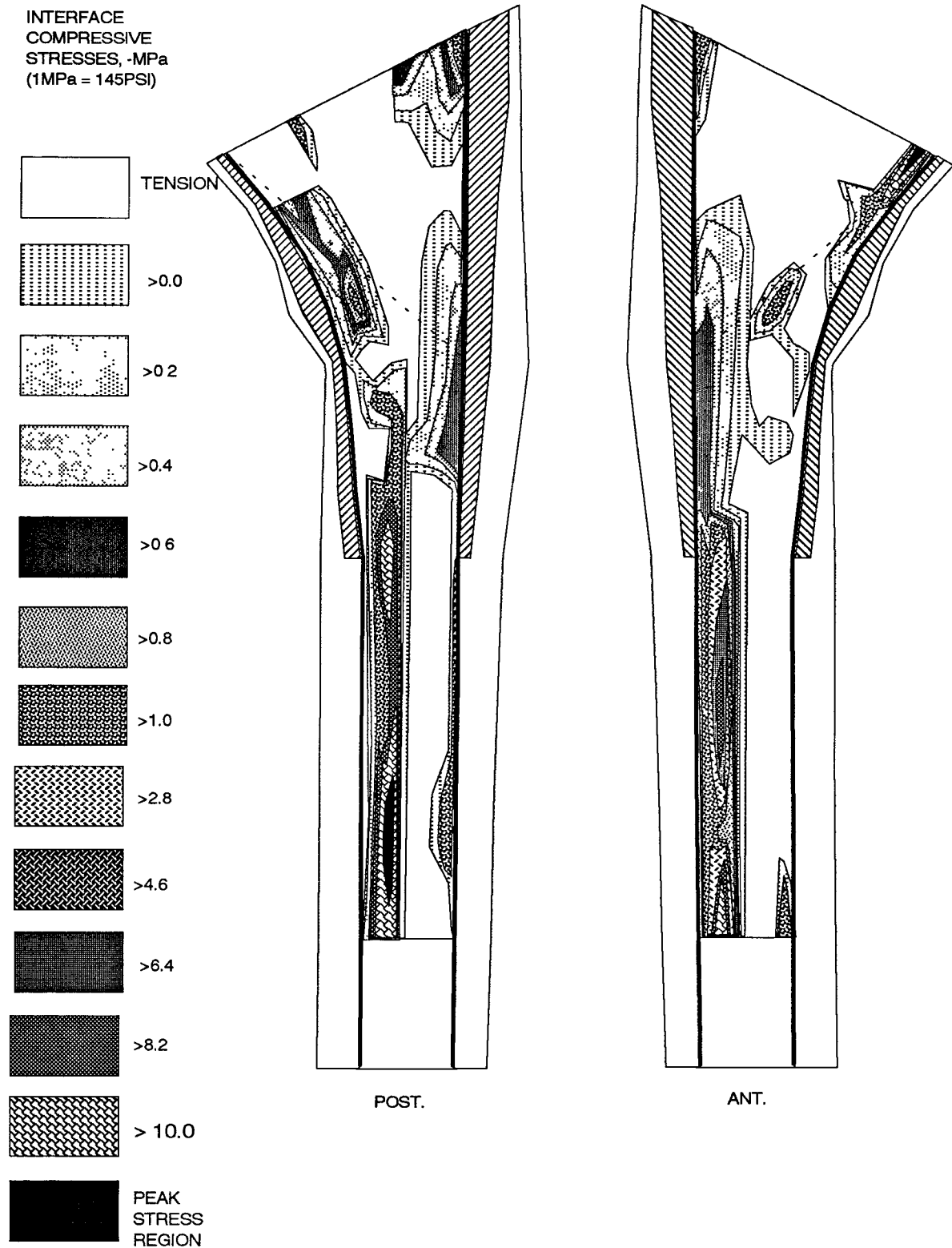


Fig.3.2-10 Interface compressive stresses on THR using laterally coated Ti stem at 4% phase of the walking cycle

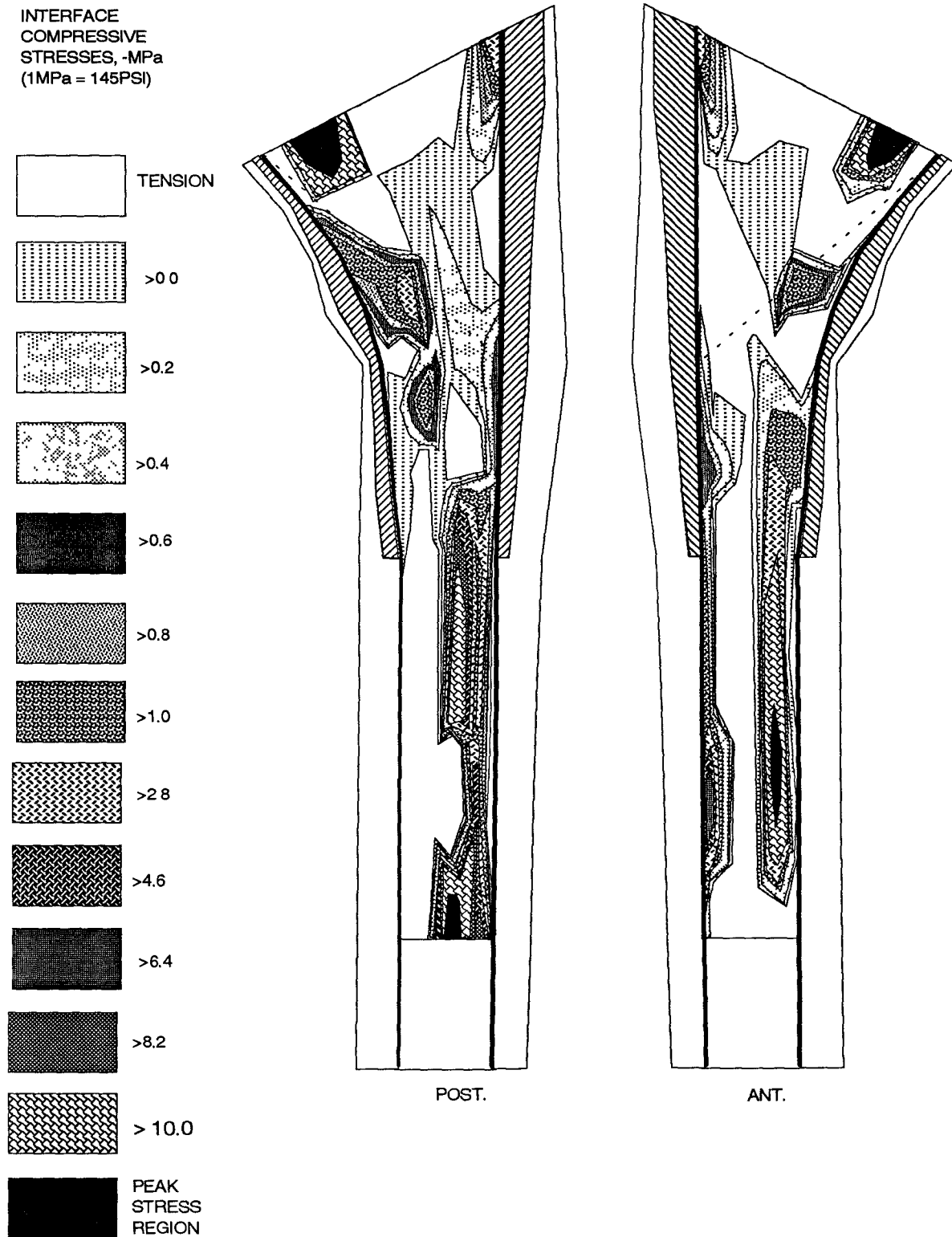


Fig.3.2-11 Interface compressive stress on THR using laterally coated CoCr stem at 41% phase of the walking cycle

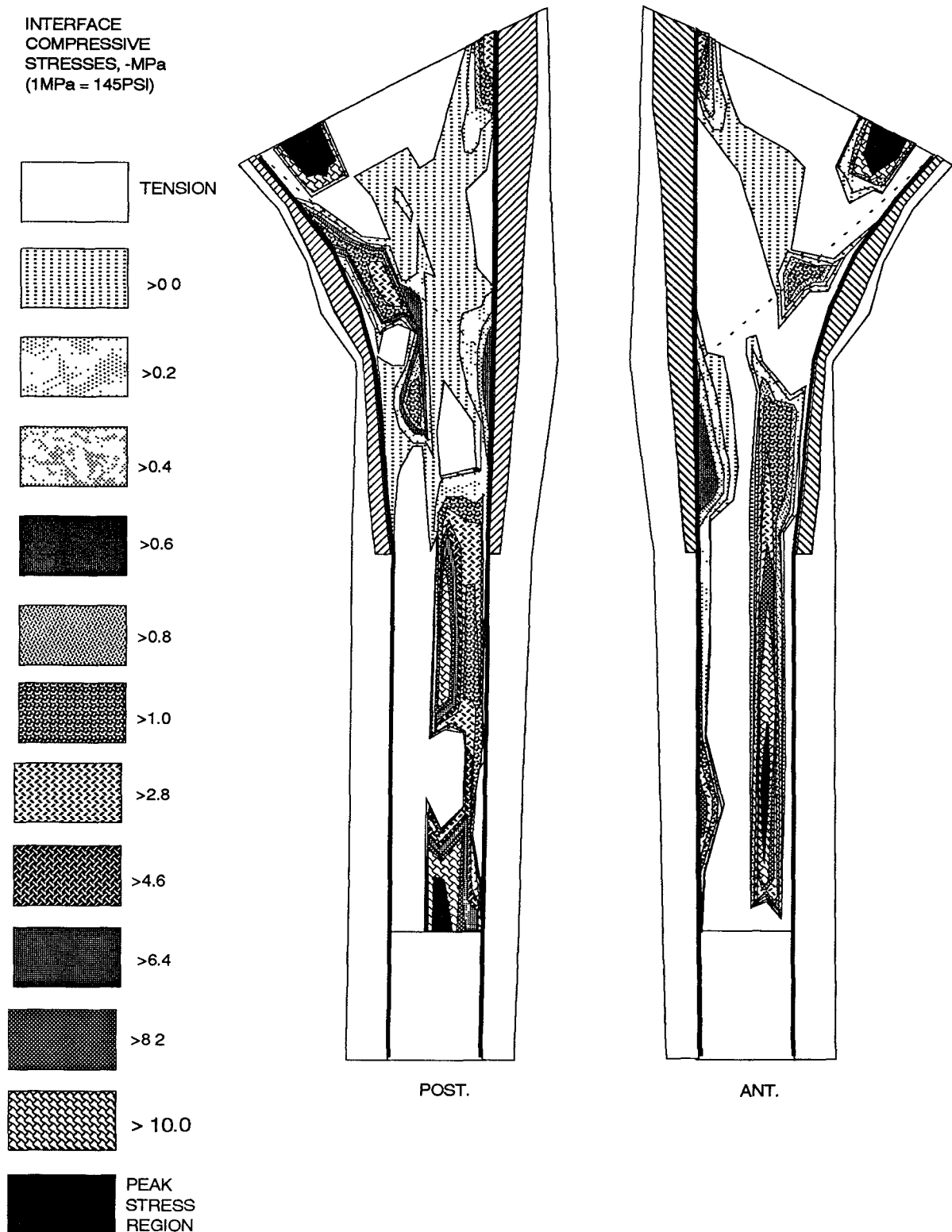


Fig.3.2-12 Interface compressive stress on THR using laterally coated Ti stem at 41% phase of the walking cycle

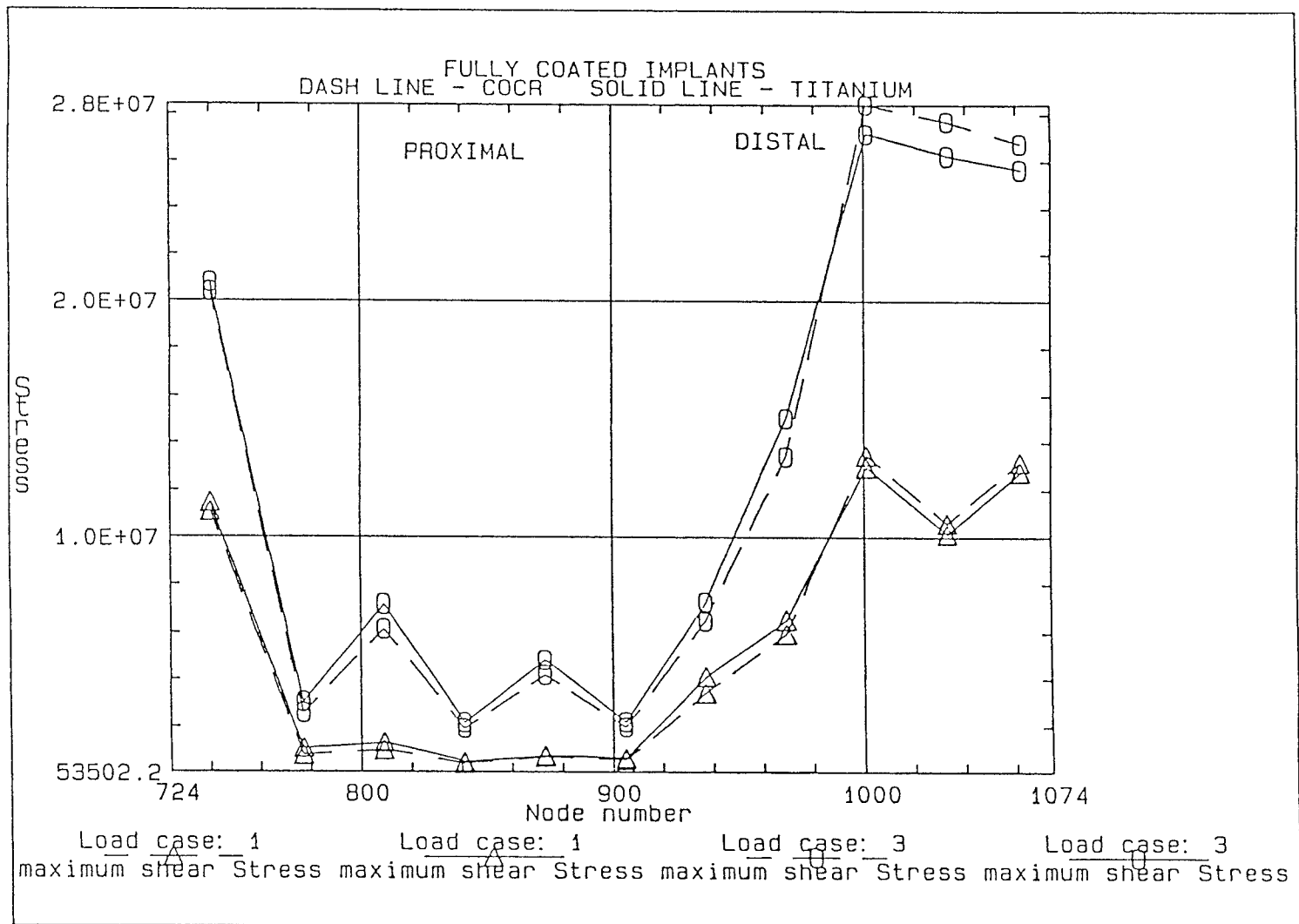


Fig. 3.3-7 Maximum shear stress for fully coated Ti and Co-Cr stems at bone interface

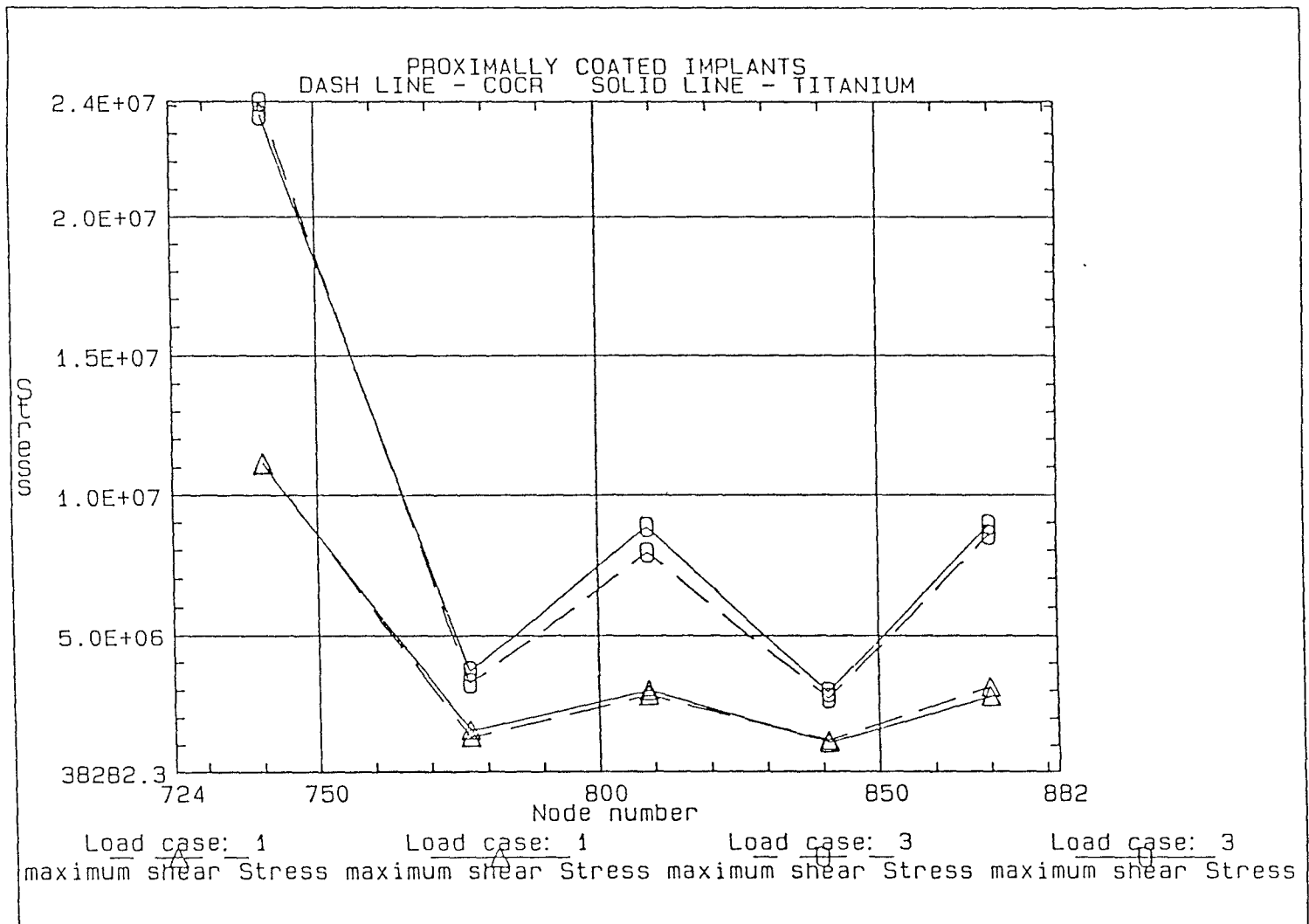


Fig. 3.3-8 Maximum shear stress for proximally coated Ti and Co-Cr stems at bone interface

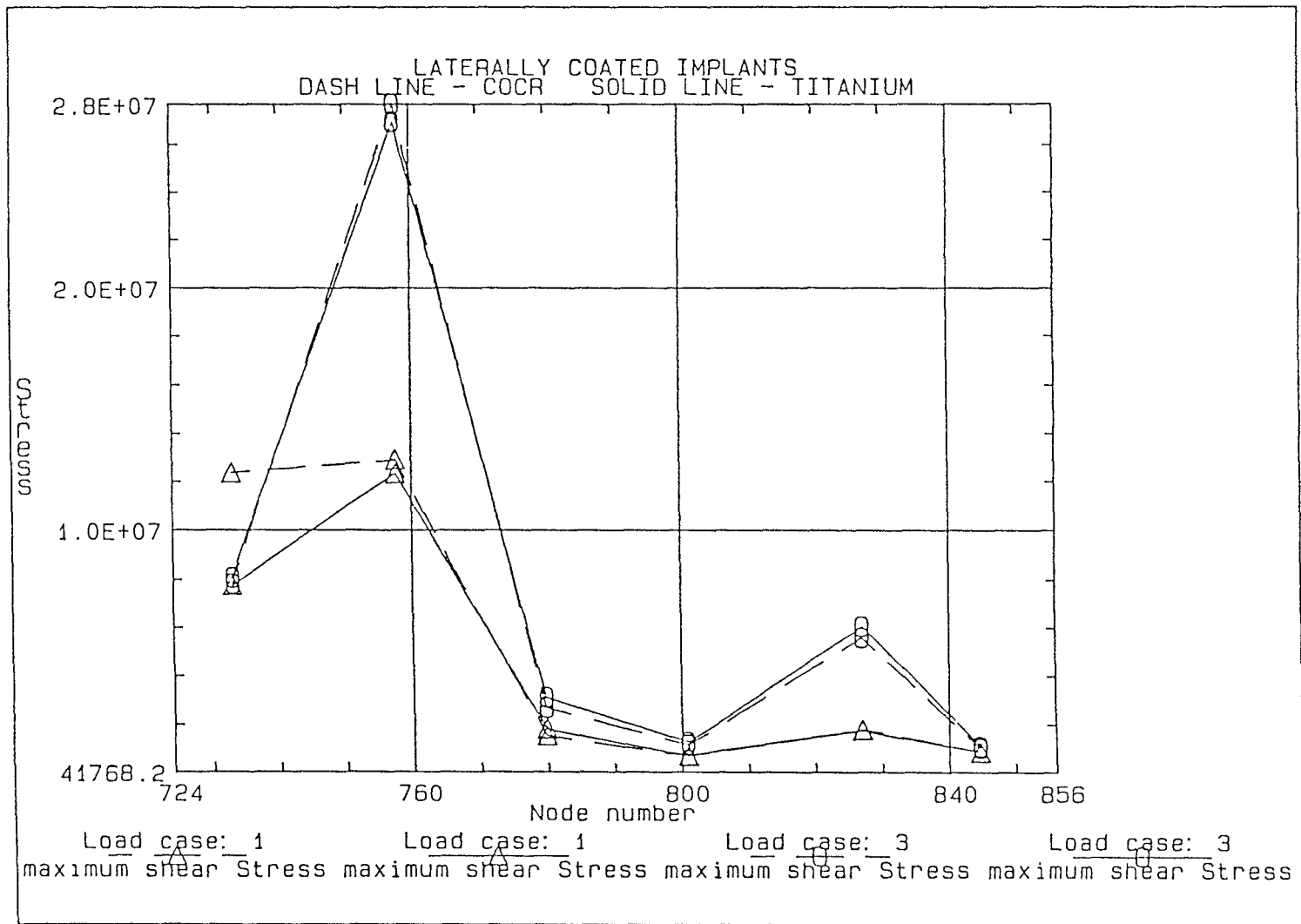


Fig. 3.3-9 Maximum shear stress for laterally coated Ti and Co-Cr stems at bone interface

3.2 COMPRESSIVE STRESSES AT BONE INTERFACE

Contour plots of compressive stresses at bone interface are shown in fig. 3.2-1 thru 3.2-12. Tension at the interface is represented by white areas on the figures. The interface compression is achieved mainly by stem-bone contact pressure resulting from the axial bending load contributed by the negative Y component of the hip joint vector. Compression at bone interface is believed to facilitate bone fixation and promote bony ingrowth. On the contrary, tension at bone interface will cause implant loosening and bone resorption.

For the 4 percent load case, compression occurs primarily on anterior-lateral and posterior-medial sides of the interface. Local stress concentration found at anterior proximal interface is caused by the negative z component of the adduction vector inserted in that region.

The stress pattern is reversed for the 41 percent load case where compression is seen on anterior-medial and posterior-lateral sides of the interface. The opposite pattern is primarily due to the opposite direction of the hip joint reaction force which is an anterior component for the 41 percent load case and a posterior component for the 4 percent load case.

Medial compression in the proximal interface is caused by the axial loading distributed by the collar while lateral compression in the proximal interface results from the effects of the positive x abductor force and the negative x hip joint force. The peak stress at the periphery of the interface is a modelling artifact and does not contribute to any clinical implications.

3.2.1 EFFECT OF DIFFERENT MATERIALS

The stress contour plots in fig.3.2-1 thru 3.2-12 reveal that titanium stems result in a more gradual stress transfer at the interface, which is contrary to the more localized stress concentrations associated with the Co-Cr stems. The difference may be accounted for the smooth bending applied by the more flexible titanium stem to the surrounding interface.

For the stiffer Co-Cr stems, they appear to induce higher stress concentration at the distal interface. Figures 3.2-13 thru 3.2-15 illustrate that the distal interface nodes represented by the last three symbols have higher calculated normal stresses for the Co-Cr stems than the titanium stems.

3.2.2 EFFECTS OF POROUS COATING CONFIGURATIONS

Stems with complete coating result in slight bone-implant contact, reflected by low levels of compressive stresses at the interface. The tension and compression at the interface are approximately in equal proportion. Local stress concentration is observed at the distal interface and its presence may lead to bone hypertrophy which may cause eventual implant failure.

The bone interface with partial coating exhibits significantly higher compressive stresses and the stress distribution shows a great deal of smoothness. Compared to the fully coated interface, partly coated interface induces more compression notably near the junction of coating and loose interface. Stresses are quantitatively higher on the bone interface with lateral coating than with proximal coating.

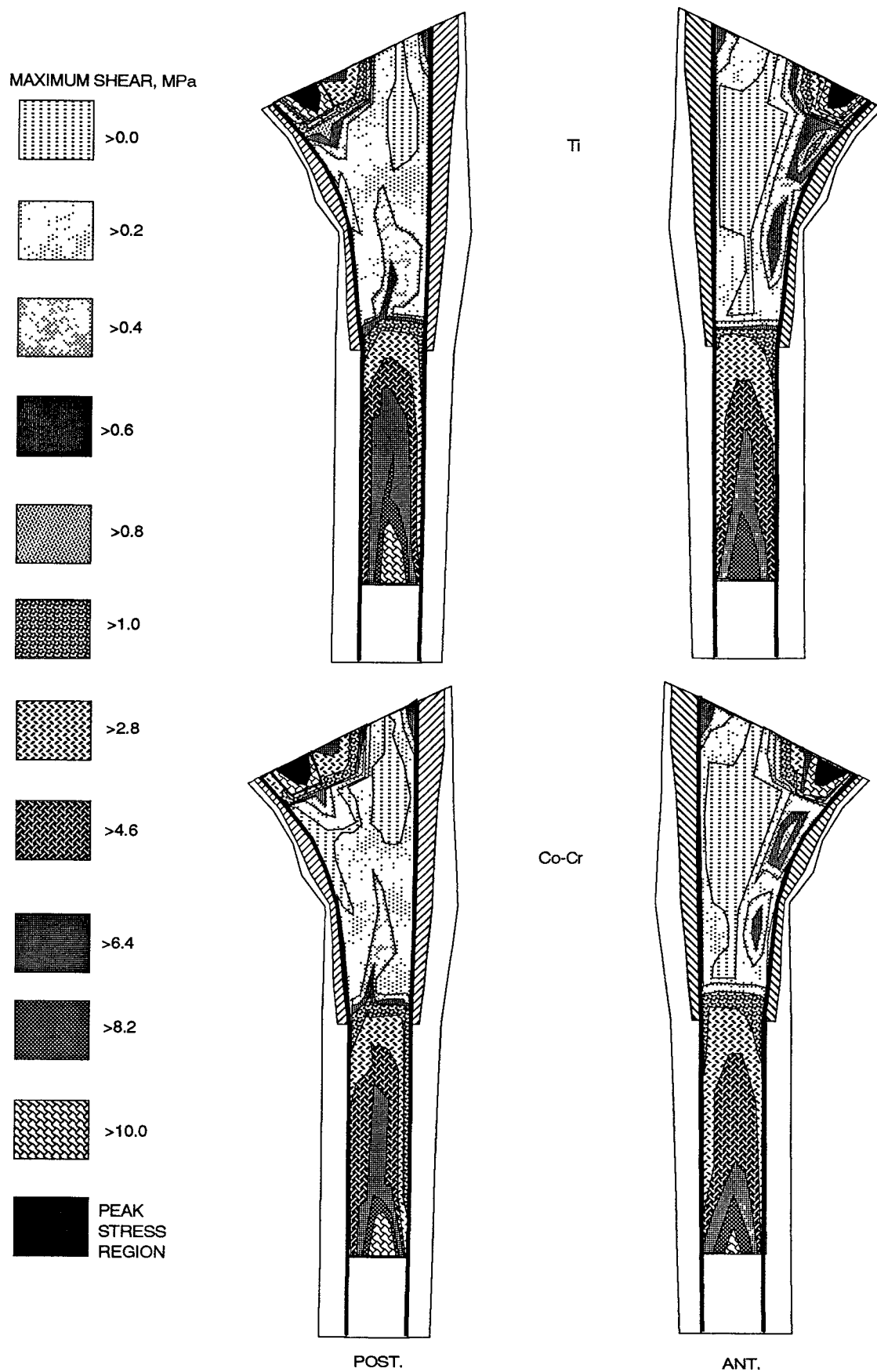


Fig.3.3-1 Maximum shear at bone interface surrounding fully coated stems at 4% load case

MAXIMUM SHEAR, MPa

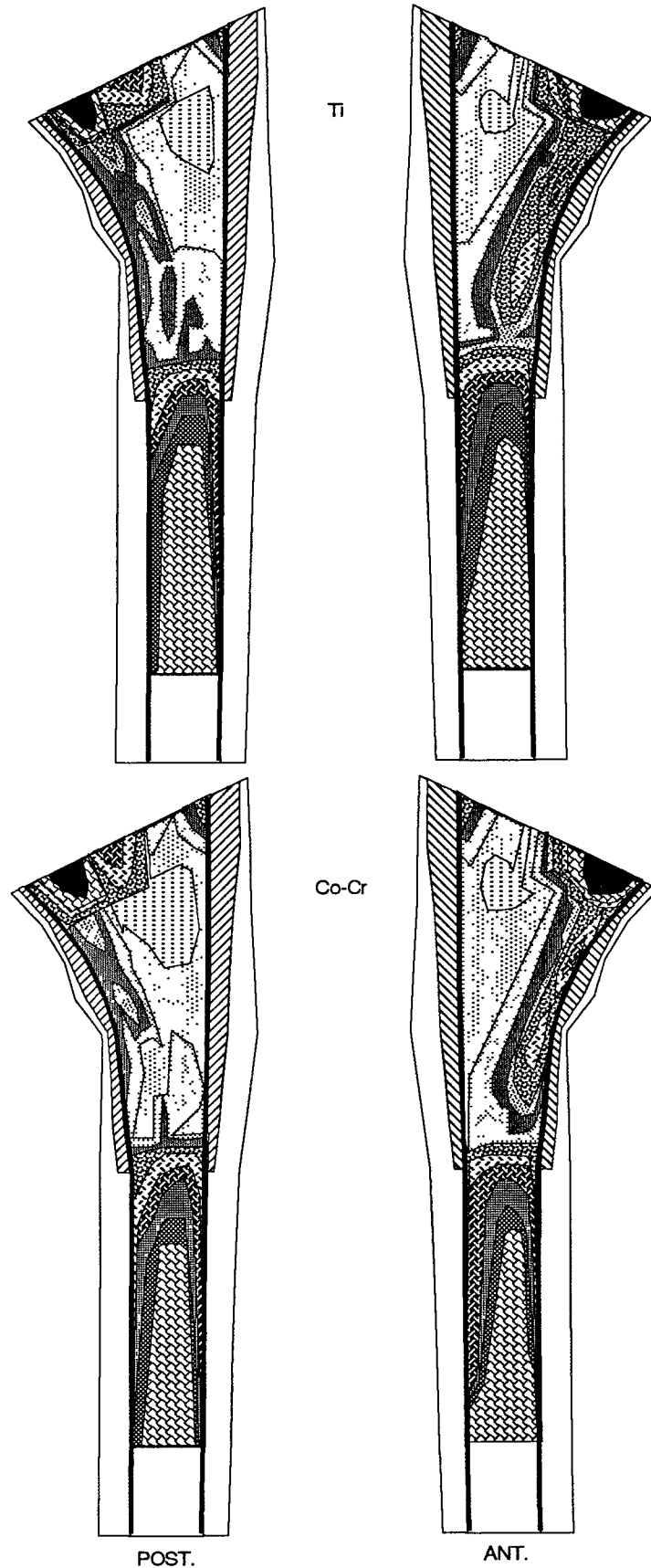
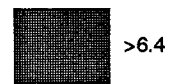
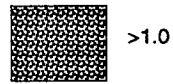
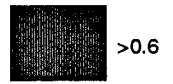
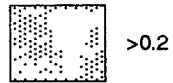
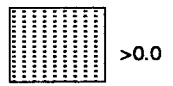


Fig.3.3-2 Maximum shear at bone interface surrounding fully coated stems at 41% load case

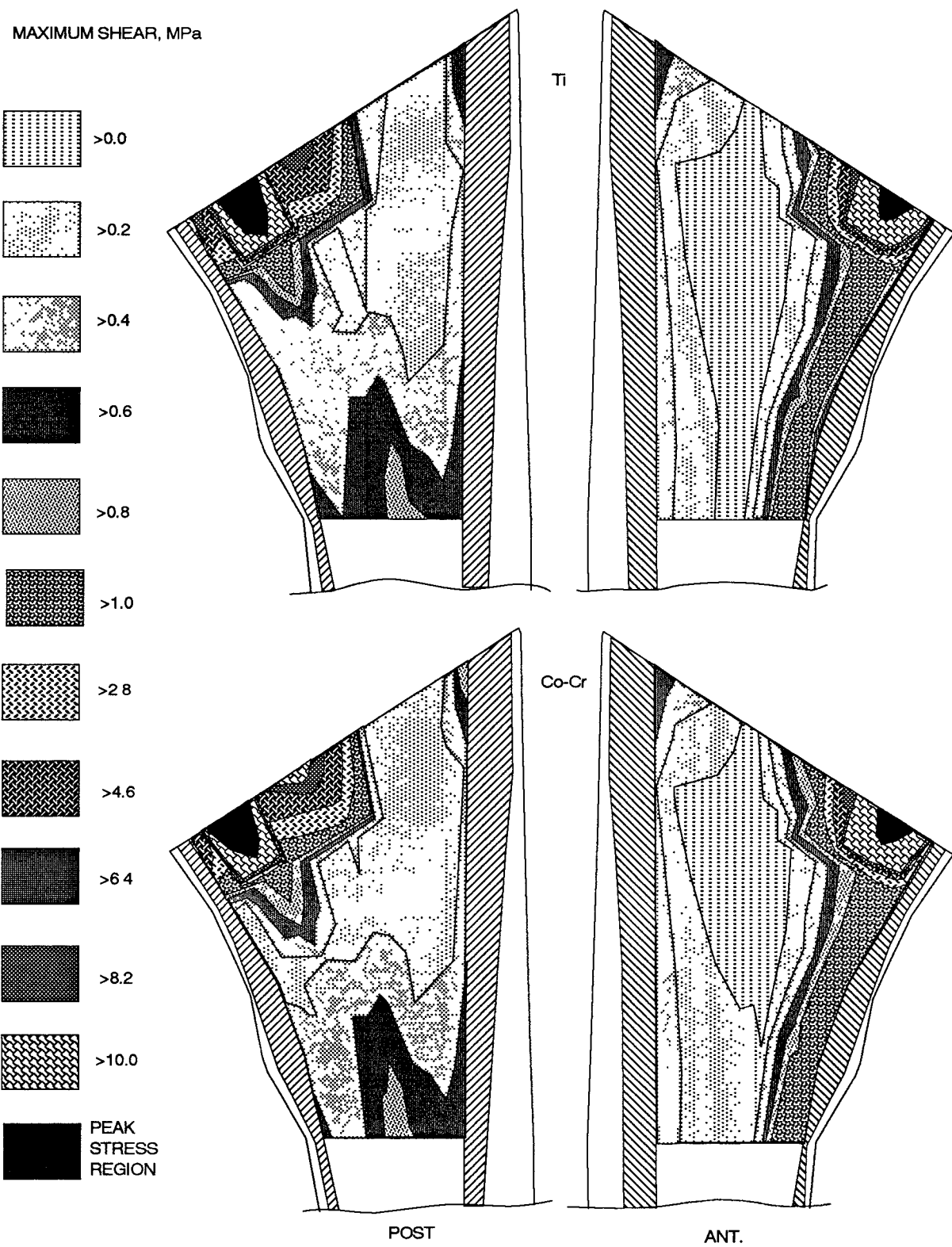


Fig.3.3-3 Maximum shear at bone interface surrounding proximaly coated stems at 4% load case

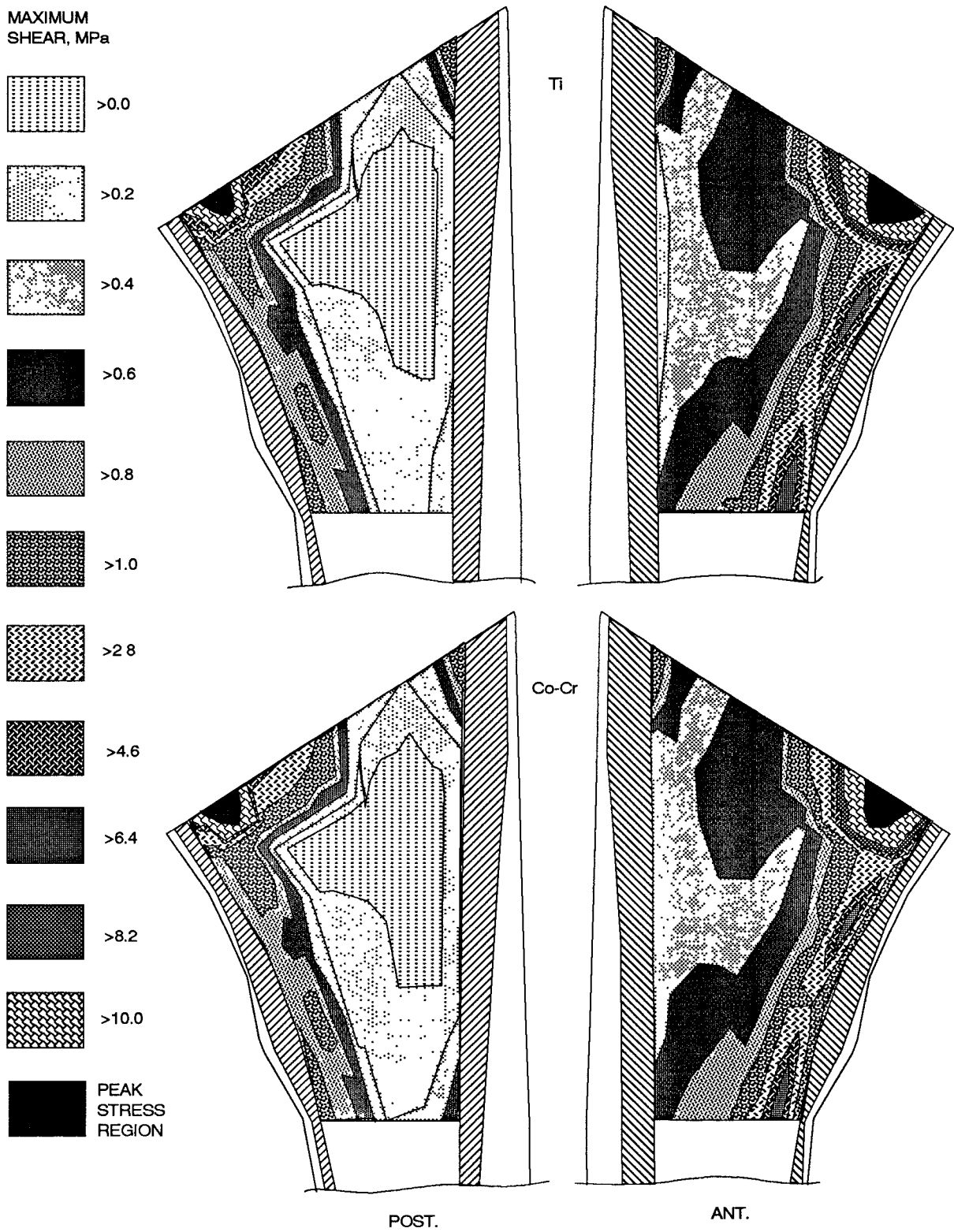
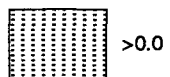


Fig.3.3-4 Maximum shear at bone interface surrounding proximally coated stems at 41% load case

MAXIMUM
SHEAR, MPa



PEAK
STRESS
REGION

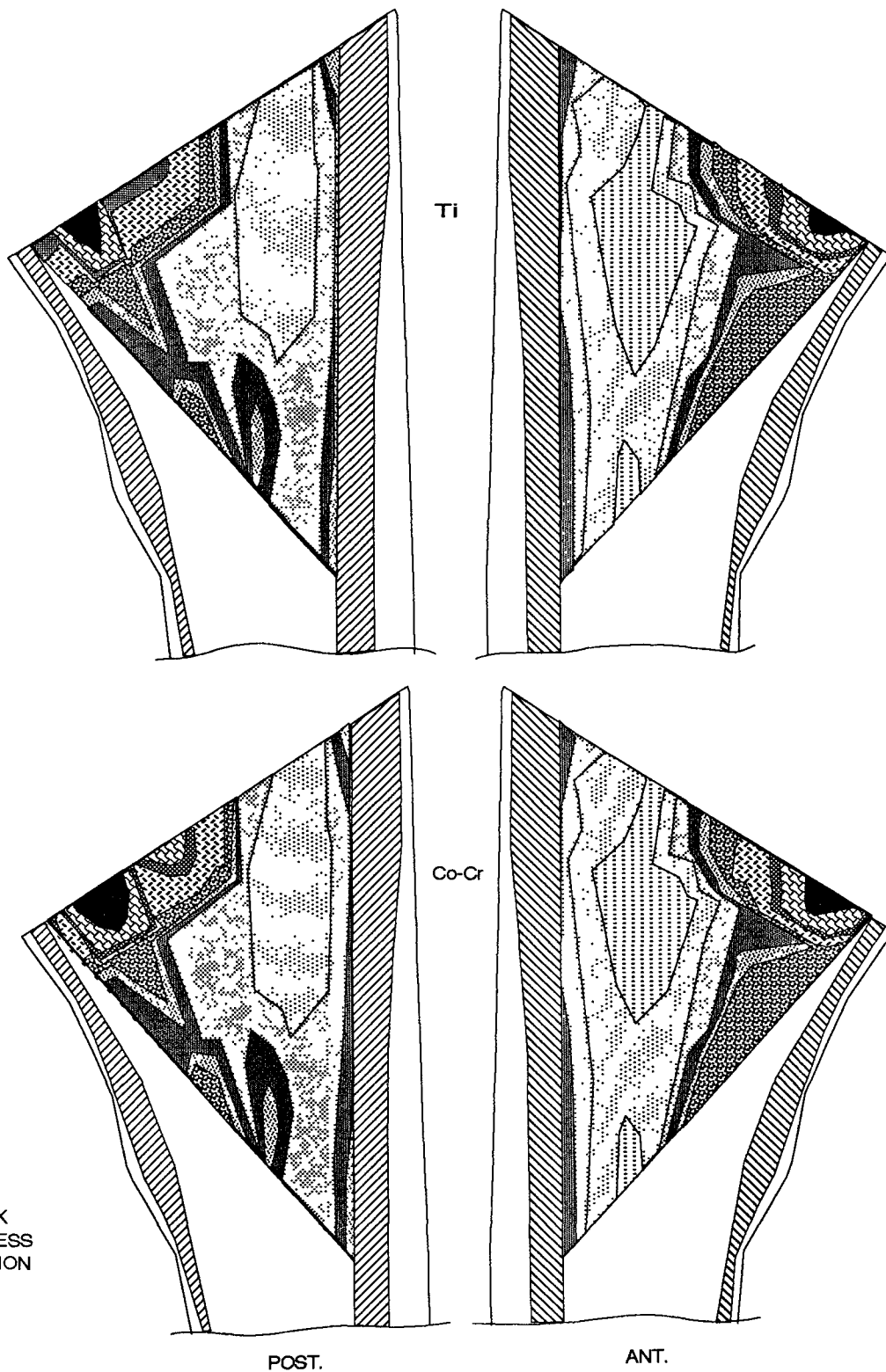


Fig.3.3-5 Interface maximum shear on THR using laterally coated stems at 4% load case



Fig.3.3-6 Maximum shear at bone interface surrounding laterally coated stems at 41% load case

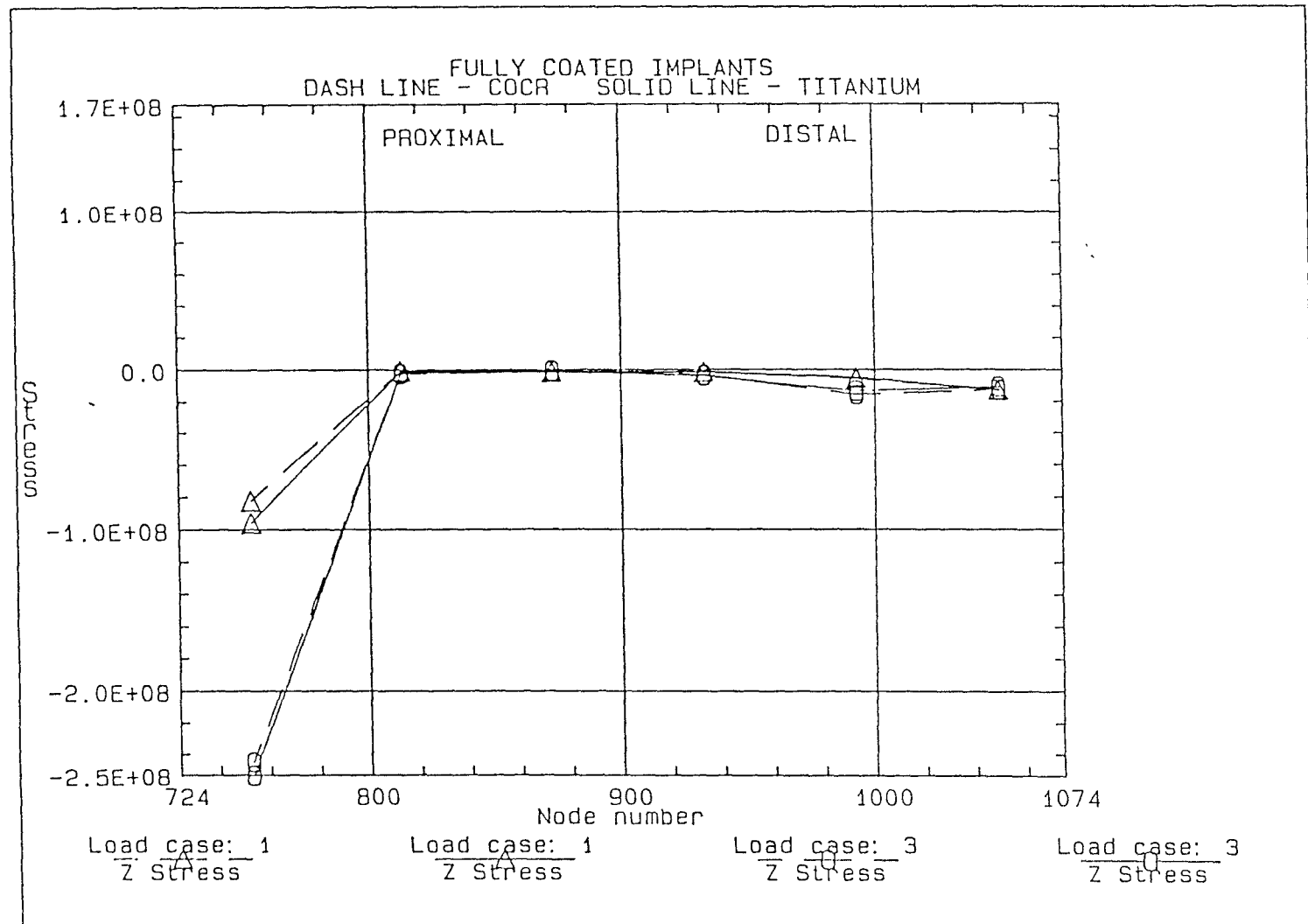


Fig. 3.2-13 Interface compressive stress for fully coated Ti and Co-Cr stems at bone interface

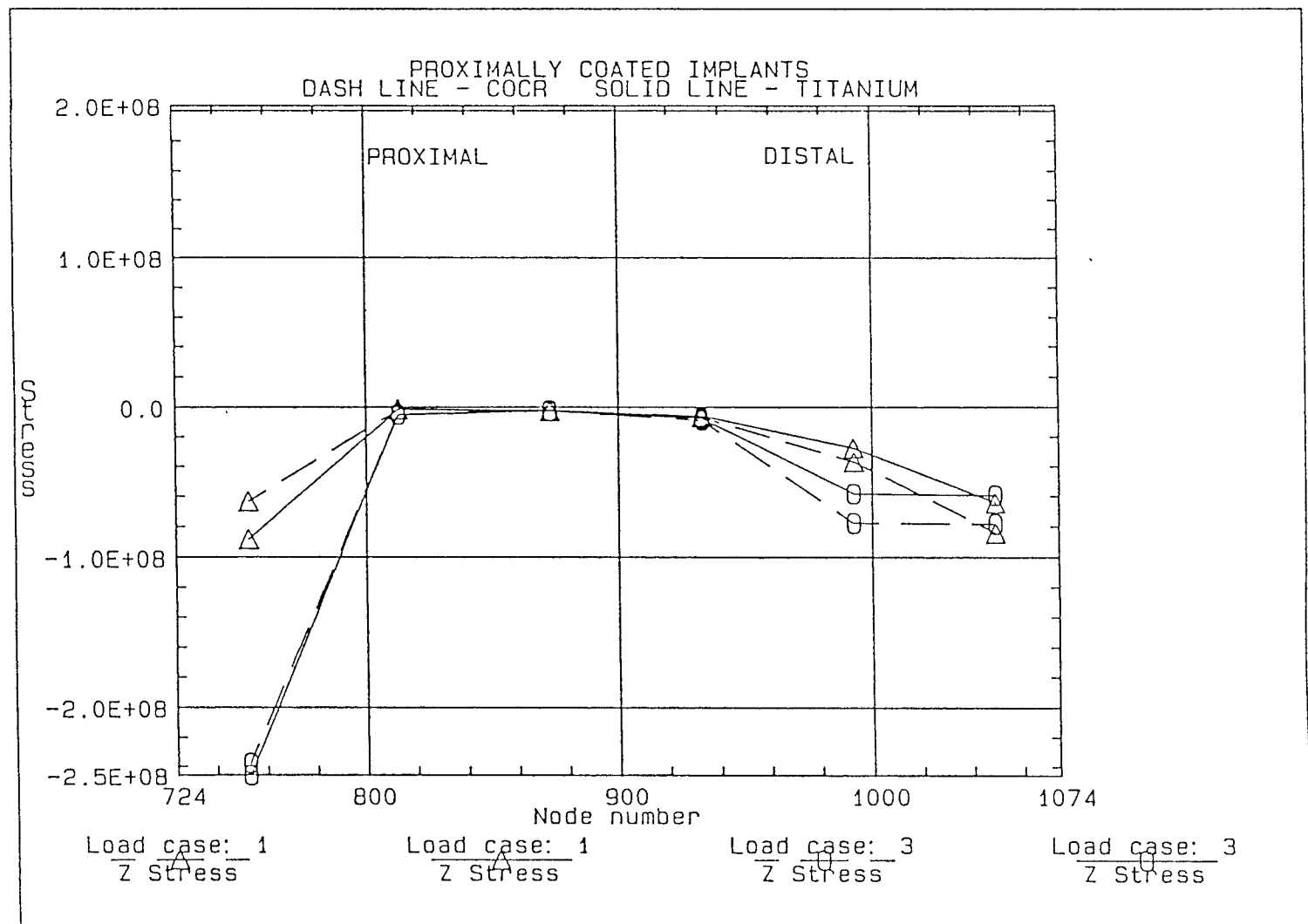


Fig. 3.2-14 Interface compressive stress for proximally coated Ti and Co-Cr stems at bone interface

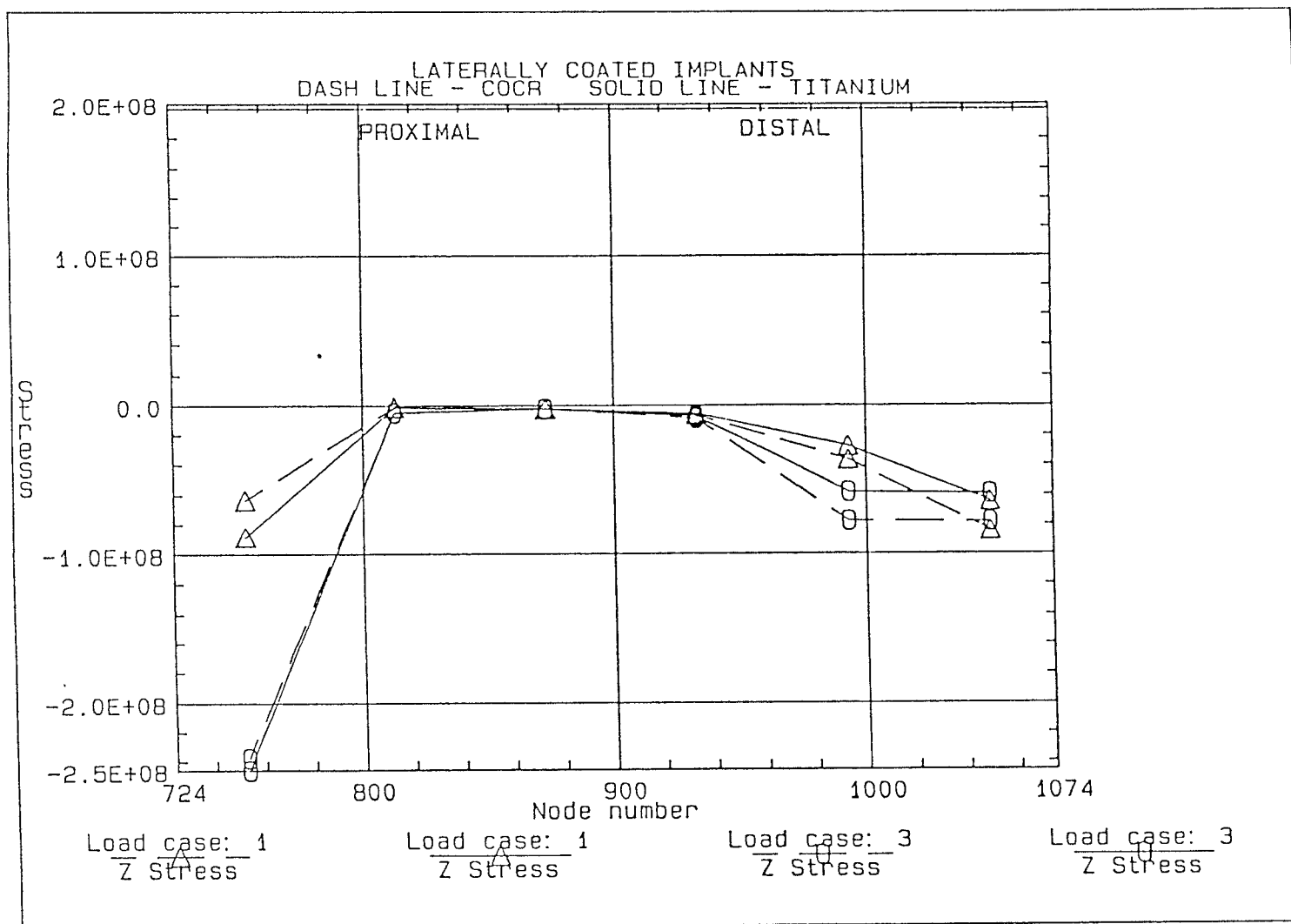


Fig. 3.2-15 Interface compressive stress for laterally coated Ti and Co-Cr stems at bone interface

3.3 MAXIMUM SHEAR STRESSES AT BONE INTERFACE

Fig. 3.3-1 thru 3.3-9 illustrate the results for the 4 percent and 41 percent load cases. The formation of shear stresses at the interface basically comes from torsional loads as well as axial loads as a result of three-dimensional loading. Peak stress at the proximal interface merely reflects the defects in model processing.

3.3-1 EFFECT OF DIFFERENT MATERIALS

The general effect of titanium stems is higher shear stresses developed at the bone interface in comparison with Co-Cr stems. Figure 3.3-7 which represents the fully coated stem shows the nodes for titanium stem has higher calculated maximum shear than those for Co-Cr stem along the interface, except in the distal regions denoted by the last three symbols of the curves. The result reflecting the stiffness effect matches closely with the characteristics of interface compressive stresses as function of materials. For the partly coated stems which frictional shear is assumed to exist only in coating area, the average maximum shear is generally higher at the bone interface surrounding titanium stem, as illustrated in figures 3.3-8 and 3.3-9.

3.3-2 EFFECT OF POROUS COATING CONFIGURATIONS

For the complete coating, maximum shear at the proximal interface is uniformly low except near the muscle force region. The maximum shear distribution at the distal interface is more

uniform, which can be attributed to the uniform canal shape and lack of applied forces. The highest shear is at the distal end where the load is distributed predominantly.

For the 4 percent load case, maximum shear is higher posteriorly than anteriorly due to the more posterior direction of the joint force. Maximum shear is higher medially at the anterior interface due to the action of adduction force inserted on the anterior side. The shear pattern is reversed for the 41 percent load case which higher shear is found at the anterior interface because of the anteriorly directed joint reaction force. Maximum shear is medially higher at both anterior and posterior interfaces. This results from the effect of the opposite-Y directions of the joint force and the adduction force inserted in lesser trochanter region. Distal shear distribution is equivalent to the 4 percent load case.

For the proximal coating, maximum shear increases laterally to medially on the anterior interface at the 4 percent load case. On the posterior interface, maximum shear increases in the downward direction. Maximum shear for the 41 percent load case follows the pattern of the 4 percent one. The only exception is that higher shear also exists medially on the posterior interface owing to the loading condition.

The general pattern for the lateral coating at 4 percent and 41 percent load cases is more uniform shear distribution across the coating interface when compared with the proximal and complete coating configurations. Area of maximum shear concentration is reduced particularly at the medial interface.

Maximum
compressive
stresses, -MPa

TENSION

>0.0

>1.0

>2.0

>3.0

>4.0

>5.0

>8.0

>11.0

>14.0

>17.0

>20.0

PEAK
STRESS
REGION

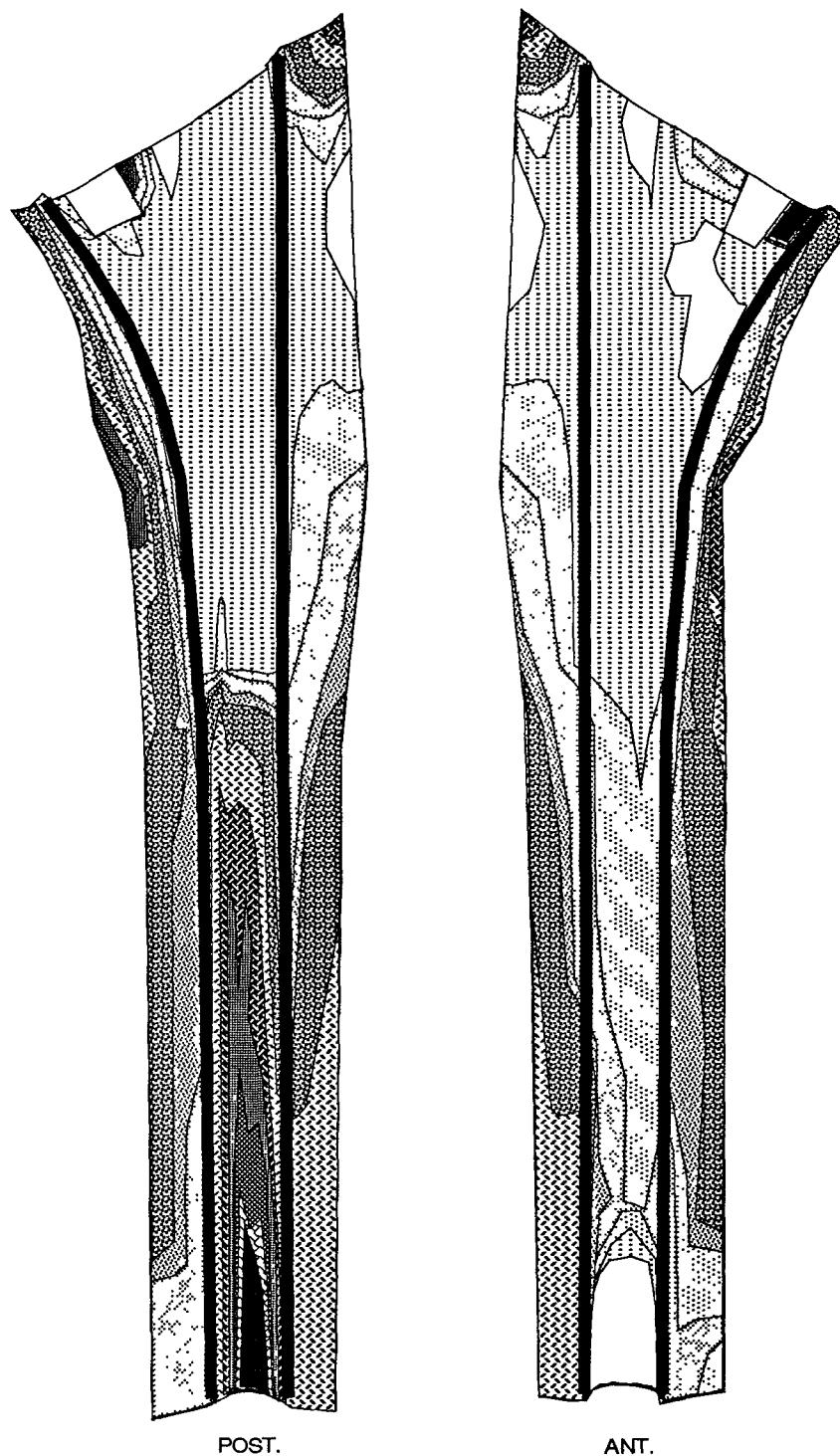


Fig. 3.4-1

Maximum compressive stresses at bone interface and surrounding bone on THR using fully coated Ti stem at 4% phase of the walking cycle

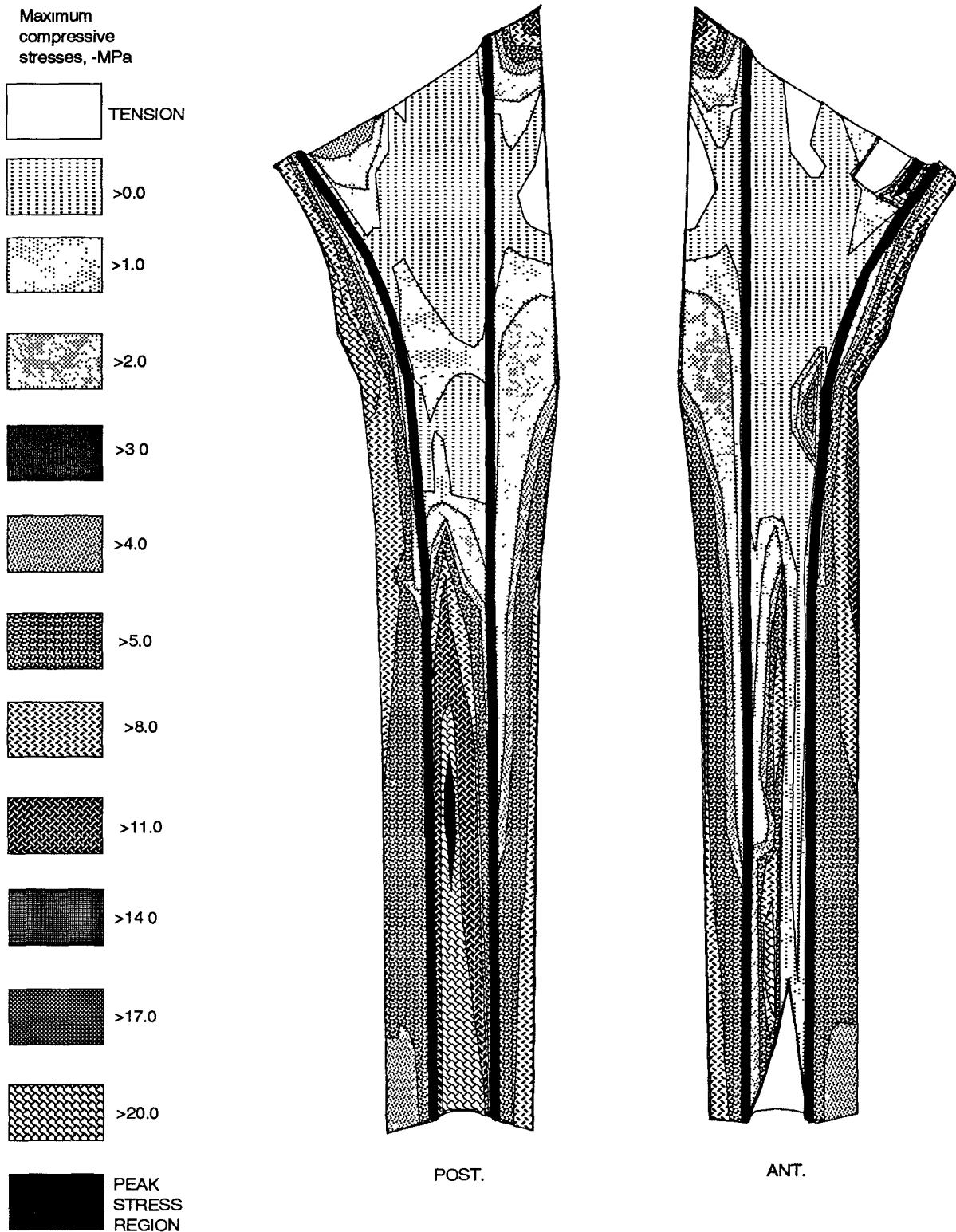


Fig. 3.4-2

Maximum compressive stresses at bone interface and surrounding bone on THR using proximally coated Ti stem at 4% phase of the walking cycle

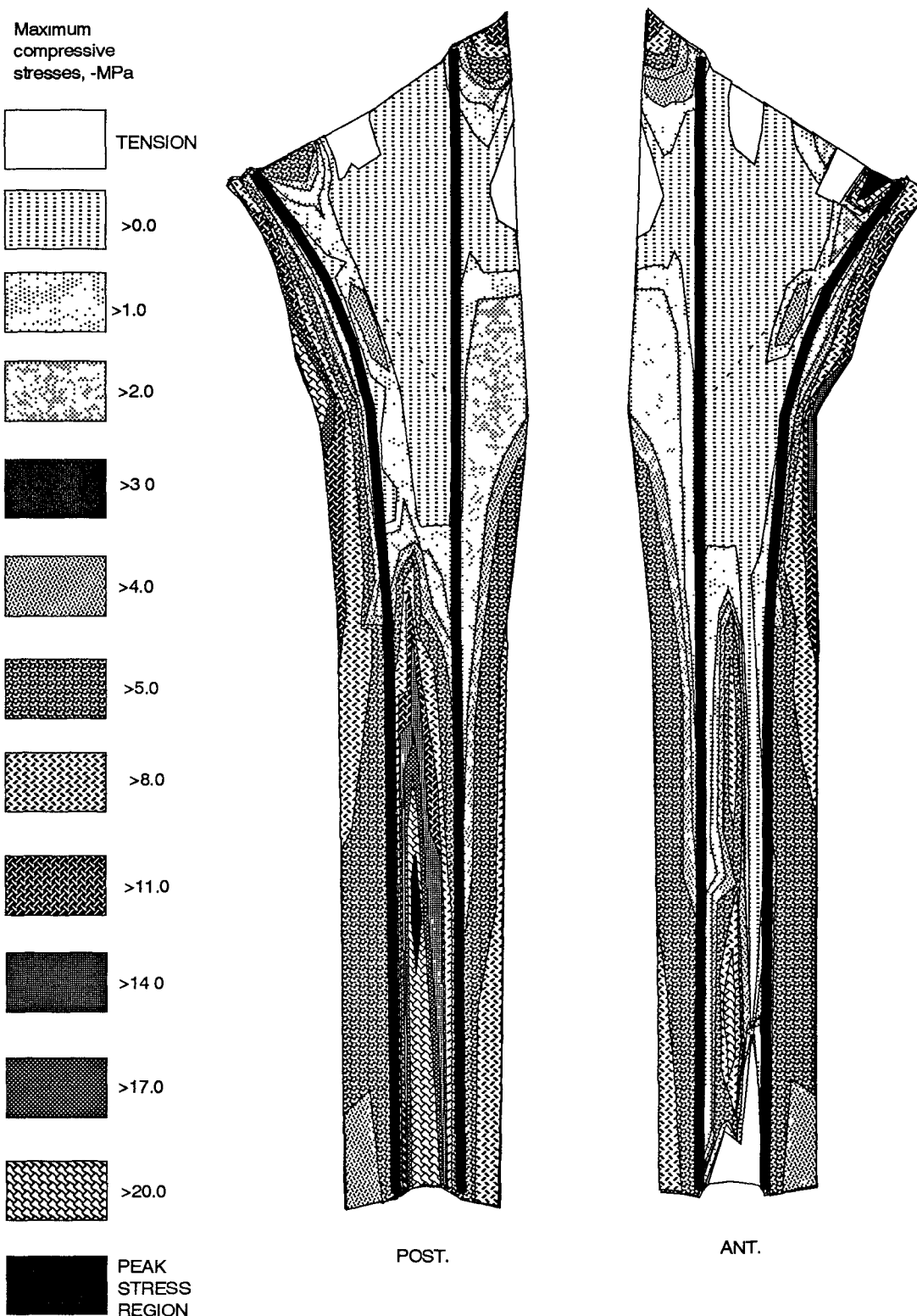


Fig. 3.4-3

Maximum compressive stresses at bone interface and surrounding bone on THR using laterally coated Ti stem at 4% phase of the walking cycle

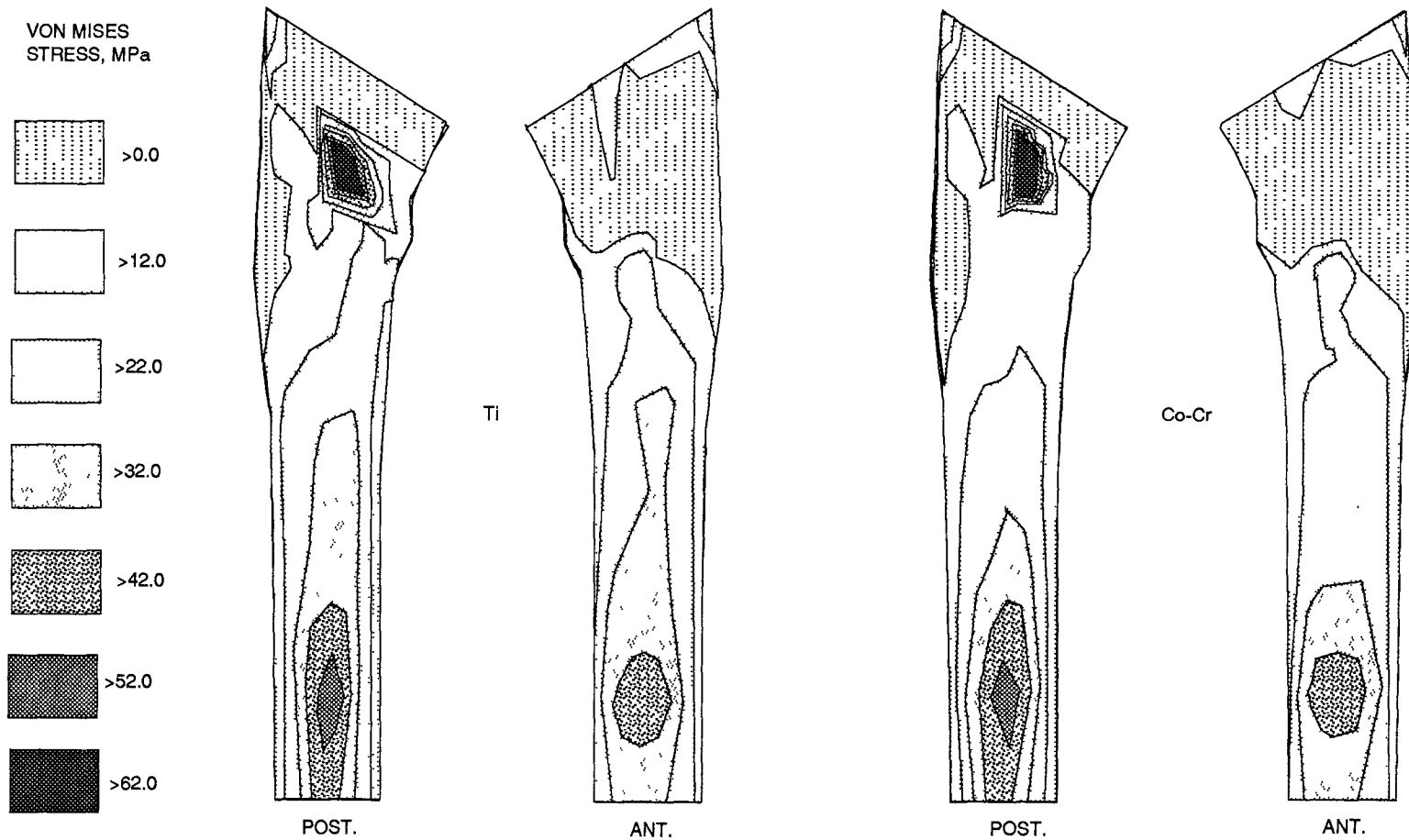
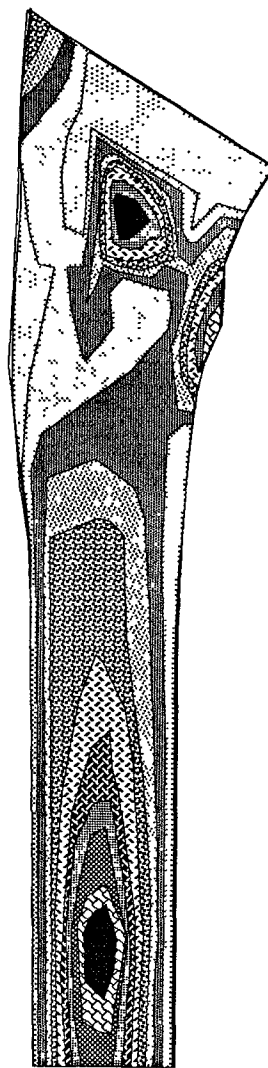
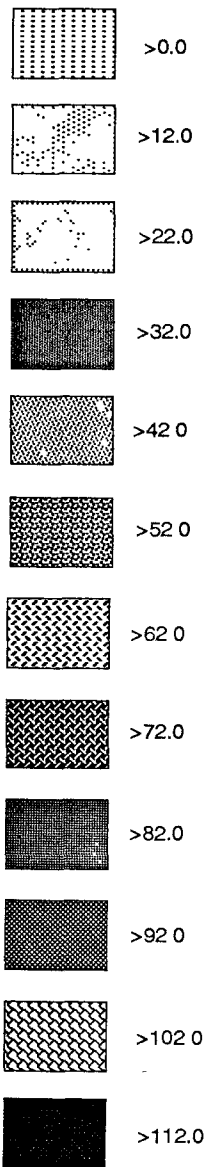
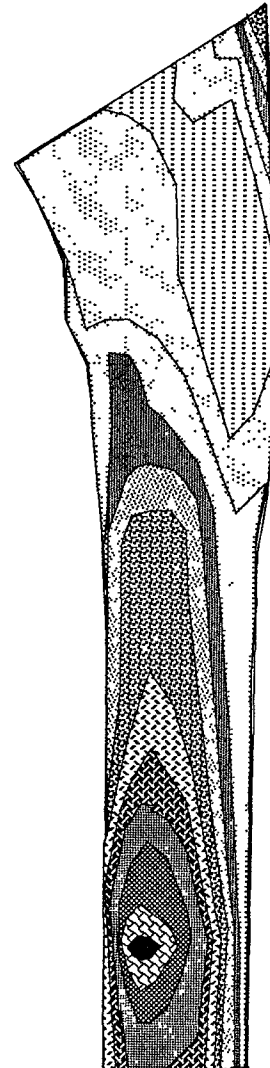


Fig.3.4-4 Von mises stress on cortical bone surface of THR using fully coated stems at 4% phase of the walking cycle

VON MISES STRESS, MPa



POST.

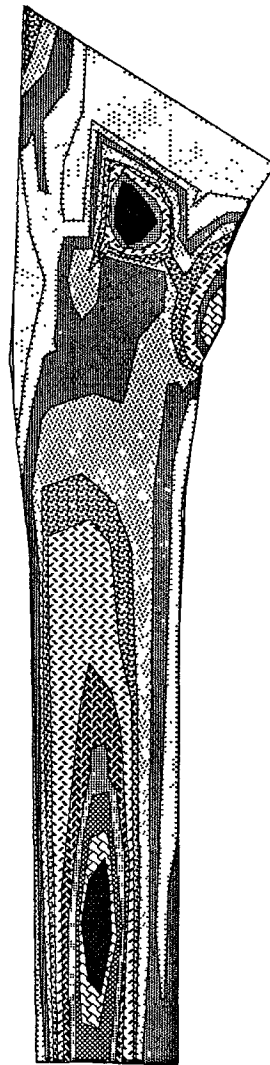
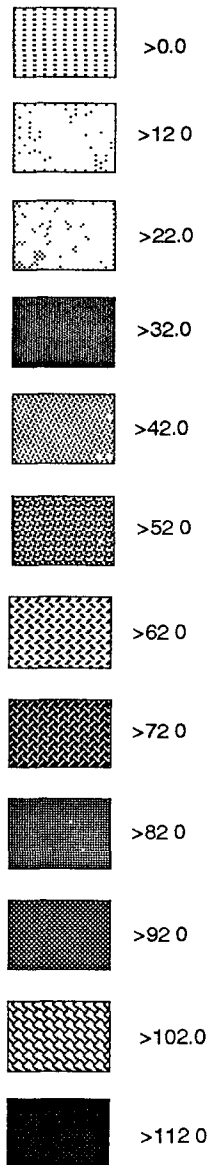


ANT.

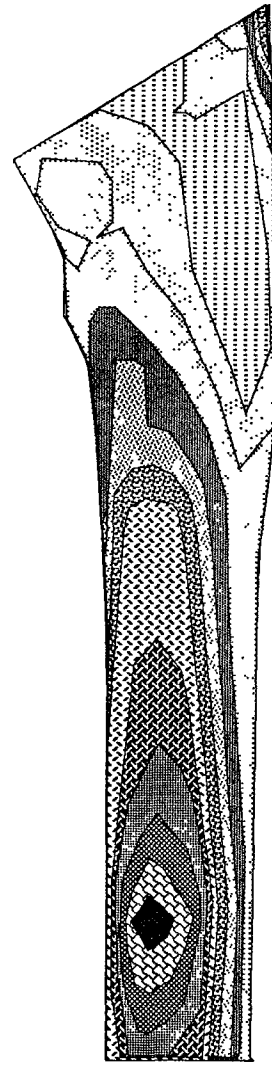
Fig.3.4-5

Von mises stress on cortical bone surface of THR using fully coated Co-Cr stem at 41% phase of the walking cycle

VON MISES STRESS, MPa



POST.



ANT.

Fig.3.4-6

Von mises stress on cortical bone surface of THR using fully coated Ti stem at 41% phase of the walking cycle

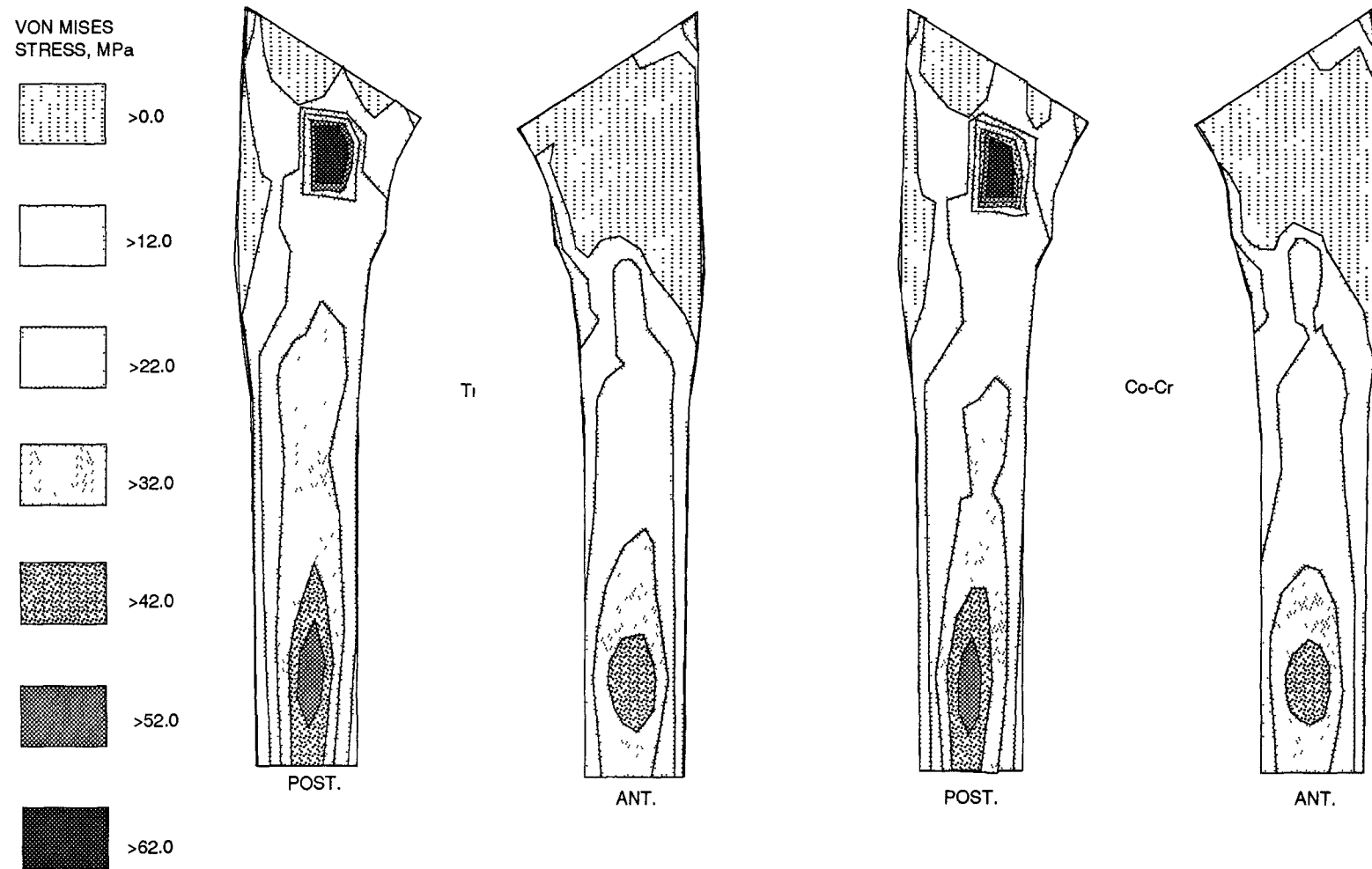
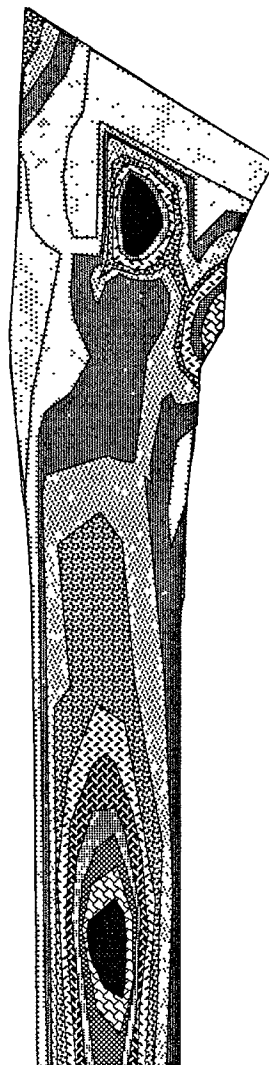
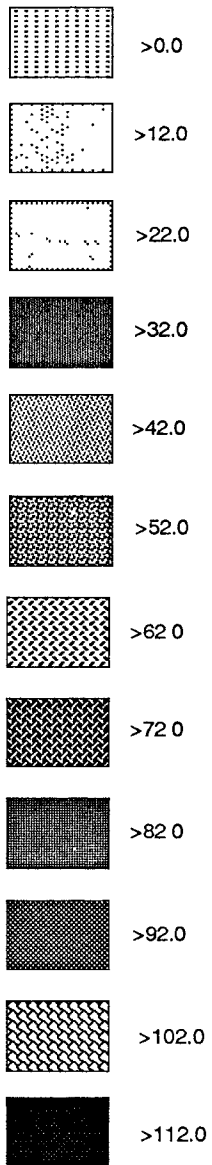
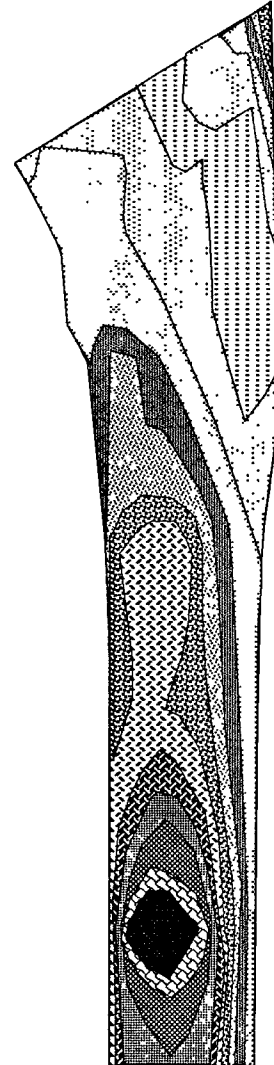


Fig.3.4-7 Von mises stress on cortical bone surface of THR using proximally coated stems at 4% phase of the walking cycle

VON MISES STRESS, MPa



POST.

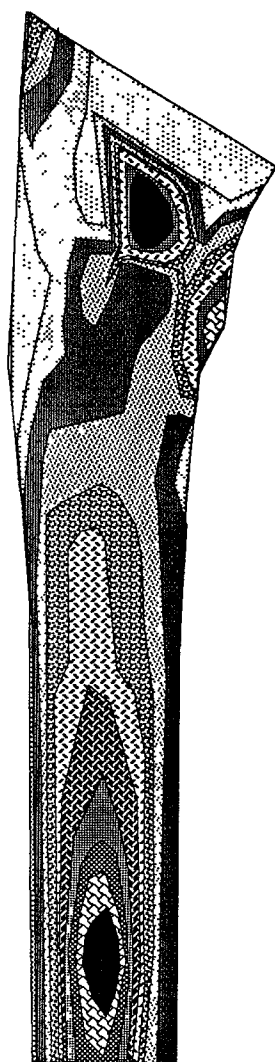
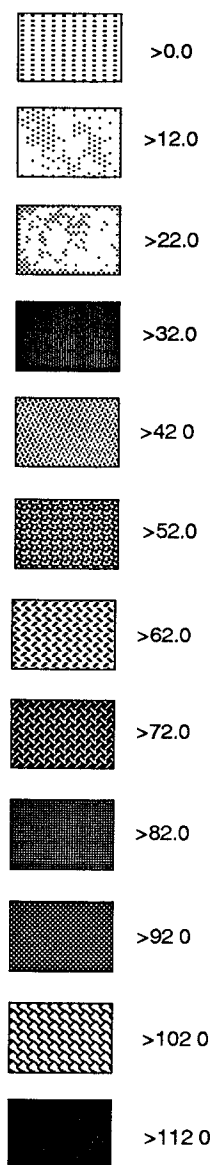


ANT.

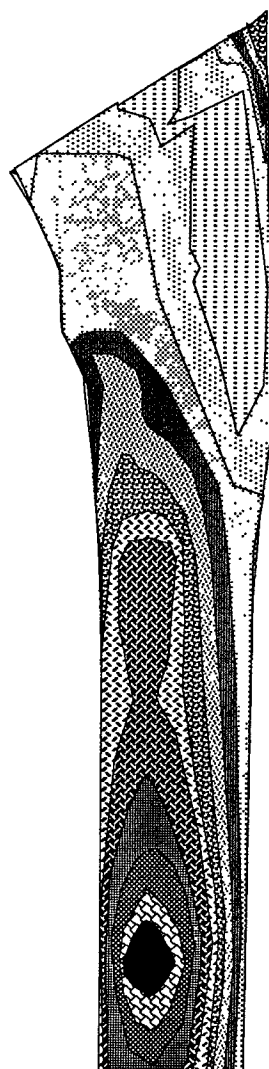
Fig.3.4-8

Von mises stress on cortical bone surface of THR using proximally coated Co-Cr stem at 41% phase of the walking cycle

VON MISES STRESS, MPa



POST.



ANT.

Fig.3.4-9

Von mises stress on cortical bone surface of THR using proximally coated Ti stem at 41% phase of the walking cycle

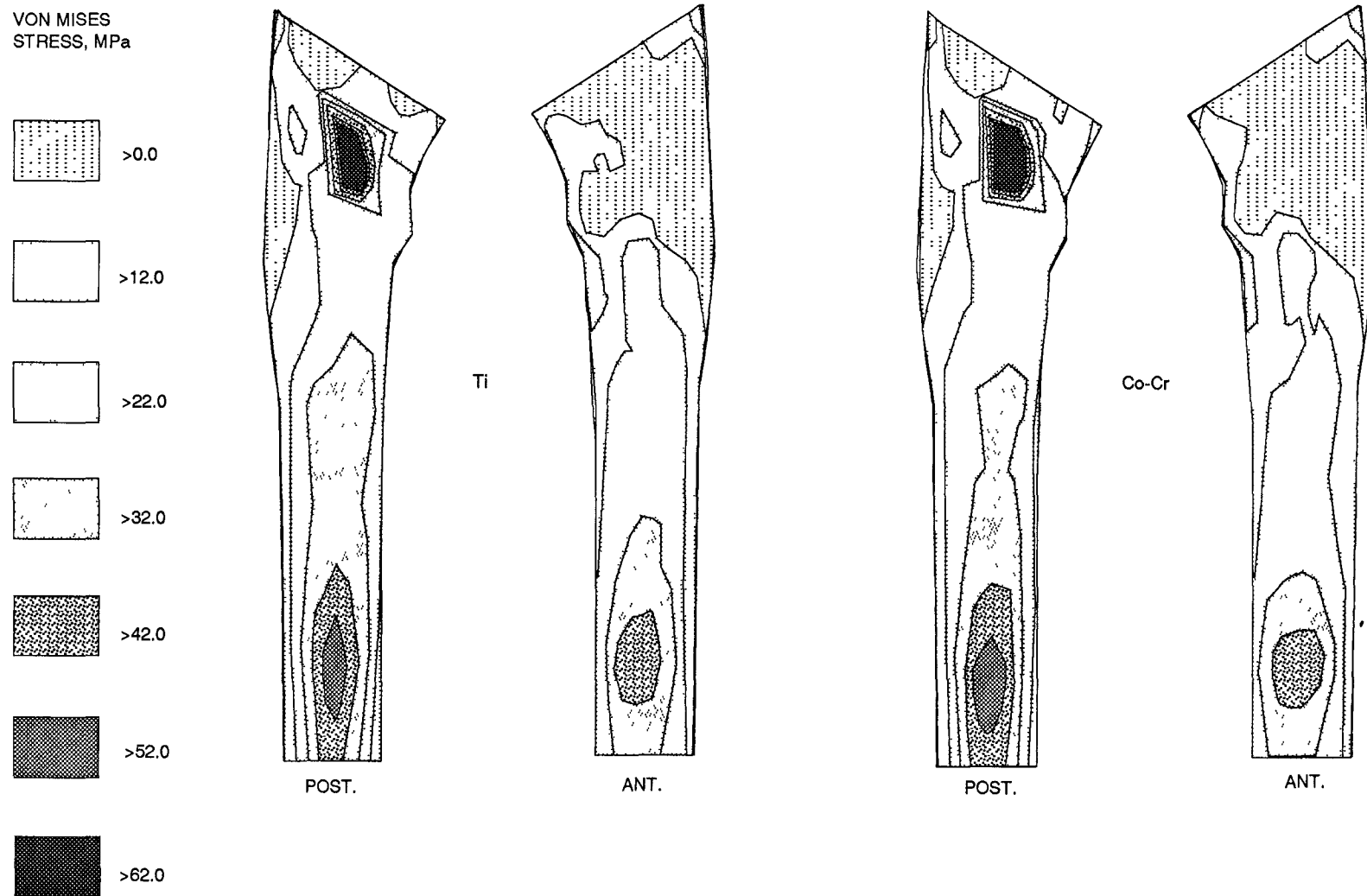
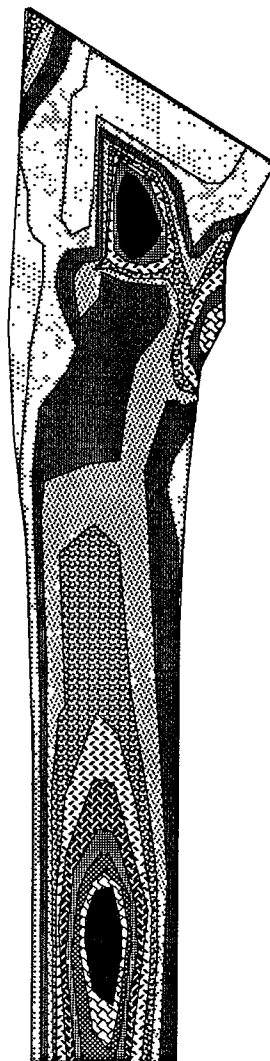
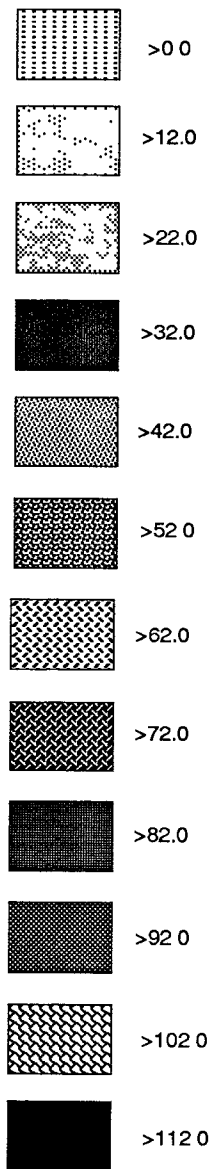
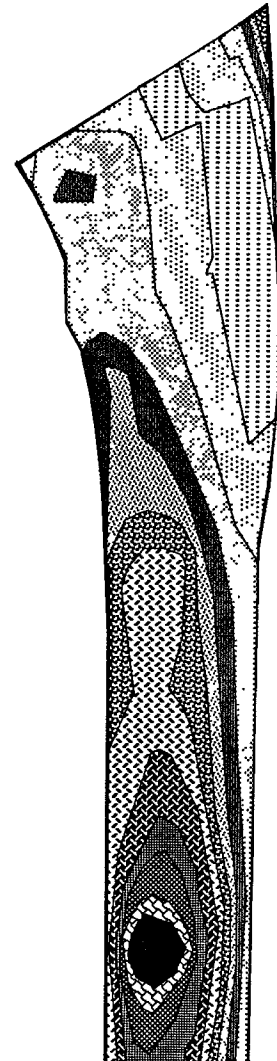


Fig.3.4-10 Von Mises stress on cortical bone surface of THR using laterally coated stems at 4% phase of the walking cycle

VON MISES STRESS, MPa



POST.

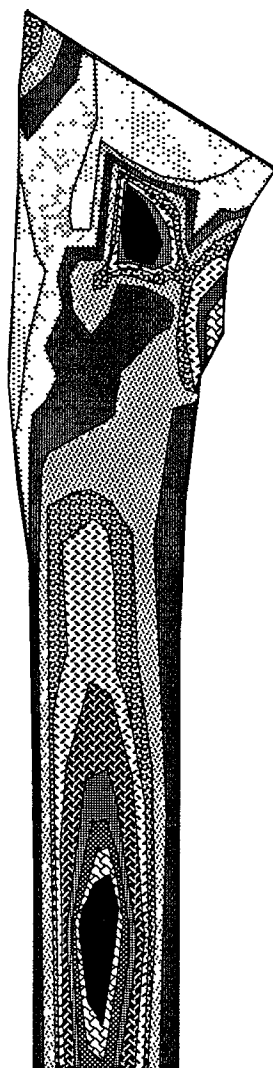
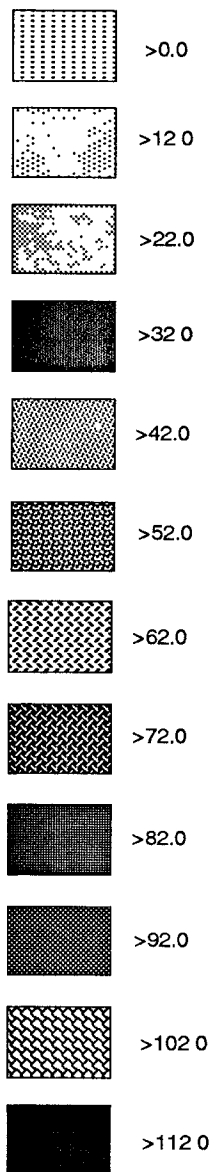


ANT.

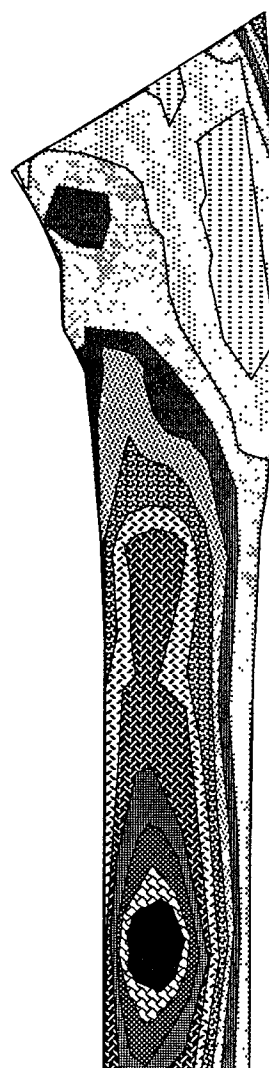
Fig.3.4-11

Von mises stress on cortical bone surface of THR using laterally coated CoCr stem at 41% phase of the walking cycle

VON MISES STRESS, MPa



POST.



ANT.

Fig.3.4-12

Von mises stress on cortical bone surface of THR using laterally coated Ti stem at 41% phase of the walking cycle

3.4 STRESSES IN FEMUR

3.4.1 EFFECT OF DIFFERENT MATERIALS

The von Mises stresses on the surface of cortical bone for the fully coated titanium stem is 9% higher on average higher than the fully coated Co-Cr stem. For the partly coated titanium stems, the average stress is 4% higher than the Co-Cr stems. More load is carried by the bone with a titanium stem due to its lower rigidity in a composite structure. The effect is more pronounced if there is an integral bond between the stem and the less rigid surrounding bone, as reflected by the results of the fully coated stems. This implies that the amount of coating significantly alters the stress transfer pattern.

3.4.2 EFFECT OF POROUS COATING CONFIGURATIONS

Figures 3.4-1 thru 3.4-3 show the maximum compressive stresses at the bone interface and the surrounding bone for different coating configurations. THR with fully coated stem demonstrates excessive stress concentration near the distal end, while the proximal region is greatly bypassed in terms of the axial load transfer. In contrast, the partly coated stems induce higher level of stress intensity over the decoupled area which produces bending and axial loading of the femoral shaft. Stress discontinuities exist near the boundary of the coating and the loose interface. The stress concentration is more evenly distributed in the distal interface.

Figures 3.4-4 thru 3.4-12 illustrates the von Mises stress on the cortical bone surface for the 4 percent and 41 percent load cases. The peak stresses in the extreme proximal region is a model artifact and as is the localized distal stress concentration at the stem tip.

For the 4 percent load case, the stress concentration at the greater trochanter is the result of the reaction of the abduction force. The same applies for the 41 percent load case which also shows the stress concentration at the lesser trochanter where the adduction force is inserted.

For the fully coated stems, the cortical bone is substantially relieved of stress notably in the proximal area when compared to the partly coated stems. It indicates the load path bypasses the proximal femur when the bone interface is completely bonded to the stem. For the partly coated stems, as shown in the stress contour plots, they elevate the level of the stress intensity significantly in the proximal region because of the decoupled area which allows the femur to move relative to the stem. Therefore, more stress can be transmitted to the proximal femur and stress shielding effect can be reduced in that region.

CHAPTER FOUR

DISCUSSION OF RESULTS

In terms of material choice, titanium is preferred over Co-Cr mainly because it produces more favorable conditions in the implant, bone, and at bone interface. Titanium reduces the peak stress in the implant to prevent implant failure. Its low rigidity alleviates the stress shielding effect of the stem and benefits the surrounding bone taking more of the shared load. In the area of bone interface, titanium stems can generate relatively high compressive stresses in the proximal area. The increased compressive stresses at the proximal bone interface would secure the component fixation and promote bone ingrowth. Titanium stem results in a smooth stress distribution at the distal interface, thereby reducing distal bone hypertrophy caused by high local stress concentrations associated with the Co-Cr filled canal.

Changing from complete coating configuration to partial coating configuration shifts the high level of maximum compressive stresses in the distal region to the proximal region near the coating boundary and without increasing the maximal values. As a result of the midstem load transfer, the stress shielding effect can be substantially reduced. This is reflected by the elevated von Mises stresses on the cortical bone surface for the cases of partly coated stems.

The augmented stresses is mainly caused by increased deformation of the bone in bending, due to the reduced stiffness of the whole structure when the implant-bone interface is no longer bonded.

With respect to the partial coating configurations, the lateral coating achieves a higher ratio of compression to tension on the interface and a more natural stress transfer in the femur when compared to the proximal coating. It produces a load path that transfers load directly to the medial calcar region and distributes the load laterally minimizing stress protection. The only shortcoming of the lateral coating configuration is the slightly higher stresses induced on the implant.

CHAPTER FIVE

CONCLUSION

Bone remodeling can be predicted by the mechanical factors such as stress shielding and altered stress transfer which depend on stem design. Material stiffness can determine the durability of the prosthesis and the extent of stress shielding effects. The results of this study indicate that titanium implant is expected to produce better performance. Stem coating geometries produce dramatical different interface conditions. A slanted coating configuration appears to achieve more physiological loading.

The model in this study stands for the initial formulation of the bone-implant interface. The bonded interface represented by spring element is defined to allow the transmission of compressive, shear and tensile forces. The loose interface represented by gap element is defined to transfer only compressive force. The forthcoming model formulation should sort out spring elements which are subject to tensile stress and then redefine them to transmit compressive force only. This process of interface redefinition followed by model reanalysis is repeated until all the interface elements simulating loose interface are free of tension. The final model can then satisfy the assumption that total fixation can occur only in the coating interface in the absence of tension.

REFERENCES

- [1] Smith-Peterson, "Arthroplasty of the Hip. A New Method" Journal of Bone and Joint Surgery, Vol.21, 1939, PP.269-288.
- [2] Moore,A.T.,Bohlman,H.R., "Metal Hip Joint. A Case Report," Journal of Bone and Joint Surgery, Vol.25, 1943, PP.688-692.
- [3] Judet,J.,Judet,R., "The Use of an Artificial Femoral Head for Arthroplasty of the Hip Joint," Journal of Bone and Joint Surgery, Vol.32B, 1950, PP.166-173.
- [4] Charnley,J., "Arthroplasty of the Hip. A New Operation", Lancet, 1(7187), 1961, PP.1129-1132.
- [5] Giliberty,R.P., "A New Concept of a Bipolar Endoprosthesis," Orthopedic Review, Vol.3, 1974, PP.40.
- [6] Bateman,J.E., "Single Assembly Total Hip Prosthesis. Preliminary Report" Orthopedic Digest, Vol.2, 1974, PP.15.
- [7] Luncford,E.M., "Total Hip Replacement Using McBride Cup and Moore Prosthesis," Clinical Orthopedics, Vol.72, 1970,PP.201-204.
- [8] McBride,E., "The Flanged Acetabular Replacement Prosthesis," Arch. Surg., Vol.83, 1961, PP.721.
- [9] Lord,G.A., Hardy,J.R., Kummer,F.J., "An Uncemented Total Hip Replacement," Clinical Orthopedics, Vol.141, 1979, PP.2-16.
- [10] Judet,R., Siguier,M., Brumpt,B.,et al., "A Noncemented Total Hip Prosthesis," Clinical Orthopedics, Vol.137, 1978, PP.76-86.
- [11] Engh,C.A., Brooker,A.F., Kenmore, P.I., Chandler, H.P., Luncford, E.M., "Porous Coated Hip Replacement," Forty-Eighth Annual Meeting of the American Academy of Orthopedic Surgeon, Las Vegas, 1981.
- [12] Carlsson, A.S., Gentz, C.F., "Mechanical Loosening of the Femoral Head Prosthesis in the Charnley Total Hip Arthroplasty," Clinical Orthopedics, Vol.147, 1980, PP.262.
- [13] Callaghan, J.J., Salvati, E.A., Pellicci, P.M., et al., "Results of Revision for Mechanical Failure after Cemented Total Hip Replacement, 1979 to 1982. A Two to Five-Year Follow-up," Journal of Bone and Joint Surgery, Vol.67A, 1985, PP.1074-1085.
- [14] Engh, C.A., "Hip Arthroplasty with a Moore Prosthesis with Porous Coating. A Five-Year Study" Clinical Orthopedics, Vol.176, 1983, PP.52-66.
- [15] Nasca, R.J., "Porous Hip Implant with Case Reports," The Alabama Journal of Medical Science, Vol.25, No.1, 1988, PP.47-53.

- [16] Jasty, M.J., Floyd, W.E., Schiller, A.L., Goldring, S.R., Harris, W.H., "Localized Osteolysis in Stable, Non-septic Total Hip Replacement," *Journal of Bone and Joint Surgery*, Vol.68A, 1986, PP.912.
- [17] Chwirut, D.J., "Long-Term Compressive Creep Deformation and Damage in Acrylic Bone Cements," *Journal of Biomedical Materials Research*, Vol.18, 1984, PP.25.
- [18] Looney, M.A., Park, J.B., "Molecular and Mechanical Property Changes During Aging of Bone Cement In Vitro and In Vivo," *Journal of Biomedical Materials Research*, Vol.20, 1986, PP.555.
- [19] Johanson, N.A., "14-Year Follow-up Study of a Patient with Massive Calcar Resorption. A Case Report" *Clinical Orthopedics*, Vol.213, 1986, PP.189.
- [20] Engh, C.A., Bobyn, J.D., Glassman, A.H., "Porous-Coated Hip Replacement: the Factors Governing Bone Ingrowth, Stress Shielding, and Clinical Results," *Journal of Bone and Joint Surgery*, Vol.69B, No.1, 1987, PP.45-54.
- [21] Pillar, R.M., "Powder Metal-Made Orthopedic Implants with Porous Surface for Fixation by Tissue Ingrowth," *Clinical Orthopedic*, Vol.176, 1983, PP.42.
- [22] Crowninshield, R.D., Brand, R.A., Johnston, R.C., Pedersen, D.R., "An Analysis of Collar Function and the Use of Titanium in Femoral Prostheses," *Clinical Orthopedics*, Vol.158, 1981, PP.270.
- [23] Engh, C.A., Bobyn, J.D., "The Influence of Stem Size and Extent of Porous Coating on Femoral Bone Resorption after Primary Cementless Hip Arthroplasty," *Clinical Orthopedics*, Vol.231, 1988, PP.7-29.
- [24] Turner, T.M., et al., "A Comparative Study of Porous Coating in a Weight-Bearing Total Hip Arthroplasty Model," *Journal of Bone and Joint Surgery*, Vol. 68A, 1986, PP.1396.
- [25] Buchert, P.K., Vaughn, B.K., Mallory, T.H., Engh, C.A., Bobyn, J.D., "Excessive Metal Release Due to Loosening and Fretting of Sintered Particles on Porous-Coated Hip Prosthesis: Report of Two Cases," *Journal of Bone and Joint Surgery*, Vol. 68A, 1986, PP.606-609.
- [26] Bobyn, J.D., Pillar, R.M., et al., "The Effects of Proximally and Fully Porous-Coated Canine Hip Stem Design on Bone Modelling," *Journal of Orthopedics Research*, Vol.5, 1987, PP.393.
- [27] Andriacchi, T.P., Galante, J.O., Belytschko, T.B., Hampton, S., "A Stress Analysis of The Femoral Stem in Total Hip Prosthesis," *Journal of Bone and Joint Surgery*, Vol.58A, 1976, PP.616-624.

- [28] Svensson, N.L., Valliappan, S., Wood, R.D., "Stress Analysis of Human Femur with Implanted Charnley Prosthesis," Journal of Biomechanics, Vol.10,
- [29] Huiskes, R., "Some Fundamental Aspects of Human Joint Replacement;Part III:Stress Analyses of Intramedullary Fixation Systems," Acta. Orth. Scand. Suppl., No.185, PP.109-200.
- [30] Crowninshield, R.D., Brand, R.A. Johnston, R.C., " An Analysis of Femoral Stem Design in Total Hip Arthroplasty," Journal of Bone and Joint Surgery, Vol.62-A, No.1, January 1980, PP.68-78.
- [31] Rohlmann, et al., "A Nonlinear Finite Element Analysis of Interface Conditions in Porous Coated Hip Endoprosthesis," Journal of Biomechanics, Vol.21, No.7, 1988, PP.605-611.
- [32] Rohlmann, A., Bergmann, G.,et al., " Finite Element Analysis and Experimental Investigation in a Femur with Hip Endoprosthesis." Journal of Biomechanics, Vol.16, 1983, PP.727-742.
- [33] Bathe,K.J., Chaudhary, A., "A Solution Method for Planar and Axisymmetric Contact Problems," Int. J. Num. Meth. Engng., Vol.21, 1985, PP.65-88.
- [34] Roesler, H., "The history of some fundamental concepts in bone biomechanics," Journal of Biomechanics, Vol.20(11/12), 1987, PP.1025-1034.
- [35] Koch, John, "The Laws of Bone Architecture," The American Journal of Anatomy, Vol.21, No.2, March 1917, PP.179-268.
- [36] Reily, S.B., Burstein, A.H., "The Elastic and Ultimate Properties of Compact Bone Tissue," Journal of Biomechanics, Vol.8, 1975, PP.393-405.
- [37] Reily, D.T., Burstein, A.H., "Mechanical Properties of Cortical Bone," Journal of Bone and Joint Surgery, Vol.56-A, 1974, PP.1001-1022.
- [38] Huiske, R., "Modelling of Long Bone in Structural Analyses," Journal of Biomechanics, Vol.15, No.1, 1982, PP.65-69.
- [39] Currey, J.D., "The Mechanical Properties of Bone," Clinical Orthopedics, Vol.73, 1964, PP.210-231.
- [40] Yamada, H., Evans, F.G., Strength of Biological Materials, Williams & Wilkins, Baltimore, 1970.
- [41] Evans, F.G., King, A.I., "Regional Differences in Some Physical Properties of Human Spongy Bone," Biomechanical Studies of the Musculoskeletal System, Springfield, Charles C. Thomas, 1961, PP.49-67.

[42] Zienkiewicz, O.C., The Finite Element Method, Third Edition, McGraw Hill, London, 1977.

[43] Crowninshield, R.D., Brand, R.A., Johnston, R.C., and Pedersen, D.R., "An Analysis of Collar Function and The Use of Titanium in Femoral Prosthesis," Clinical Orthopedics, Vol.270, 1981, PP.270.

[44] Whiteside, L.A., Amador, D.D., and Russell, K.W., "The Effects of The Collar on Total Hip Femoral Component Subsidence," Clinical Orthopedics, Vol.231, 1988, PP.120.

[45] Crowninshield, R., "Prosthetic Materials for Fixation," Clinical Orthopedics, Vol.235, 1988, PP.166.

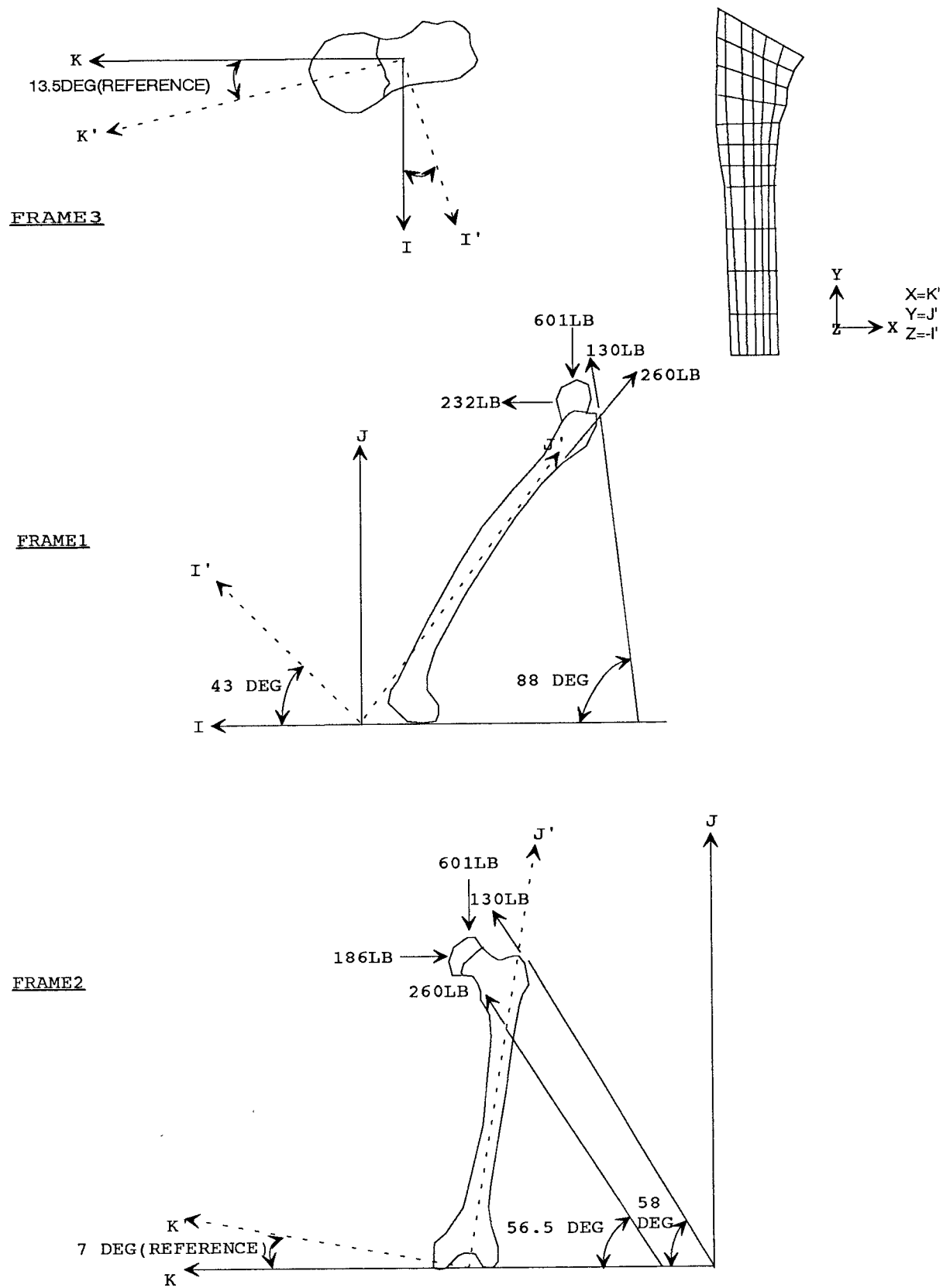
[46] Paul, J.P., "Load Actions on the Human Femur in Walking and Some Resultant Stresses," Experimental Mechanics, March 1971, PP.121-125.

APPENDIX

ILLUSTRATION OF COORDINATE SYSTEMS TRANSFORMATION ON

4 PERCENT PHASE OF THE WALKING CYCLE
9 PERCENT PHASE OF THE WALKING CYCLE
41 PERCENT PHASE OF THE WALKING CYCLE
52 PERCENT PHASE OF THE WALKING CYCLE

Fig. A-1 Force actions on left femur at 4 percent phase of the walking cycle



4 PERCENT PHASE OF THE WALKING CYCLE

$$\text{TRANSFORMATION MATRIX } T, \begin{vmatrix} C_{I'I} & C_{I'J} & C_{I'K} \\ C_{J'I} & C_{J'J} & C_{J'K} \\ C_{K'I} & C_{K'J} & C_{K'K} \end{vmatrix}$$

$C_{i'i}$ = ANGLE OF COSINE BETWEEN OLD AXIS AND NEW AXIS

$$\text{FRAME 1, } T_1 = \begin{vmatrix} \cos 43^\circ & \cos 47^\circ & \cos 90^\circ \\ \cos 133^\circ & \cos 43^\circ & \cos 90^\circ \\ \cos 90^\circ & \cos 90^\circ & \cos 0^\circ \end{vmatrix}$$

$$\text{FRAME 2, } T_2 = \begin{vmatrix} \cos 0^\circ & \cos 90^\circ & \cos 90^\circ \\ \cos 90^\circ & \cos 7^\circ & \cos 97^\circ \\ \cos 90^\circ & \cos 83^\circ & \cos 7^\circ \end{vmatrix}$$

$$\text{FRAME 3, } T_3 = \begin{vmatrix} \cos 13.5^\circ & \cos 90^\circ & \cos 76.5^\circ \\ \cos 90^\circ & \cos 0^\circ & \cos 90^\circ \\ \cos 103.5^\circ & \cos 90^\circ & \cos 13.5^\circ \end{vmatrix}$$

NEW MATRIX = (RESULTANT MATRIX) (OLD MATRIX)

$$\text{RESULTANT MATRIX} = T_1 * T_2 * T_3 = \begin{vmatrix} 0.73 & 0.68 & 0.09 \\ -0.64 & 0.72 & -0.25 \\ -0.23 & 0.12 & 0.96 \end{vmatrix}$$

FROM FIGURE A-1,

$$1 \text{ LB} = 4.448 \text{ N}$$

HIP JOINT COMPONENTS,

$$\begin{aligned} H_I &= 232 \text{ lb.} = 1031.9 \text{ N} \\ H_J &= -601 \text{ lb.} = -2673.2 \text{ N} \\ H_K &= -186 \text{ lb.} = -827.3 \text{ N} \end{aligned}$$

COMPONENTS OF HIP ABDUCTOR FORCE(130LB),

$$\begin{aligned} AB_I &= 130 * 4.448 * \cos 88^\circ = 20.18 \text{ N} \\ AB_J &= 130 * 4.448 * \cos 32^\circ = 489.96 \text{ N} \\ AB_K &= 130 * 4.448 * \cos 58^\circ = 306.42 \text{ N} \end{aligned}$$

COMPONENTS OF HIP ADDUCTOR FORCE(260LB),

$$\begin{aligned} AD_I &= 260 * 4.448 * \cos 133^\circ = -788.72 \text{ N} \\ AD_J &= 260 * 4.448 * \cos 61.3^\circ = 554.92 \text{ N} \\ AD_K &= 260 * 4.448 * \cos 56.5^\circ = 638.30 \text{ N} \end{aligned}$$

4 PERCENT PHASE OF THE WALKING CYCLE, CONT'D

$$\text{OLD MATRIX BECOMES} \left| \begin{array}{ccc} 1031.9 & 20.18 & -788.72 \\ -2673.2 & 489.96 & 554.92 \\ -827.3 & 306.42 & 638.30 \end{array} \right| \begin{array}{l} \dots\dots I \\ \dots\dots J \\ \dots\dots K \end{array}$$

NEW MATRIX IS EQUAL TO

$$\begin{array}{c} \left| \begin{array}{ccc} 0.73 & 0.68 & 0.09 \\ -0.64 & 0.72 & -0.25 \\ -0.23 & 0.12 & 0.96 \end{array} \right| \left| \begin{array}{ccc} 1031.9 & 20.18 & -788.72 \\ -2673.2 & 489.96 & 554.92 \\ -827.3 & 306.42 & 638.30 \end{array} \right| \\ = \left| \begin{array}{ccc} -1138.95 & 375.48 & -140.97 \\ -2378.30 & 263.25 & 744.75 \\ -1352.33 & 348.32 & 860.76 \end{array} \right| \begin{array}{l} \dots\dots I' \\ \dots\dots J' \\ \dots\dots K' \end{array} \end{array}$$

INPUT FORCE COMPONENTS APPLIED TO THE FINITE ELEMENT MODEL :

$$\begin{array}{l} H_X = -1352.33N \\ H_Y = -2378.30N \\ H_Z = 1138.95N \end{array}$$

$$\begin{array}{l} AB_{130-X} = 348.32N \\ AB_{130-Y} = 263.25N \\ AB_{130-Z} = -375.48N \end{array}$$

$$\begin{array}{l} AD_{260-X} = 860.76N \\ AD_{260-Y} = 744.75N \\ AD_{260-Z} = 140.97N \end{array}$$



9 PERCENT PHASE OF THE WALKING CYCLE

$$\text{TRANSFORMATION MATRIX } T, \begin{vmatrix} C_{I'I} & C_{I'J} & C_{I'K} \\ C_{J'I} & C_{J'J} & C_{J'K} \\ C_{K'I} & C_{K'J} & C_{K'K} \end{vmatrix}$$

$C_{i'i}$ = ANGLE OF COSINE BETWEEN OLD AXIS AND NEW AXIS

$$\begin{aligned} \text{FRAME 1, } T_1 &= \begin{vmatrix} \cos 37.5^\circ & \cos 52.5^\circ & \cos 90^\circ \\ \cos 127.5^\circ & \cos 37.5^\circ & \cos 90^\circ \\ \cos 90^\circ & \cos 90^\circ & \cos 0^\circ \end{vmatrix} \\ &= \begin{vmatrix} 0.79 & 0.60 & -0.07 \\ -0.61 & 0.79 & -0.1 \\ 0 & 0.12 & 1 \end{vmatrix} \end{aligned}$$

$$\begin{aligned} \text{FRAME 2, } T_2 &= \begin{vmatrix} \cos 0^\circ & \cos 90^\circ & \cos 90^\circ \\ \cos 90^\circ & \cos 7^\circ & \cos 97^\circ \\ \cos 90^\circ & \cos 83^\circ & \cos 7^\circ \end{vmatrix} \\ &= \begin{vmatrix} 1 & 0 & 0 \\ 0 & 0.99 & -0.12 \\ 0 & 0.12 & 0.99 \end{vmatrix} \end{aligned}$$

$$\begin{aligned} \text{FRAME 3, } T_3 &= \begin{vmatrix} \cos 13.5^\circ & \cos 90^\circ & \cos 76.5^\circ \\ \cos 90^\circ & \cos 0^\circ & \cos 90^\circ \\ \cos 103.5^\circ & \cos 90^\circ & \cos 13.5^\circ \end{vmatrix} \\ &= \begin{vmatrix} 0.97 & 0 & 0.23 \\ 0 & 1 & 0 \\ -0.23 & 0 & 0.97 \end{vmatrix} \end{aligned}$$

NEW MATRIX = (RESULTANT MATRIX) (OLD MATRIX)

$$\text{RESULTANT MATRIX} = T_1 * T_2 * T_3 = \begin{vmatrix} 0.78 & 0.60 & 0.12 \\ -0.57 & 0.79 & -0.24 \\ -0.23 & 0.12 & 0.96 \end{vmatrix}$$

FROM FIGURE A-2,

HIP JOINT COMPONENTS,

$$\begin{aligned} H_I &= 234 \text{ lb.} = 1040.8\text{N} \\ H_J &= -577 \text{ lb.} = -2566.5\text{N} \\ H_K &= -253 \text{ lb.} = -1125.3\text{N} \end{aligned}$$

9 PERCENT PHASE OF THE WALKING CYCLE, CONT'D

COMPONENTS OF HIP ABDUCTOR FORCE(202LB) ,

$$\begin{aligned} AB_I &= 0 \\ AB_J &= 202 * 4.448 * \cos 31^\circ \\ &= 770.16N \\ AB_K &= 202 * 4.448 * \cos 59^\circ \\ &= 462.76N \end{aligned}$$

COMPONENTS OF HIP ADDUCTOR FORCE(374LB) ,

$$\begin{aligned} AD_I &= 374 * 4.448 * \cos 135^\circ \\ &= -1176.3N \\ AD_J &= 374 * 4.448 * \cos 66.85^\circ \\ &= 653.9N \\ AD_K &= 374 * 4.448 * \cos 54^\circ \\ &= 977.8N \end{aligned}$$

$$\text{OLD MATRIX BECOMES} \quad \left| \begin{array}{ccc} 1040.8 & 0 & -1176.3 \\ -2566.5 & 770.16 & 653.9 \\ -1125.3 & 462.76 & 977.8 \end{array} \right| \quad \begin{array}{l} \dots\dots I \\ \dots\dots J \\ \dots\dots K \end{array}$$

NEW MATRIX IS EQUAL TO

$$\begin{aligned} & \left| \begin{array}{ccc} 0.78 & 0.60 & 0.12 \\ -0.57 & 0.79 & -0.24 \\ -0.23 & 0.12 & 0.96 \end{array} \right| \quad \left| \begin{array}{ccc} 1040.8 & 0 & -1176.3 \\ -2566.5 & 770.16 & 653.9 \\ -1125.3 & 462.76 & 977.8 \end{array} \right| \\ &= \left| \begin{array}{ccc} -863.11 & 517.63 & -407.84 \\ -2350.72 & 497.36 & 952.4 \\ -1627.65 & 536.67 & 1287.7 \end{array} \right| \quad \begin{array}{l} \dots\dots I' \\ \dots\dots J' \\ \dots\dots K' \end{array} \end{aligned}$$

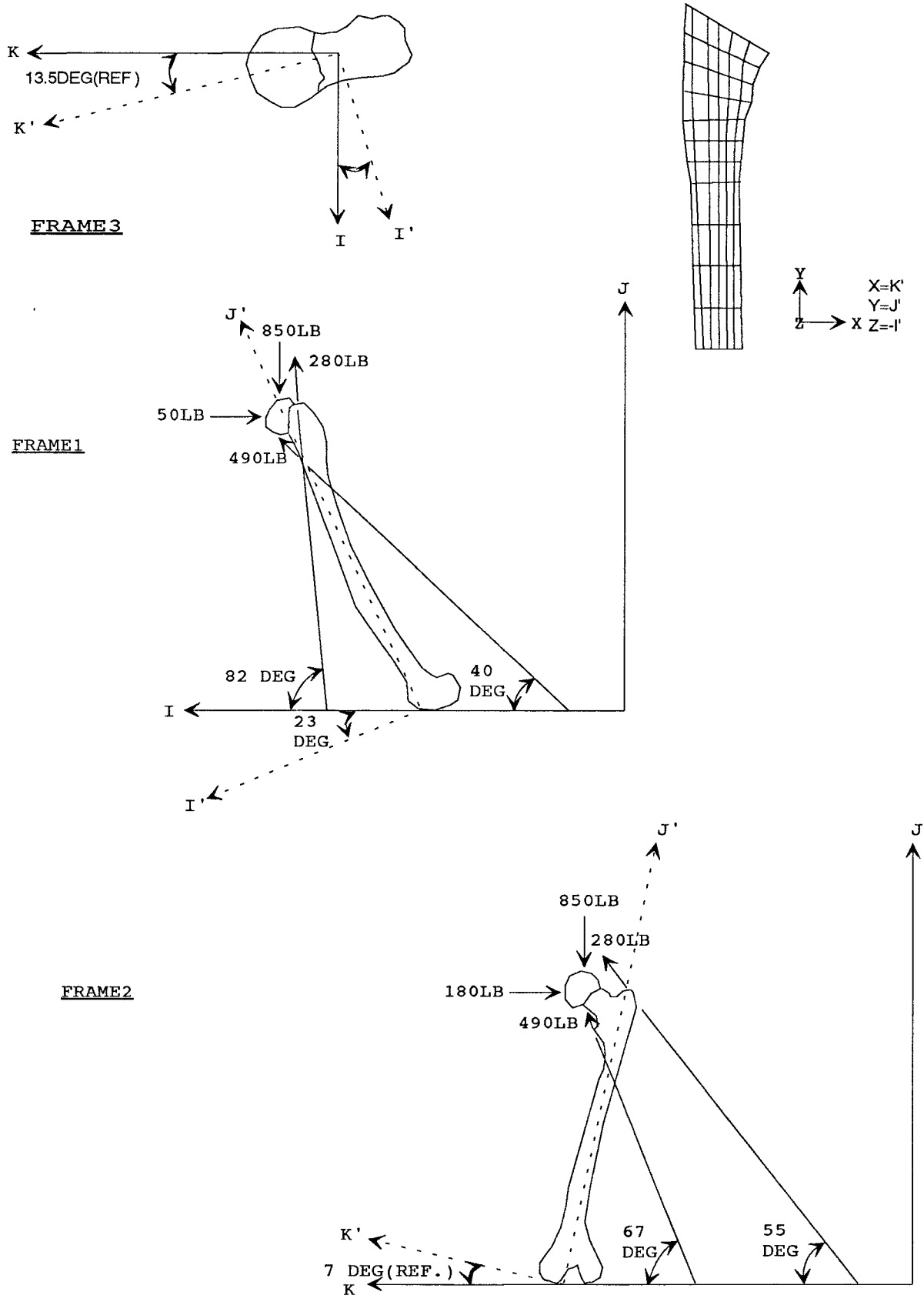
INPUT FORCE COMPONENTS APPLIED TO THE FINITE ELEMENT MODEL :

$$\begin{aligned} H_X &= -1627.65N \\ H_Y &= -2350.72N \\ H_Z &= 863.11N \end{aligned}$$

$$\begin{aligned} AB_{202-X} &= 536.67N \\ AB_{202-Y} &= 497.36N \\ AB_{202-Z} &= -517.63N \end{aligned}$$

$$\begin{aligned} AD_{374-X} &= 1287.7 \text{ N} \\ AD_{374-Y} &= 952.4 \text{ N} \\ AD_{374-Z} &= 407.84N \end{aligned}$$

Fig.A-3 Force actions on left femur at 41 percent phase of the walking cycle



41 PERCENT PHASE OF THE WALKING CYCLE

$$\text{TRANSFORMATION MATRIX } T, \begin{vmatrix} C_{I'I} & C_{I'J} & C_{I'K} \\ C_{J'I} & C_{J'J} & C_{J'K} \\ C_{K'I} & C_{K'J} & C_{K'K} \end{vmatrix}$$

$C_{i'i}$ = ANGLE OF COSINE BETWEEN OLD AXIS AND NEW AXIS

$$\text{FRAME 1, } T_1 = \begin{vmatrix} \cos 23^\circ & \cos 113^\circ & \cos 90^\circ \\ \cos 67^\circ & \cos 23^\circ & \cos 90^\circ \\ \cos 90^\circ & \cos 90^\circ & \cos 0^\circ \end{vmatrix}$$

$$= \begin{vmatrix} 0.92 & -0.39 & 0 \\ 0.39 & 0.92 & 0 \\ 0 & 0 & 1 \end{vmatrix}$$

$$\text{FRAME 2, } T_2 = \begin{vmatrix} \cos 0^\circ & \cos 90^\circ & \cos 90^\circ \\ \cos 90^\circ & \cos 7^\circ & \cos 97^\circ \\ \cos 90^\circ & \cos 83^\circ & \cos 7^\circ \end{vmatrix} = \begin{vmatrix} 1 & 0 & 0 \\ 0 & 0.99 & -0.12 \\ 0 & 0.12 & 0.99 \end{vmatrix}$$

$$\text{FRAME 3, } T_3 = \begin{vmatrix} \cos 13.5^\circ & \cos 90^\circ & \cos 76.5^\circ \\ \cos 90^\circ & \cos 0^\circ & \cos 90^\circ \\ \cos 103.5^\circ & \cos 90^\circ & \cos 13.5^\circ \end{vmatrix} = \begin{vmatrix} 0.97 & 0 & 0.23 \\ 0 & 1 & 0 \\ -0.23 & 0 & 0.97 \end{vmatrix}$$

NEW MATRIX = (RESULTANT MATRIX) (OLD MATRIX)

$$\text{RESULTANT MATRIX} = T_1 * T_2 * T_3 = \begin{vmatrix} 0.88 & -0.39 & 0.26 \\ 0.40 & 0.91 & -0.01 \\ -0.23 & 0.12 & 0.96 \end{vmatrix}$$

FROM FIGURE A-3,

HIP JOINT COMPONENTS,

$$H_I = -50 \text{ lb.} = -222.4\text{N}$$

$$H_J = -850 \text{ lb.} = -3780.8\text{N}$$

$$H_K = -180 \text{ lb.} = -800.6\text{N}$$

COMPONENTS OF HIP ABDUCTOR FORCE(280LB),

$$\begin{aligned} AB_I &= 280 * 4.448 * \cos 82^\circ \\ &= 173.33\text{N} \end{aligned}$$

$$\begin{aligned} AB_J &= 280 * 4.448 * \cos 35^\circ \\ &= 1005.37\text{N} \end{aligned}$$

$$\begin{aligned} AB_K &= 280 * 4.448 * \cos 55^\circ \\ &= 714.35\text{N} \end{aligned}$$

41 PERCENT PHASE OF THE WALKING CYCLE, CONT'D

COMPONENTS OF HIP ADDUCTOR FORCE(490LB) ,

$$\begin{aligned}AD_I &= 490 * 4.448 * \cos 40^\circ \\&= 1669.61N \\AD_J &= 490 * 4.448 * \cos 59^\circ \\&= 1112.42N \\AD_K &= 490 * 4.448 * \cos 67^\circ \\&= 851.61N\end{aligned}$$

$$\text{OLD MATRIX BECOMES} \quad \left| \begin{array}{ccc} -222.4 & 173.33 & 1669.61 \\ -3780.8 & 1005.37 & 1112.42 \\ -800.6 & 714.35 & 851.61 \end{array} \right| \quad \begin{array}{l} \dots\dots I \\ \dots\dots J \\ \dots\dots K \end{array}$$

NEW MATRIX IS EQUAL TO

$$\begin{aligned}& \left| \begin{array}{ccc} 0.88 & -0.39 & 0.26 \\ 0.40 & 0.91 & -0.01 \\ -0.23 & 0.12 & 0.96 \end{array} \right| \quad \left| \begin{array}{ccc} -222.4 & 173.33 & 1669.61 \\ -3780.8 & 1005.37 & 1112.42 \\ -800.6 & 714.35 & 851.61 \end{array} \right| \\&= \left| \begin{array}{ccc} 1070.64 & -53.83 & 1256.83 \\ -3521.48 & 977.07 & 1671.63 \\ -1171.12 & 766.55 & 567.02 \end{array} \right| \quad \begin{array}{l} \dots\dots I' \\ \dots\dots J' \\ \dots\dots K' \end{array}\end{aligned}$$

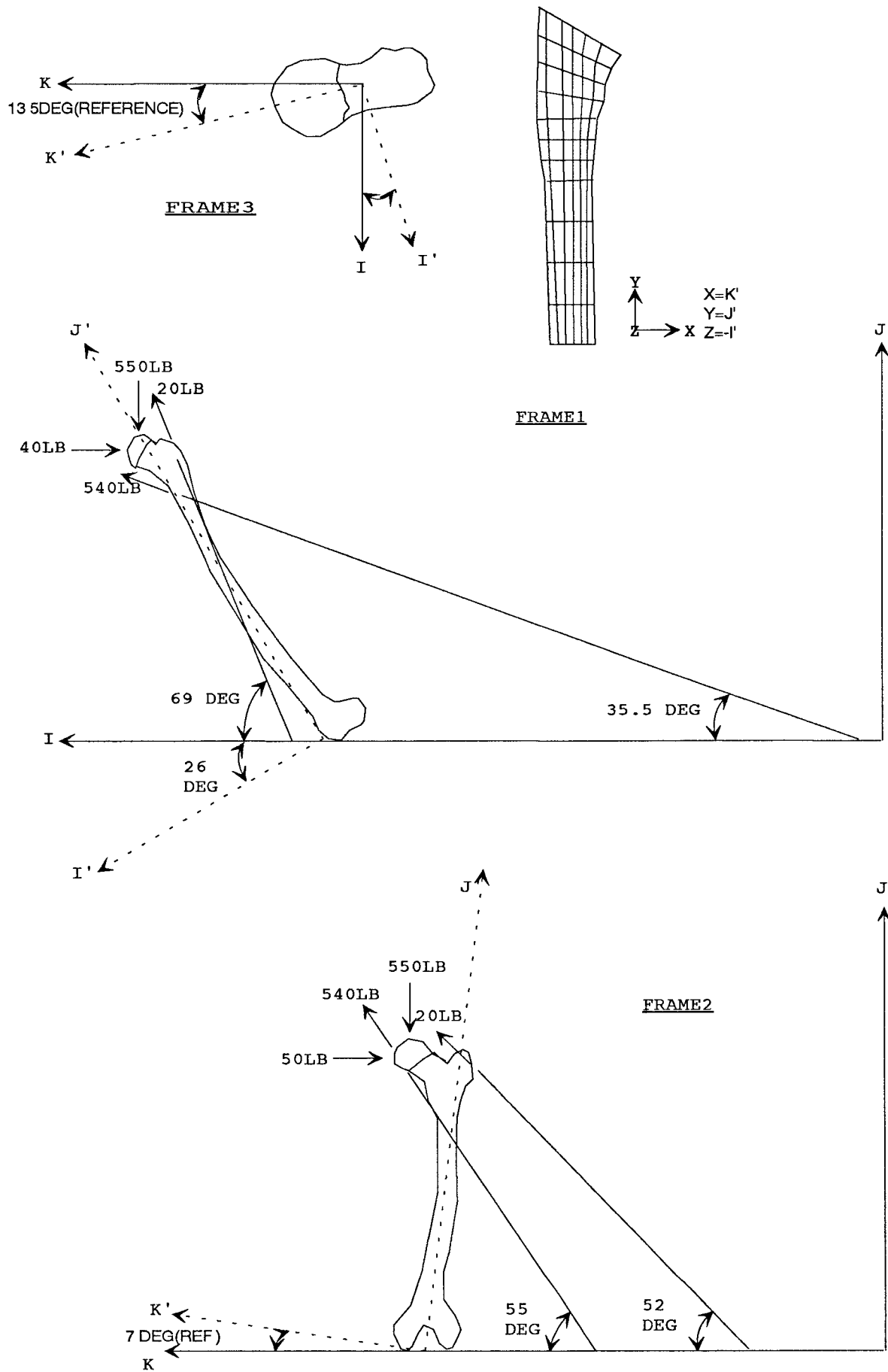
INPUT FORCE COMPONENTS APPLIED TO THE FINITE ELEMENT MODEL :

$$\begin{aligned}H_X &= -1171.12N \\H_Y &= -3521.48N \\H_Z &= -1070.64N\end{aligned}$$

$$\begin{aligned}AB_{280-X} &= 766.55N \\AB_{280-Y} &= 977.07N \\AB_{280-Z} &= 53.83N\end{aligned}$$

$$\begin{aligned}AD_{490-X} &= 567.02N \\AD_{490-Y} &= 1671.63N \\AD_{490-Z} &= -1256.83N\end{aligned}$$

Fig.A-4 Force actions on left femur at 52 percent phase of the walking cycle



52 PERCENT PHASE OF THE WALKING CYCLE

$$\text{TRANSFORMATION MATRIX } T, \begin{vmatrix} C_{I'I} & C_{I'J} & C_{I'K} \\ C_{J'I} & C_{J'J} & C_{J'K} \\ C_{K'I} & C_{K'J} & C_{K'K} \end{vmatrix}$$

$C_{i'i}$ = ANGLE OF COSINE BETWEEN OLD AXIS AND NEW AXIS

$$\begin{aligned} \text{FRAME 1, } T_1 &= \begin{vmatrix} \cos 26^\circ & \cos 116^\circ & \cos 90^\circ \\ \cos 64^\circ & \cos 26^\circ & \cos 90^\circ \\ \cos 90^\circ & \cos 90^\circ & \cos 0^\circ \end{vmatrix} \\ &= \begin{vmatrix} 0.90 & -0.44 & 0 \\ 0.44 & 0.90 & 0 \\ 0 & 0 & 1 \end{vmatrix} \end{aligned}$$

$$\begin{aligned} \text{FRAME 2, } T_2 &= \begin{vmatrix} \cos 0^\circ & \cos 90^\circ & \cos 90^\circ \\ \cos 90^\circ & \cos 7^\circ & \cos 97^\circ \\ \cos 90^\circ & \cos 83^\circ & \cos 7^\circ \end{vmatrix} \\ &= \begin{vmatrix} 1 & 0 & 0 \\ 0 & 0.99 & -0.12 \\ 0 & 0.12 & 0.99 \end{vmatrix} \end{aligned}$$

$$\begin{aligned} \text{FRAME 3, } T_3 &= \begin{vmatrix} \cos 13.5^\circ & \cos 90^\circ & \cos 76.5^\circ \\ \cos 90^\circ & \cos 0^\circ & \cos 90^\circ \\ \cos 103.5^\circ & \cos 90^\circ & \cos 13.5^\circ \end{vmatrix} \\ &= \begin{vmatrix} 0.97 & 0 & 0.23 \\ 0 & 1 & 0 \\ -0.23 & 0 & 0.97 \end{vmatrix} \end{aligned}$$

NEW MATRIX = (RESULTANT MATRIX) (OLD MATRIX)

$$\text{RESULTANT MATRIX} = T_1 * T_2 * T_3 = \begin{vmatrix} 0.86 & -0.43 & 0.26 \\ 0.45 & 0.89 & -0.004 \\ -0.23 & 0.12 & 0.96 \end{vmatrix}$$

FROM FIGURE A-4,

HIP JOINT COMPONENTS,

$$\begin{aligned} H_I &= -40 \text{ lb.} = -177.9\text{N} \\ H_J &= -550 \text{ lb.} = -2446.4\text{N} \\ H_K &= -50 \text{ lb.} = -222.4\text{N} \end{aligned}$$

52 PERCENT PHASE OF THE WALKING CYCLE, CONT'D

COMPONENTS OF HIP ABDUCTOR FORCE(20LB) ,

$$AB_I = 20 * 4.448 * \cos 69^\circ \\ = 31.88N$$

$$AB_J = 20 * 4.448 * \cos 45^\circ \\ = 62.43N$$

$$AB_K = 20 * 4.448 * \cos 52^\circ \\ = 54.77N$$

COMPONENTS OF HIP ADDUCTOR FORCE(540LB) ,

$$AD_I = 540 * 4.448 * \cos 35.5^\circ \\ = 1955.44N$$

$$AD_J = 540 * 4.448 * \cos 85^\circ \\ = 218.57N$$

$$AD_K = 540 * 4.448 * \cos 55^\circ \\ = 1377.68N$$

OLD MATRIX BECOMES	$\begin{matrix} -177.9 & 31.88 & 1955.44 \\ -2446.4 & 62.43 & 218.57 \\ -222.4 & 54.77 & 1377.68 \end{matrix}$	$\begin{matrix} \dots\dots I \\ \dots\dots J \\ \dots\dots K \end{matrix}$
--------------------	--	--

NEW MATRIX IS EQUAL TO

$\begin{vmatrix} 0.86 & -0.43 & 0.26 \\ 0.45 & 0.89 & -0.004 \\ -0.23 & 0.12 & 0.96 \end{vmatrix}$	$\begin{vmatrix} -177.9 & 31.88 & 1955.44 \\ -2446.4 & 62.43 & 218.57 \\ -222.4 & 54.77 & 1377.68 \end{vmatrix}$	
$= \begin{vmatrix} 841.13 & 14.81 & 1945.89 \\ -2256.46 & 69.69 & 1068.96 \\ -466.15 & 52.74 & 899.05 \end{vmatrix}$		$\begin{matrix} \dots\dots I' \\ \dots\dots J' \\ \dots\dots K' \end{matrix}$

INPUT FORCE COMPONENTS APPLIED TO THE FINITE ELEMENT MODEL :

$$\begin{aligned} H_X &= -466.15N \\ H_Y &= -2256.46N \\ H_Z &= -841.134N \end{aligned}$$

$$\begin{aligned} AB_{20-X} &= 52.74N \\ AB_{20-Y} &= 69.69N \\ AB_{20-Z} &= -14.81N \end{aligned}$$

$$\begin{aligned} AD_{540-X} &= 899.05N \\ AD_{540-Y} &= 1068.96N \\ AD_{540-Z} &= -1945.89N \end{aligned}$$